Universitat Autònoma de Barcelona

Study of vegetation dynamics from satellite: phenological responses to climate change

Kevin Bórnez Mejías

ADVERTIMENT. L'accés als continguts d'aquesta tesi queda condicionat a l'acceptació de les condicions d'ús establertes per la següent llicència Creative Commons: http://cat.creativecommons.org/?page_id=184

ADVERTENCIA. El acceso a los contenidos de esta tesis queda condicionado a la aceptación de las condiciones de uso establecidas por la siguiente licencia Creative Commons: http://es.creativecommons.org/blog/licencias/

WARNING. The access to the contents of this doctoral thesis it is limited to the acceptance of the use conditions set by the following Creative Commons license: https://creativecommons.org/licenses/?lang=en

Study of vegetation dynamics from satellite: phenological responses to climate change

Doctoral thesis

Kevin Bórnez Mejías

To apply for the degree of Doctor

Directors: **Dr. Josep Peñuelas** & **Dr. Aleixandre Verger**

PhD in Terrestrial Ecology

Centre for Ecological Research and Forestry Applications (CREAF)

Universitat de Autònoma de Barcelona

Bellaterra, July 2021

"However difficult life may seem, there is always something you can do and succeed at."

Stephen Hawking

Acknowledgements

Todo comenzó allá por el año 2016. Por aquel entonces, me encontraba finalizando mi segundo máster en Granada; cuando mi madre, ilusionada porque su hijo encontrara un trabajo después de los estudios, me envió una captura de pantalla con una oferta laboral. Se trataba de una oferta en la que un tal Dr. Aleixandre Verger buscaba candidatos para optar a un contrato FPU durante 4 años en Barcelona. Tras una deliberación, decidí realizar la solicitud para ser el candidato para optar a esa ayuda FPU y, por suerte fui seleccionado.

Tras disfrutar mi último verano de estudiante, me fui con mis enseres personales a Barcelona, concretamente a Cerdanyola del Vallès. La elección del lugar para buscar piso, no fue nada fácil, pero teniendo en cuenta que me gustar tener todo a mano y poder ir a los sitios caminando, la decisión estaba tomada. Tras unos días de toma de contacto por la ciudad, llegó el tres de octubre, día en el que la vida que conocía daría un cambio de 360º (nuevo trabajo, nuevos compañeros, hábitos, etc.). Y aquí estoy hoy, cinco años después, finalizando esta etapa. El tiempo ha pasado tan rápido que apenas me he dado cuenta. De no ser por el tamaño que ha alcanzado el *potus* del despacho, pensaría que llevo aquí unos meses.

Durante esta etapa he tenido la suerte de encontrarme con personas fantásticas, a las que querría agradecer que hayan estado junto a mí por unos motivos u otros. Quiero agradecer en primer lugar a Aleixandre que me diera esta oportunidad, lo que me ha permitido crecer como persona, aumentar conocimientos e introducirme en el mundo de la ciencia, del que conocía poco. Desde que te fuiste de vuelta a Valencia no nos hemos visto mucho, pero por unos métodos u otros siempre has estado ahí para guiarme y ayudarme. Agradecerte también que, tras finalizar la ayuda predoctoral, no dudaras en contratarme durante unos meses adicionales, que sirvieron para poder llevar a buen puerto esta tesis. Josep, gracias por ayudarme en todo lo que he necesitado durante estos años, y aunque también sé que siempre estás ocupado, nunca has dejado de atenderme, aunque fuera fin de semana o festivo. También quiero agradecer al Ministerio de Educación que haya financiado mi contrato durante el periodo predoctoral.

Nunca olvidaré el primer día que Aleixandre me enseñó aquel despacho (-148). Había tal desorden que hasta él mismo se sorprendió. Era difícil ver a los compañeros con los que trabajaría entre aquel montón de cajas y armarios repletos de material de campo, cuyos delitos ya habían prescrito hacía décadas. Con el paso de los días, ese despacho gris y marrón empezaba a tomar un color verde intenso gracias al gran *potus*, que se extendía por los armarios dejando atrás todas aquellas cajas, convirtiéndose en la envidia de todo aquel que osaba asomarse por la puerta.

Pero lo mejor de ese despacho no han sido las plantas, sino los grandes compañeros/as y amigos que me han acompañado en esta andadura. Unos se fueron y otros seguirán, pero sin lugar a dudas, he aprendido algo de cada uno de ellos. A pesar de que este último año haya sido un poco diferente y no nos hayamos podido ver las caras, siempre que veníais a hacer una visita, me alegráis el día. Marina, Helena, gracias por vuestras mañanas de cháchara intentando arreglar el planeta y sacarnos unos eurillos extra, que junto con los días de tertulias con Laura, Irene y Paolo hacían cada jornada un poco más amena. También mencionar a una de las jóvenes promesas del despacho, Luca, que tendrás que ser el encargado de cuidar las plantas, aunque he de decir que te dejaré una nota con las instrucciones de riego. Me siento orgulloso de haber estado en el mejor despacho del CREAF y con los mejores compañeros.

También querría agradecer al resto de personas con las que he tenido el placer de cruzarme por estos pasillos, especialmente aquellos que apostaron por una navidad 2021 feliz con la celebración de la *Kevineta*, que, aunque sean de un despacho rival, me han terminado cayendo bien. Manu (compañero de noches y festivos), Victor (no es persona sin un café mañanero), Carlos, Javi, Aina, M.ª Ángeles, Judit, ha sido un placer conoceros y espero que, aunque pasen los años, el día en que haya un reencuentro parezca que no ha pasado el tiempo. También quisiera agradecer a otros compañeros/as con los que he compartido experiencias y charlas, aunque sea por los pasillos del CREAF, Albert, Luciana, Jordi, Susana, Adrià. Y en general, gracias a toda la familia del CREAF, por la acogida, y por aquellas celebraciones pre-covid cada vez que había un cumpleaños o una festividad, que terminaban convirtiéndose en una forma de relacionarse, de conocerse, y que servían para apartar un momento los ojos de la pantalla del ordenador y volver con las pilas recargadas.

No puedo olvidarme de que durante el segundo año de tesis tuve la oportunidad de realizar una estancia de investigación en Estados Unidos, que se convirtió en una de las mejores experiencias que he vivido. Thanks to Andrew Richardson and its research group at Northern Arizona University for making me feel at home at all times; and for the learning and experiences I had during those three months. Por otro lado, entre las experiencias relativas al aprendizaje y formación como estudiante de doctorado, he tenido la posibilidad de realizar un gran número de horas de docencia en distintos grados universitarios de la UAB, y principalmente las he realizado con Miquel, al que quería agradecer el tratamiento que ha tenido hacia mí y lo que he aprendido con él desde el punto de vista docente.

Para ir finalizando con los agradecimientos, y aunque seguro que me he dejado a alguien por el camino, quería agradecerte a ti, Marta, que me has apoyado en esta última etapa de la tesis, tanto sentimental como logísticamente, haciendo que los agobios finales no lo fueran tanto y, sobre todo, teniendo mucha paciencia conmigo.

Por último, agradecer a mi familia los esfuerzos que han realizado a lo largo de mi vida para que finalmente haya podido realizar el doctorado. A mi madre, que seguro me ha echado mucho de menos durante todos estos años lejos de casa; a mi hermana "reto", que, aunque es la peque de la familia, siempre ha estado ahí en los momentos buenos y malos; y a mi padre, que allá donde estés siempre formarás parte de mí y me acompañarás en el corazón. Seguro que los tres estaréis orgullosos de que aquel pequeño travieso haya llegado a convertirse en la persona que es ahora y que esté escribiendo estas palabras para finalizar su etapa predoctoral.

.

Cerdanyola de Vallès,

Julio 2021

Table of Contents

List of Tables

List of Figures

Acronyms

AGF: Asymmetric Gaussian Function

AVHRR: Advanced Very High-Resolution Radiometer

BBCH: Biologische Bundesanstalt, Bundessortenamt and Chemical industry

CCI: Climate Change Initiative

CGLS: Copernicus Global Land Service

DN: Digital Numbers

DoY: Day of the Year

EoS: End of the Season

EVI: Enhanced Vegetation Index

FAO: Food and Agriculture Organization

FAPAR: Fraction of Absorbed Photosynthetically Active Radiation

FCOVER: Fraction of Vegetation Cover

FPU: Formación del Profesorado Universitario

GCC: Green Chromatic Coordinates

GCOS: Global Climate Observing System

GEE: Google Earth Engine

GMES: Global Monitoring of the Environment and Security

GPP: Gross Primary Production

IPCC: Intergovernmental Panel on Climate Change

LAI: Leaf Area Index

LC: land-cover

LFP: Low Pass Filtering

LoS: Length of the growing Season

LSP: Land Surface Phenology

MERIS: Medium Resolution Imaging Spectrometer

MODIS: Moderate Resolution Imaging Spectroradiometer

NDVI: Normalized Difference Vegetation Index

NIR: Red and Near Infrared

PEP: Pan European Phenology

PET: Potential Evapotranspiration

RGB: Red-Green-Blue

RMA: Reduced Major Axis regression

RMSE: Root Mean Square Error

SGF: Adaptive Savitzky-Golay Filter

SoS: Start of the Season

SPEI: Standardized Precipitation-Evapotranspiration Index

SPI: Standardized Precipitation Index

SPIRITS: Software for the Processing and Interpretation of Remotely Sensed Image Time Series

SPOT – VGT: VEGETATION on board the Satellite Pour l'Observation de la Terre

SWIR: Short-Wave Infrared

TOC: Top Of the Canopy

TS: Theil-Sen

US: The United States

USA-NPN: United States of America - National Phenology Network

VIIRS: Visible Infrared Imaging Radiometer Suite

Abstract

Phenology is key to control physicochemical and biological processes, especially albedo, surface roughness, canopy conductance and fluxes of carbon, water and energy. High-quality retrieval of land surface phenology (LSP) is thus increasingly important for understanding the effects of climate change on ecosystem function and biosphere–atmosphere interactions. Remote sensing is a useful tool for characterizing LSP although no consensus exists on the optimal satellite dataset and the method to extract phenology metrics.

I aimed to (i) improve the retrieval of Land Surface Phenology from satellite data, (ii) validate LSP with ground observations and near surface remote sensing, and (iii) understand the relationships between climate variables and phenology in a climate change context, as well as to assess the responses of vegetation to extreme events. These three main research objectives are explored in the three chapters of the thesis.

In chapter 2, I investigated the sensitivity of phenology to (I) the input vegetation variable: normalized difference vegetation index (NDVI), leaf area index (LAI), fraction of absorbed photosynthetically active radiation (FAPAR), and fraction of vegetation cover (FCOVER); (II) the smoothing and gap filling method for deriving seasonal trajectories; and (III) the phenological extraction method: threshold, logistic-function, moving-average and first derivative based approaches. The threshold-based method applied to the smoothed and gap-filled Copernicus Global Land LAI V2 time series agreed the best with the ground phenology, with root mean square errors of ~10 d and ~25 d for the timing of the start of the season (SoS) and the end of the season (EoS), respectively.

In the third chapter, I took advantage of PhenoCam and FLUXNET capability of continuous monitoring of vegetation seasonal growth at very high temporal resolution (every 30 minutes). This allows a more robust and accurate comparison with LSP derived from satellite time series avoiding problems related to the differences in the definition of phenology metrics. I validated LSP estimated from LAI time series with

near-surface PhenoCam and eddy covariance FLUXNET data over 80 sites of deciduous broadleaf forest. Results showed a strong correlation ($R^2 > 0.7$) between the satellite LSP and ground-based observations from both PhenoCam and FLUXNET for the timing of the start (SoS) and $R^2 > 0.5$ for the end of season (EoS). The threshold-based method performed the best with a root mean square error of ~9 d with PhenoCam and ~7 d with FLUXNET for the timing of SoS, and ~12 d and ~10 d, respectively, for the timing of EoS.

In the fourth chapter, I investigated the spatio-temporal patterns of the response of deciduous forests to climatic anomalies in the Northern Hemisphere using LSP derived in Chapter 1 and validated in Chapter 1 and Chapter 2, and multi-source climatic data sets for 2000–2018 at resolutions of 0.1°. I also assessed the impact of extreme heatwaves and droughts on deciduous forest phenology. Analyses of partial correlations of phenological metrics with the timing of the start of the season (SoS), end of the season (EoS), and climatic variables indicated that changes in preseason temperature played a stronger role than precipitation in the interannual variability of SoS anomalies: the higher the temperature, the earlier the SoS in most deciduous forests in the Northern Hemisphere (mean correlation coefficient of -0.31). Both temperature and precipitation contributed to the advance and delay of EoS. A later EoS was significantly correlated with a positive standardized precipitation-evapotranspiration index (SPEI) at the regional scale (~30% of deciduous forests). The timings of EoS and SoS shifted by >20 d in response to heat waves throughout most of Europe in 2003 and in the United States of America in 2012.

1

Introduction

1.1. Land surface phenology under climate change

Phenology is defined as the study of the timing of recurrent biological events (such as plant growing, migration and breeding of birds, or emergence of insects), as well as the causes of their timing with regard to biotic and abiotic forces, and the relationship among phases of the same or different species (Lieth, 1974). In this thesis I focus on the field of vegetation phenology, which deals with the seasonal life-cycle phenophases of plants, from the start of the greenness to senescence and their biotic or abiotic drivers (Saxena and Rao, 2020). Fluctuations in vegetation phenology are related to factors such as carbon, energy, and climate within terrestrial ecosystems (Estiarte and Peñuelas, 2015; Garrity et al., 2011).

The scientific discipline of vegetation phenology has a long history. The first robust studies date from the 1950s (Schnelle, 1955). However, vegetation phenology has received increasing scientific attention in more recent times, by the early 1990s (Bajocco et al., 2019; Donnelly and Yu, 2017; Saxena and Rao, 2020) due to the growing evidence that the timing of growing stages is mostly dependent on environmental cues (Chuine and Regniere, 2017), especially as phenological events are deeply sensitive to climate variations (Menzel et al., 2006). Moreover, vegetation phenology has raised an increasing interest as a key indicator of climate change (IPCC, 2007, 2013, 2014) due to its important role as regulator of processes in terrestrial ecosystems, including carbon and water cycle (Peñuelas et al., 2009; Richardson et al., 2013; Verger et al., 2016).

Unlike human and animals with the ability to quickly move from one region to another, vegetation is fixed to a location, with slow and limited migrations, so it has to withstand the climatic changes (Saxena and Rao, 2020). Vegetation phenology varies greatly between species and geographic gradients (Peñuelas et al., 2009; Zhao et al., 2013), and it is the outcome of the interaction of inherent attributes of each specie and their sensitivity to external factors, such as radiation (photoperiod) (Borchert and Rivera, 2001), temperature (Wang et al., 2019), and precipitation (Chuine, 2010; Ibáñez et al., 2010; Visser et al., 2010; Zhao et al., 2013). Assessing phenological transitions dates has played an important role for understanding the climatic drivers of interannual variability and for analyzing how vegetations respond to climate conditions (Chmielewski and Rötzer, 2001; Cleland et al., 2007; Menzel et al., 2006; Schwartz et al., 2006; Walther, 2010).

Climate change is recognized for being a direct consequence of greenhouse gas emissions, and it is especially reflected in a significant and continuous increase in the average temperature of the earth (IPCC, 2007, 2013). The Intergovernmental Panel on Climate Change (IPCC) 4th Assessment Report on Impacts, Adaptation and Vulnerability highlighted that the average global temperature has risen by 0.85 °C, over the period 1880–2012 and projections indicate that it will continue to rise (IPCC, 2007, 2013). Most studies in the late 1990s and early twenty-first century highlighted that elevated temperatures have contributed to the increase of vegetation greening through the early leaf unfolding (Chmielewski and Rötzer; Menzel and Fabian, 1999; Zhang et al., 2004) and later senescence (Delbart et al., 2008; Menzel and Fabian 1999; Menzel, 2006), which extends the length of the growing season in most areas of the Northern Hemisphere (Saxena and Rao. 2020).

Global climate change and particularly extreme weather events such as floods, droughts and heatwaves are reflected in vegetation phenology anomalies (IPCC, 2007, 2012; Tang et al., 2017). Therefore, understanding the responses of vegetation phenology to climate extremes is crucial and challenging, considering that climatic projections indicate that future anomalies in the climate will become more intense and frequent than those experienced in the past decades (IPCC, 2007, 2012; Jentsch et al., 2009; Reichstein et al., 2013; Tang et al., 2017; Zheng et al., 2018; Zhao et al., 2018). Studies on vegetation and climatic interactions have demonstrated that vegetation phenology respond directly to climate, and phenological shifts in turn disturb climate through feedback, affecting the CO_2 uptake in function of the water availability in the soil, regional characteristics, as well as the plant species and location (Atkinson et al., 2013; Chen et al., 2018; Keenan et al., 2014; Peñuelas et al., 2001, 2009; Richardson et al., 2013), which would alter the hydrological cycle through changes in the evapotranspiration pattern (Berg et al., 2016; Bonan et al., 2008; Buermann et al., 2013, 2018; Peñuelas et al., 2009).

1.2. Vegetation phenology estimation

Traditionally, phenological datasets were compiled from annual ground-based observations of the timing of specific phenological events for particular plant species based on periodic visual inspection by scientists or by volunteer observers (Morin et al., 2009; Peñuelas et al., 2002; Richardson et al., 2006; Schwartz et al., 2002, 2013). Human observations of plant phenology phases have been conducted for centuries (Templ et al., 2018). The earliest known phenological data collection date from the ninth century in Japan, where local citizens recorded the spring cherry blossoms and maple leaves for the timing of autumn (Aono and Kazui, 2008; Aono and Tani, 2014). In the sixteenth and seventeenth century records of phenology are also found in England, recording the growth of more than 20 different species of plants, including records of tree-leaf out from temperate forest (Sparks and Carey, 1995; Thompson and Clark, 2008). In France, the scientists and farmers have also a long tradition observing the grapevine phenology since the 1950s (García de Cortazar et al., 2017).

In the late twentieth and early twenty-first centuries, several international initiatives including PEP725 (Pan European Phenology), PlantWatch program (Templ et al.,2018; Vliet et al., 2003), and USA-NPN (National Phenology Network) (Mayer, 2010), aim to manage and coordinate the databases of phenological records, establishing common protocols and techniques to support and standardize phenological data collection across large geographical areas in order to provide detailed plant phenology data at species-scale or individual plant scale (Donnelly and Yu, 2017; Morin et al., 2009; Richardson et al., 2006; Schwartz et al., 2012; Templ et al., 2018).

Most of the ground-based observations and phenological networks are usually carried out by observing the vegetation and recording only a small choice of phenophases (e.g. leaf unfolding, senescence), avoiding the possibility of analyzing the progression of the seasonality (Templ et al., 2018). Moreover, the number of ground-based observations are insufficiently distributed, mainly near to the cities, agricultural fields, or in low altitude areas, and usually are restricted to a few species (Liang et al., 2011). To solve these issues, the scientific community has begun to take advantage of (1) near-surface observations (Hufkens et al., 2012; Richardson et al., 2009; Sonnentag et al., 2012; Zhang et al., 2018) and (2) satellite remote sensing data (Bórnez et al., 2020a, 2020b;

Verger et al., 2016; Wu et al., 2014; Zhang et al., 2018), which allow more objective, long-term and continuous phenological observations of different plant species over a broad area (Morisette et al., 2009).

Near-surface observations usually includes imagery acquired from visible-wavelength digital cameras, such as PhenoCam (Hufkens et al., 2012; Richardson et al., 2009; Sonnentag et al., 2012) with RGB (Red, Green and Blue) bands (Wingate et al., 2015; Vrieling et al., 2018), and continuous CO_2 flux measurements based on eddy covariance technique (e.g. FluxNet Network) (Gonsamo et al., 2013; Wu et al., 2013). Near-surface observations (e.g. PhenoCam and FluxNet) provide higher temporal resolution and greater spatial coverage than ground measurements, allowing to analyze site-level phenological variation and mechanisms (Vrieling et al., 2018). Near-surface imagery acquired by PhenoCam are based on optical principles similar to those used by sensors onboard on satellites, bridging the scale between ground and satellite-based data (Figure 1.1) (Moura et al., 2017; Sonnentag et al., 2012).

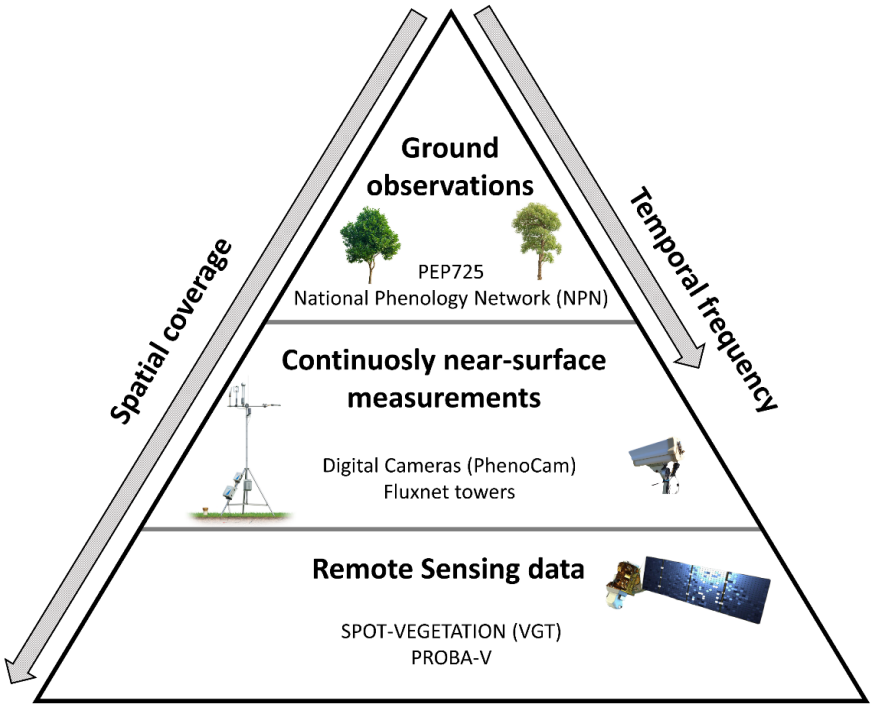

Figure 1.1: Diagram showing the data sources used in the thesis for the phenological estimation, as well as their properties regarding the temporal frequency and the spatial coverage and representability of the measurements. Ground measurements have the lowest temporal resolution while near surface remote sensing data and eddy covariance observations as well as satellite remote sensing provide more frequent observations and higher spatial coverage

1.2.1. Land surface phenology: the role and importance of remote sensing for vegetation monitoring

Attention to changes in vegetation phenophases such as the start (SoS), end (EoS) or length (LoS) of the growing season has increased over the last three decades (Donnelly and Yu, 2017) with the use of remote sensing technology and climate models (Daham et al., 2019; Shen et al., 2015; Wang et al., 2019), which allows to collect climatic and phenological data over larger scales (Donnelly and Yu, 2017). Remote sensing imagery has been improving the spatial resolutions ranging from centimeters to kilometers and the temporal frequencies ranging from months or weeks to minutes (Xie et al., 2008). Therefore, unlike in-situ observations, CO_2 flux data or PhenoCam imagery, sensors onboard satellites allow to measure phenological events over larger areas. The study of the seasonal pattern of variation in vegetated land surfaces from remote sensing is commonly known as Land Surface Phenology (LSP) (de Beurs and Henebry, 2005).

The first monitoring of LSP began with the Landsat I satellite in the early 1970s with frequency temporal acquisition of images (16-day) at 30m of spatial resolution (Tucker, 1979). However, for monitoring vegetation, frequent observations are necessary (Miao et al., 2013), so other satellites and sensors have been developed over the last few decades for monitoring vegetation with higher temporal resolution, but with lower spatial resolution (>250 m), such as the Advanced Very High-Resolution Radiometer (AVHRR) sensor launched in the 1980‘s (Duchemt al. 1999; Heumann et al., 2007; Lloyd, 1990; Reed et al., 1994), the Moderate resolution Imaging Spectroradiometer (MODIS) (Tan et al., 2011; Zhang et al., 2003), Visible Infrared Imaging Radiometer Suite (VIIRS) (Liu et al., 2017; Zhang et al., 2018), Système Pour L'Observation de la Terre (SPOT)-VEGETATION (VGT) (Atzberger and Eilers, 2011; Verger et al., 2015; Xie et al., 2008), Medium Resolution Imaging Spectrometer (MERIS) (Brown et al., 2017), PROBA-V (Bórnez et al., 2020a, 2020b, Guzman et al., 2019; Verger et al., 2017), and more recently, Sentinel-2A/B tandem satellites, which unlike the previous ones, have been used for the estimation of LSP at greater spatial resolution ranging from 10 to 60 m and frequent revisit times <5 d (Addabbo et al., 2016; Descals et al., 2020).

LSP dynamics reflect the response of vegetation to seasonal and annual changes in the climate and hydrologic cycle (de Beurs and Henebry, 2004, 2010). The application of

remote sensing imagery to study vegetation phenology and climate relationship found a great catalyst with the development of vegetation indices, and its implementation in Landsat and the AVHRR sensor in the late 1970s (Jones and Vaughan, 2010). From that moment, a broad variety of vegetation products have been developed for the study of LSP and climate at multiple scales (Henebry and de Beurs, 2013; Zeng et al., 2020). The European Union has developed operational land monitoring services, known as Copernicus Global Land Service (CGLS), as continuity of the Global Monitoring of the Environment and Security (GMES) (Verger et al., 2014). CGLS provides a series of bio-geophysical products and vegetation indices (VI), describing the status and dynamics of vegetation at global scale from time series of remote sensing observations (Verger et al., 2014).

VI and biophysical products use the land surface reflectance through the spectral signatures of photosynthetically and non-photosynthetically of green healthy vegetation (leaves) over the 0.4–2.6 μm wavelengths (Figure 1.2) to estimate the greenness (Gonsamo et al., 2013). The vegetation signature shows low spectral reflectance in the visible and middle-infrared wavelengths (high chlorophyll and water absorption) and high reflectance in the near-infrared (NIR) wavelengths (Gates, 1970; Zheng et al., 2020), which aids to monitor the seasonal cycle of vegetation. Time series of VIs and biophysical variables are commonly used to identify seasonal transitions in vegetation, especially for deciduous forests, since they have a clearly defined seasonal response (e.g. Figure 1.3) compared to the small seasonal variations of evergreen vegetation. (Garrity et al., 2011; Liu et al., 2016; Melaas et al., 2013).

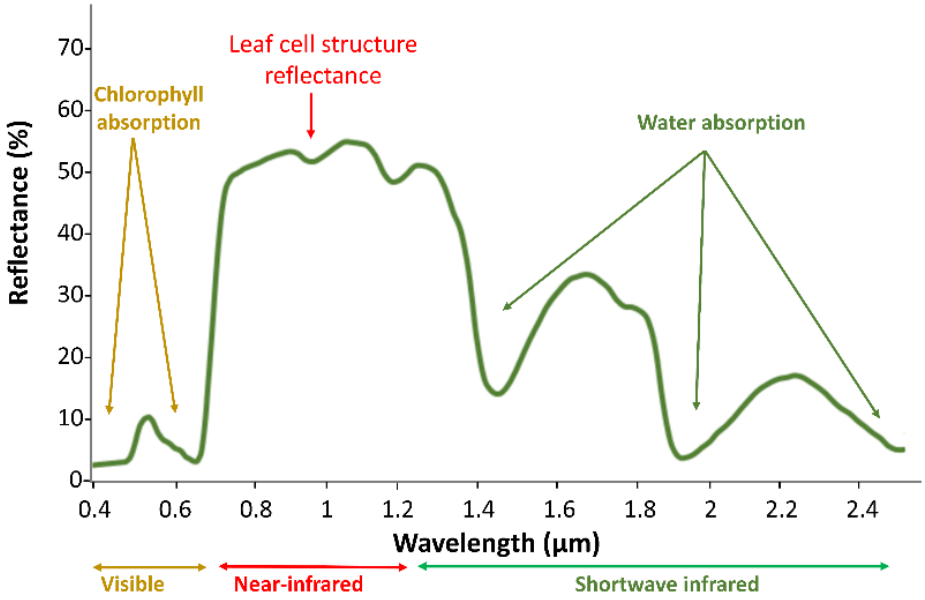

Figure 1.2**:** The spectral response patterns of vegetation, that remote sensors use to estimate vegetation indices. It shows the area of absorption by chlorophyll pigment in the visible spectrum, the reflectance of the leaves mainly in the near infrared, and the absorption of radiation by the water content in most of the incoming radiation over the shortwave infrared region. Note that the figure shows the average spectral signature of the vegetation, which varies slightly between different vegetation types and species. To explore the spectral response characteristics of specific species, visit the ASTER Spectral Library https://speclib.jpl.nasa.gov/library/ecoviewplot, California Institute of Technology, 2002.

Among the different vegetation products, most previous approaches for estimating LSP have been based on the use of biophysical variables, including the Leaf Area Index (LAI) (Bórnez et al., 2020b; Hanes and Schwartz, 2011; Kang et al., 2003; Verger et al., 2015; Wang et al., 2017), Fraction of Absorbed Photosynthetic Active Radiation (FAPAR) (Meroni et al., 2014; Verger 2016, 2017), the fraction of vegetation cover (FCover) (Verger et al., 2016), as well as spectral vegetation indices such as the Normalized Difference Vegetation Index (NDVI) (Fischer, 1994; Yu et al., 2003; Wu et al., 2014), and Enhanced Vegetation Index (EVI) (Zhang et al., 2003; Wang et al., 2017). All of them are associated with the biophysical and biochemical properties of vegetation (Gonsamo et al., 2012), being recognized as essential climate variables by the Global Climate Observing System (GCOS) (Verger et al., 2014).

NDVI has been the most widely used index to estimate vegetation phenology because of its easy calculation and its broad acceptance into the scientific community (Jeong et al., 2011; Myneni et al., 2002; Reed et al., 1994; White et al., 2014). However, biophysical variables such the LAI are being increasingly studied to describe plant

canopy structure (Figure 1.3) because it represents direct biophysical measures of vegetation, estimated by models, and it is more sensitive than NDVI or FPAR for larger vegetation amounts (Myneni and Williams, 1994; Verger et al., 2013). It is based on leaf development rather than on proxies provided by vegetation indices which avoid distortions associated with the canopy structure and the biochemical composition of the existing foliage (Richardson et al., 2009; Verger et al., 2014, 2016).

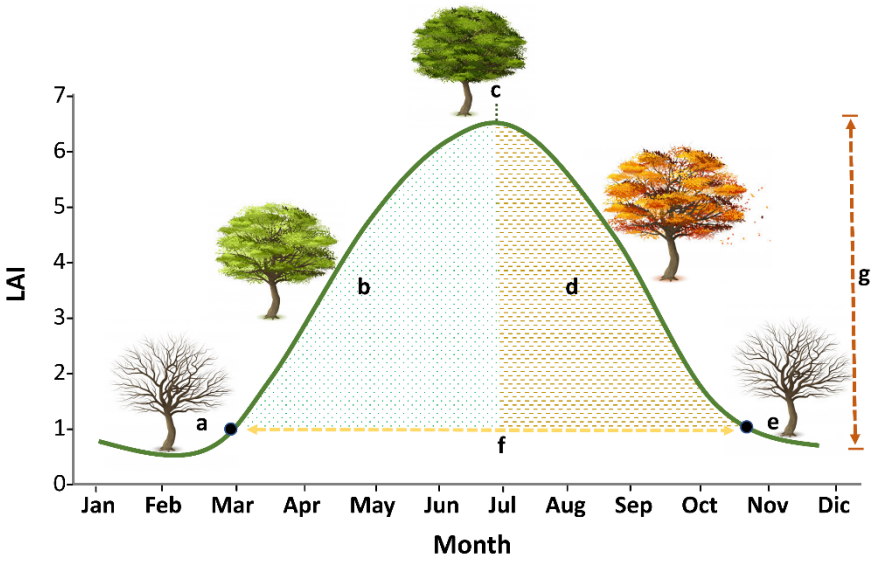

Figure 1.3: Example of determining growing season of vegetation from seasonal patterns of the Leaf Area Index (LAI) over deciduous forest. Phenology can be extracted from the seasonal LAI curve (in green), as defined in Bórnez et al., 2020b. Phenological date vary according to the method for phenological estimation used. In this example (a) Start of season, (b) Greenup phase, (c) Maximum LAI, (d) Senescence phase, (e) End of season, (f) Length of season, (g) Seasonal amplitude are shown.

Various methods have been developed to estimate phenological transitions from a time series of VI and biophysical variables. The main metrics of interest in the studies of LSP have been the start (SoS) (White et al., 2009; Liang et al., 2011) and the end of the growing season (EoS) due to its importance within the context of climate change (Garrity et al., 2011; Menzel, 2002). The methodologies on LSP estimation are mainly based on a two-step approach (Verger et al., 2016; Zeng et al., 2020) including (1) curve-fitting and (2) extraction of phenology metrics. Firstly, the original remote sensing products typically have noisy and spurious points, so to perform the curve fitting approach smoothing methods are typically applied to the time-series datasets to filter and minimize residual noise and fill in the gaps, since noise and missing data in satellite time series can introduce uncertainties in the phenological estimates. Several smoothing techniques are available, including low pass filtering (LPF), Whittaker smoother,

Adaptive Savitzky-Golay filter (SGF), and asymmetric Gaussian function (AGF) (Verger et al., 2016).

Regarding the methods for phenological estimation from the reconstructed daily time series, a broad variety of strategies has been designed. The most commonly used strategies are based on thresholds (Myneni et al., 1997; White et al., 1997), moving averages (Reed et al., 1994), first derivatives (Tateishi and Ebata, 2004; White et al., 2009), and curvature of piecewise logistic functions (Zhang et al., 2003). De Beurs and Henebry (2010) indicated that there is no better method to estimate phenology for all the vegetation types and areas. White et al. (2009) and Atkinson et al. (2012) investigated the effects of using different methodologies to derive LSP metrics, highlighting that also phenological metrics estimation accuracy varies among the different methods and VI or biophysical variables. Therefore, the method and variable selected for phenological estimation can significantly influence the performance of the phenology extraction from the smoothed time series (Kandasamy et al., 2013; Atkinson et al., 2012), and this is especially important for analyzing the interrelationships between phenological estimates and climate variables.

Understanding the relationship between the different elements of global climate change and LSP is one of the most studied and challenged topics of the 21st century (Sykes, 2009). The 4th Assessment Report of the IPCC indicated that spring onset has been advancing by about 2.3 and 5.2 days per decade since the 1970s to early twenty-first century (Parmesan, 2007) and it concluded that phenology "is perhaps the simplest process in which to track changes in the ecology of species in response to climate change" (IPCC, 2007). In this sense, the LSP estimated in this thesis from remote sensing data serves for detecting the response of vegetation to environmental changes at multiple scales by analyzing the anomalies in time series.

1.3. Thesis objectives

The general objective of the thesis is to analyze the dynamics of vegetation phenology in response to climatic change, through the use of satellite imagery from CGLS vegetation products. Particularly, I aim to estimate Land Surface Phenology from satellite data, validate it with ground observations and near surface remote sensing and

understand the relationships between climate variables and phenology in a climate change context, as well as to assess the responses of vegetation to extreme events.

Meeting this goal is challenging due to the wide availability of vegetation variables and phenological estimation methods from which phenology metrics can be obtained (de Beurs and Hennery, 2010; Schwartz and Hanes, 2010; White et al., 2009), which requires a series of previous steps, including the identification of the biophysical variable or vegetation index that best assesses the vegetation phenology found in ground observations (chapter 2). In order to evaluate the robustness of the phenological metrics estimated from satellite, and compared with ground measurement, near surface remote sensing and eddy covariance techniques were used by using continuous time series GCC (from PhenoCam) and GPP (from FluxNet), which allowed me to validate the results (chapter 3). Finally, I analyzed the response of phenology to the changes in climate variables as a result of global climate change, focusing on anomalies and extreme climatic events (chapter 4).

The thesis is thus structured in three research chapters:

Chapter 2. Phenological metrics estimation from remote sensing time series and validation with ground measurements

The objectives of Chapter 2 are (1) to select the best biophysical variable or vegetation index for estimating phenological metrics on a global scale within the portfolio of the CGLS vegetation products (NDVI, LAI, FCOVER or FAPAR) from time series of the sensors SPOT-VGT and PROBA-V, and (2) to define the method that best matched with ground data (using PEP725 and NPN). I evaluated four methods for estimating phenology: the threshold method based on percentiles, the derivative method, the autoregressive moving-average method, and the logistic-function method.

Chapter 3. Validation of satellite phenological metrics by using near-surface remote sensing and eddy covariance flux data

In the s third chapter, I completed the validation of LSP retrievals developed in Chapter 2 by taking advantage of continuous measurements of near surface remote sensing (PhenoCam) and eddy covariance CO_2 flux measurements (FluxNet) at very high temporal resolution. The aim was to conduct a more robust and accurate comparison

with LSP derived from satellite time series avoiding problems related to the differences in the definition of phenological metrics. In this chapter, I evaluated the same four methods as in Chapter 2 for estimating phenology: the threshold method based on percentiles, the derivative method, the autoregressive moving-average method, and the logistic-function method. These methods were applied both to satellite CGLS LAI V2 time series and ground observations from PhenoCam GCC and eddy covariance flux data.

Chapter 4. Assessment of phenological response to climate and extreme events

In this chapter, I explored the relationship between the LSP estimated from LAI time series and climate variables. Specifically, the objectives of this chapter were: (1) to identify and quantify statistically the spatial pattern of correlation between the anomalies of vegetation phenology and climate (temperature, precipitation and drought) to this way identify the main cause of phenological change, (2) to quantify the sensitivity of phenology to climate; and (3) to determine the consequences of extreme events on phenology in the areas with the highest sensitivity to climate.

2

Land surface phenology from VEGETATION and PROBA-V data. Assessment over deciduous forests

Kevin Bórnez, Adrià Descals, Aleixandre Verger, Josep Peñuelas

Published in *International Journal of Applied Earth Observation and Geoinformation* (2020), Vol.84: 101974. https://doi.org/10.1016/j.jag.2019.101974

Scan this code to download the published version

Abstract

Land surface phenology has been widely retrieved although no consensus exists on the optimal satellite dataset and the method to extract phenology metrics. This study is the first comprehensive comparison of vegetation variables and methods to retrieve land surface phenology for 1999-2017 time series of Copernicus Global Land products derived from SPOT-VEGETATION and PROBA-V data. We investigated the sensitivity of phenology to (I) the input vegetation variable: normalized difference vegetation index (NDVI), leaf area index (LAI), fraction of absorbed photosynthetically active radiation (FAPAR), and fraction of vegetation cover (FCOVER); (II) the smoothing and gap filling method for deriving seasonal trajectories; and (III) the method to extract phenological metrics: thresholds based on a percentile of the annual amplitude of the vegetation variable, autoregressive moving averages, logistic function fitting, and first derivative methods. We validated the derived satellite phenological metrics (start of the season (SoS) and end of the season (EoS)) using available ground observations of *Betula pendula*, *B. alleghaniensis*, *Acer rubrum*, *Fagus grandifolia*, and *Quercus rubra* in Europe (Pan-European PEP725 network) and the USA (National Phenology Network, USA-NPN). The threshold-based method applied to the smoothed and gap-filled LAI V2 time series agreed best with the ground phenology, with root mean square errors of ~10 d and ~25 d for the timing of SoS and EoS respectively. This research is expected to contribute for the operational retrieval of land surface phenology within the Copernicus Global Land Service.

2.1. Introduction

Phenology is the study of the timing of recurrent biological and seasonal events and their biotic and abiotic factors (Beaumont et al., 2015). Studies of plant phenology focus on how these events and factors are influenced by seasonal and interannual variations in climate and how they modulate abundance and diversity (Beaumont et al., 2015). Phenology is, moreover, key to control physicochemical and biological processes, especially albedo, surface roughness, canopy conductance and fluxes of carbon, water and energy (Peñuelas et al., 2009; Richardson et al., 2013). Phenological metrics are thus relevant parameters for modeling land surface processes and the global carbon cycle (Wu et al., 2014).

Phenological metrics are estimated based on ground observations and data derived from satellites. Ground observations provide accurate timing of vegetation phenophases but cannot cover continuously large-scale areas (Garrity et al., 2011; Yu et al., 2017). Satellite sensors with moderate spatial resolutions, including AVHRR, MODIS, MERIS, SPOT-VEGETATION and PROBA-V, provide long-term time series of daily observations that allow improving the characterization of land surface phenology on a global scale (Atkinson et al., 2012; Verger et al., 2016; Zhang et al., 2004). However, the noise in the data and missing observations mainly due to cloud contamination may induce significant uncertainties in the estimation of phenological metrics (Kandasamy et al., 2013; Verger et al., 2013). The literature shows a broad variety of time-series processing methods designed to reconstruct gap-filled vegetation seasonal trajectories from noisy satellites signals. This includes the best index slope method (Viovy et al., 1992), mean filters (Reed et al., 1994), moving-window filters (Sweets et al. 1999), asymmetric Gaussian functions (Jönsson and Eklundh, 2002), Savitzky–Golay filters (Chen et al., 2004) or the Whittaker smoother (Eilers, 2003). However, no single method always performs better than others for smoothing vegetation time series (Cai et al., 2017) and their performance vary spatially and temporally with land surface conditions and cloud influence (Atkinson, et al. 2012; Kandasamy and Fernandes, 2015).

A broad variety of statistical methods have been designed to extract phenological metrics from satellite time series. Metrics typically include the start of the season (SoS), the end of the season (EoS), the timing of maximum growth and the length of the

growing season (LoS) (Reed et al., 1994; Zhang et al., 2004). De Beurs and Henebry (2010) provided a comprehensive review of the exiting phenology retrieval approaches that can be classified in four main categories: thresholds and percentile based methods (Atzberger and Eilers, 2011; Verger et al., 2016), moving averages (Reed et al., 1994), first derivatives (White et al., 2009) and fitted models (de Beurs and Henebry, 2005). White, et al. (2009) compared ten different phenology retrieval methods applied to AVHRR NDVI in North America and found large discrepancies of up to two months in the detection of the SoS.

In addition to the sensitivity to the smoothing and phenological extraction algorithm, the derived phenological metrics are also dependent on the sensor, spatial and temporal resolution, processing chain, and satellite data set. The satellite-derived spectral vegetation indices (e.g. the Normalized Difference Vegetation Index (NDVI)) vary in their strength of phenological prediction across sites and plant functional types (Wu et al., 2014). Unlike previous studies based on vegetation indices, the present study aimed to characterize the phenology not only with NDVI but also with biophysical variables: the leaf area index (LAI), the fraction of absorbed photosynthetically active radiation (FAPAR), the fraction of vegetation cover (FCOVER). We used NDVI version V2.1 (Toté et al., 2017), LAI, FAPAR and FCOVER V1 (Baret et al., 2013) and V2 (Verger et al., 2014) time series derived within the Copernicus Global Land Service (CGLS) from SPOT-VEGETATION and PROBA-V data. Verger et al. (2017) showed that the phenology derived from the interannual climatology of LAI V1 improved other existing products including MODIS-EVI when compared to ground observations for the average date of the SoS and EoS. However, their study was limited to the baseline LAI phenology as derived from a single extraction method. This paper is a continuation of the previous paper by Verger et al. (2017) and we address now the interannual variation of the yearly phenology, the impact of the input vegetation variable and the phenological extraction method. Further, we incorporate LAI, FAPAR and FCOVER V2 that improved continuity (no missing data in V2) and smoothness as compared to V1.

Our study had two main objectives: to select the best biophysical variable or vegetation index for estimating phenological metrics on a global scale within the portfolio of the CGLS vegetation products (NDVI, LAI, FCOVER or FAPAR) and to define the method that best matched the ground data.

2.2. Materials and Methods

2.2.1. Phenological ground observations

Ground-based phenological data from PEP725 and USA-NPN were examined, focusing on the dates of leaf out and leaf senescence for *Betula* (birch) in Europe (Figure 2.1a) and the USA and for *Quercus* (oak), *Fagus* (beech) and *Acer* (maple) in the USA (Figure 2.1b). These genera were chosen because they are present in both Europe and the USA and have large numbers of records in the combined data set.

The PEP725 Pan-European Phenology database (Templ et al., 2018) (www.pep725.eu) has complete records from 1990 to the present. The phenophases defined in PEP725 are based on BBCH (Biologische Bundesanstalt, Bundessortenamt and Chemical industry) code (Meier et al., 2009). We used the phenophases corresponding to the first visible leaves (BBCH 11) as the reference for the timing of SoS and the date corresponding to 50% of leaves with autumn coloration (BBCH 94) for the timing of EoS.

The USA National Phenology Network was established in 2007 to collect, store and share historical and contemporary phenological data on a North American scale (Schwartz et al., 2012). The data are freely available at https://www.usanpn.org/. This network provides measurements of several phenophases. We used the phenophases "leaves" which corresponds to first visible leaves and "increasing leaf size" for SoS and "colored leaves" for EoS.

We discarded ground sites with less than four yearly measurements to obtain consistent data records over the time series. We used ground-site located pixels. The spatial heterogeneity hamper comparing ground-based phenology for individual plants with satellite phenology at a resolution of 1 km. We filtered the ground sites located in agricultural or urban areas using high-resolution images from Google Earth (https://earth.google.com/) and the ESA Land Cover Map (CCI-LC) (http://maps.elie.ucl.ac.be/CCI/viewer/index.php). In Europe, we used only the points with forest coverages >5% using a tree cover map for European forests (Brus et al., 2012).

2.2.2. Satellite time series

The time series of satellite imagery used for estimating the phenological metrics were from the SPOT-VEGETATION (1999-2013) and PROBA-V satellites (2014-2017) with spatial resolutions of 1 km and temporal frequencies of 10 d. In particular, we used LAI, FAPAR, FCOVER V1 (Baret et al., 2013) and V2 (Verger et al., 2014) and NDVI V2.1 (Toté et al., 2017) products generated within the CGLS (https://land.copernicus.eu/global/themes/vegetation) (Table 2.1).

Time series of LAI, FAPAR and FCOVER V1 and NDVI V2.1 contained frequent disturbances caused by residual cloud contamination, atmospheric variability, snow and bi-directional effects (Figure 2.2). These time series required the application of smoothing and gap filling techniques to generate consistent and gap filled seasonal trajectories (section 2.2.3) before the extraction of phenological metrics. The LAI and FCOVER V2 products improved over the V1 products in terms of temporal consistency and continuity (Figure 2.2). The V2 algorithm included multi-step data filtering, smoothing and gap-filling techniques that rendered the products suitable for phenological estimation without additional pre-processing. Filtering of outliers is based on an upper envelope approach, the pixel climatology (interannual mean) is used to fill missing data and a Savitzky-Golay filter is used for the smoothing (Verger et al., 2014).

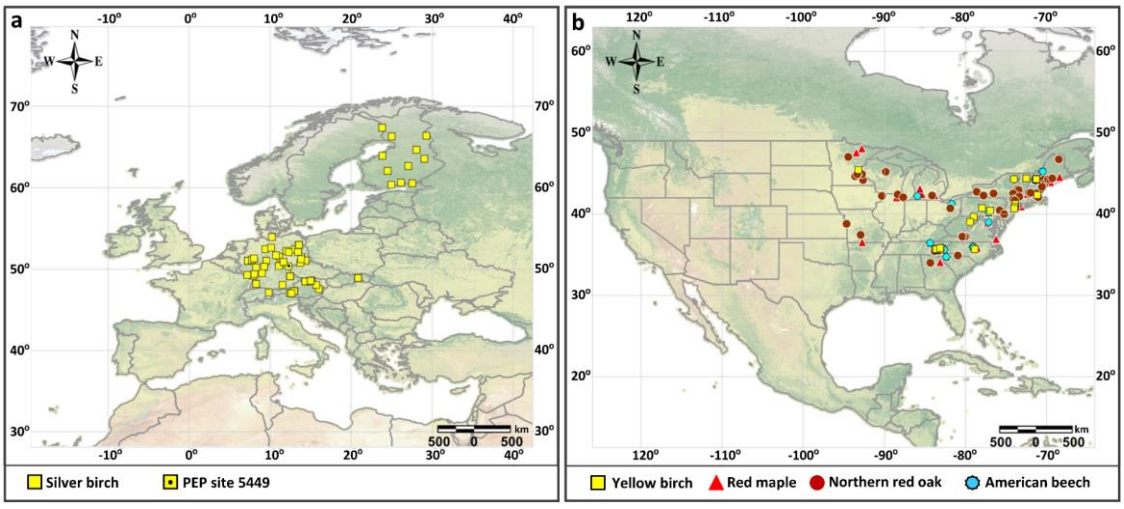

Figure 2.1: Location of selected phenological ground observations at (a) PEP725 sites for Silver birch (*Betula pendula*) and (b) USA – NPN sites for Red maple (*Acer rebrum*), Yellow birch (*Betula alleghaniensis*), American beech (*Fagus grandifolia*) and Nothern red oak (*Quercus rubra*).

Table 2.1**:** Algorithm principles of NDVI V2.1, and LAI, FAPAR, FCOVER V1 and V2.

	NDVI Version 2.1	**LAI, FAPAR, FCOVER Version 1**	**LAI, FAPAR, FCOVER Version 2**
Inputs	Top of the canopy (TOC) reflectances in the red and near infrared (NIR) spectral bands	Nadir normalized TOC reflectances in the red, NIR and short-wave infrared (SWIR) spectral bands, and cosine of the sun zenith angle at 10:00 local time	TOC reflectances in the red, NIR and SWIR spectral bands, and cosine of the 3 angles of sun and view directions
Temporal composition	10 d compositing period. The maximum NDVI value in the composition window is retained. Starting date of composition:1st, 11th and 21th day of the month	30 d compositing period with Gaussian weighting (minimum of two valid observations) Nominal dates: 3rd, 13th and 21-24th day of each month	Adaptive compositing within 15 and 60d semi-periods defined by the availability of 6 valid observations at each side of the date being processed Nominal dates: 10th, 20th and last day of the month
Temporal smoothing and gap filling	Not applied	Not applied	Multi-step filtering, temporal smoothing and gap-filling

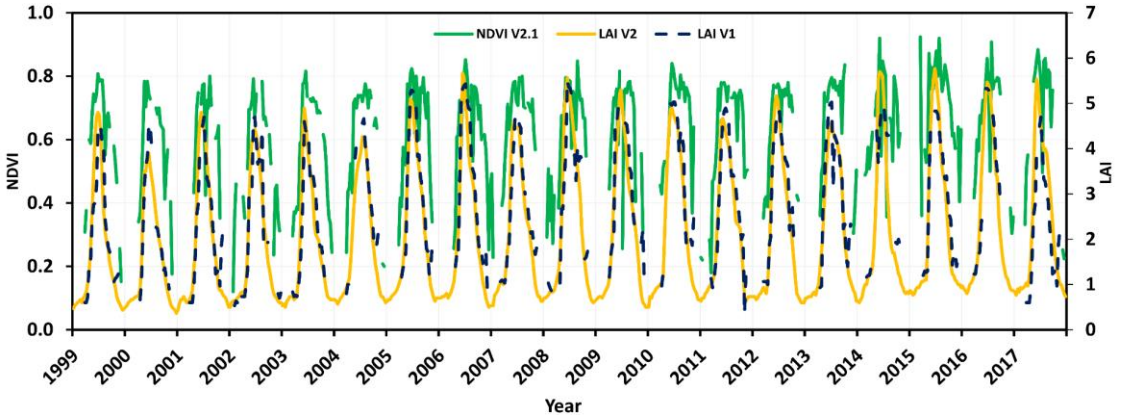

Figure 2.2: LAI (V1 and V2) and NDVI (V2.1) time series for the PEP725 site 5449 (50º42'20.49"N, 13º46'59.55"E) representative of birch forest in Europe.

2.2.3. Smoothing methods

We tested several smoothing methods for reducing noise and reconstructing gap filled seasonal trajectories from CGLS time series (Eerens and Haesen, 2015):

- *WHITTAKER smoother* (Atzberger and Eilers, 2011): It minimizes a cost function describing the balance between fidelity (quadratic difference between estimates and actual observations) and roughness (quadratic difference between successive estimates).

- *BISE (Best Index Slope Extraction)* (Viovy et al., 1992)*:* It retains the good observations in a local window and replaces missing or eliminated suspect values by linear interpolation.
- *MEAN*: A linear interpolation is first applied to fill missing data. A running mean filter with a sliding window of 50 d length is then applied.
- *SWETS method* (Swets et al., 1999): A linear interpolation is first applied to fill missing data. A weighted linear regression over a local window is then applied.

2.2.4. Methods for extracting phenological metrics

We tested four state of the art methods to extract phenological metrics from CGLS time series (Figure 2.3):

- *Thresholds based on a pixel percentile value:* SoS is defined as the day of the year (DoY) when a vegetation variable exceeds a particular threshold. EoS is defined as the DoY when an index remains below a particular threshold. We established dynamic thresholds per pixel based on a percentile of the annual amplitude of the vegetation variable (Verger et al., 2016). The selected percentiles were determined based on the comparison with available ground measurements. We tested the 20th, 30th, 40th and 50th percentiles of the annual amplitude for SoS, and the 30th, 40th, 50th and 60th percentiles for EoS. This method is also the basis of SPIRITS phenological approach.
- *Autoregressive moving average:* A moving average is first computed at a randomly chosen time lag (Ivits et al., 2009). We tested time lags from 50 to 150 d and selected a time lag of 100 d based on the comparison with ground measurements. SoS and EoS are then defined as the DOY when the moving average curves cross the original curve of the vegetation variable.
- *First derivative:* SoS is defined as the DoY of the maximum increase (maximum first derivative) in the curve (Tateishi and Ebata, 2004). EoS is defined as the DoY of the maximum decrease in the curve.
- *Logistic function:* SoS is defined as the DoY of the first local maximum rate of change in the curvature of a logistic function fitted to the time series (Zhang et al., 2003). EoS is defined as the DoY of the first local minimum rate of change in the curvature.

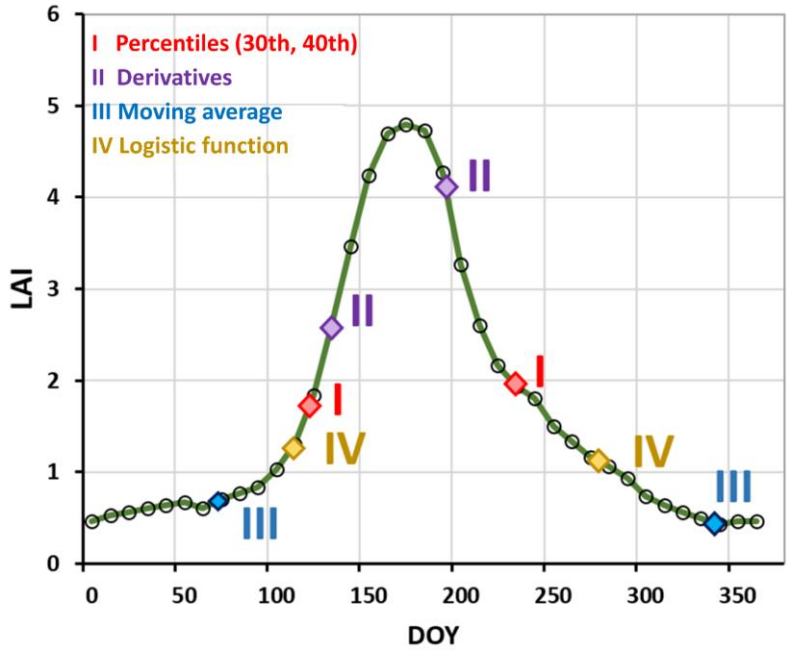

Figure 2.3**:** Schematic representation of SoS (on the left of the peak) and EoS (on the right of the peak) retrieved with the four methods for the PEP725 site 4959 (50º42'20.49"N, 13º46'59.55"E) for 2011. The black circles correspond to the original LAI data at a 10-d frequency, and the green line corresponds to the data interpolated at daily steps, which is used for phenological estimation.

2.2.5. Methodological approach

The several satellite-derived vegetation variables, smoothing methods and phenological extraction approaches lead to a large number of combinations. We sequentially investigated the impact of smoothing, variable and extraction method based on an initial set of modalities. The initial modalities were defined *a posteriori* based on the analysis of all the combinations:

1. Sensitivity analysis of the smoothing method: We used LAI V1 as input dataset and the percentile phenology method.
2. Sensitivity analysis of the vegetation variable: We used the SWETS smoothing method and the percentile phenology method.
3. Sensitivity analysis of the method to extract phenological metrics: We used the LAI V2. Note that in this case the application of a smoothing method is not required because LAI V2 is already smoothed and gap-filled.

The analysis 1 and 2 were carried out in Europe and for the validation we used ground measurements of *Betula Pendula*, which showed a greater latitudinal distribution. The analysis 3 was performed at the global scale. For the sensitivity analysis 1 and 2, we used the Software for the Processing and Interpretation of Remotely Sensed Image Time

Series (SPIRITS) (Eerens et al., 2014; Eerens and Haesen, 2015). For the sensitivity analysis 3, we used Google Earth Engine (GEE) (https://earthengine.google.org) which allowed implementing dedicated algorithms while only the threshold method is available in SPIRITS. The input 10 d time series were linearly interpolated at daily steps before phenological retrieval. For SPIRITS, the precision of phenological estimates is limited by the frequency of the input time series (10 d in our case) (non interpolation). For pixels with multiple growing seasons, we computed the phenological metrics for the growing season having the highest LAI amplitude.

The agreement between metric estimates from satellite imagery and ground-based measurements was quantified using the slope of the linear regression, the Pearson correlation coefficient (*R*), bias, i.e. the average difference between the satellite-derived phenology and the observed date (a positive bias indicated that SoS and EoS occurred later than the observed leaf out and autumnal coloring, respectively), the absolute bias and root mean square error (RMSE) calculated (e.g. for SoS) as:

$$RMSE_{SoS} = \sqrt{\frac{1}{n}\sum_{j=1}^{n}\left(SoS_{ground} - SoS_{est.}\right)^2} \quad (1)$$

where n is the number of samples

2.3. Results

2.3.1. Sensitivity analysis of the smoothing method

The SWETS method performed the best for the reconstruction of seasonal trajectories and the estimation of phenological metrics:16 d in terms of RMSE and 1 d in terms of bias for the timing of SoS, and 34 d (RMSE) and 12 d (bias) for the timing of EoS (Table 2.2).

Table 2.2: Statistics of comparisons between the derived phenology metrics from reconstructed LAI V1 time series using the different smoothing methods and PEP725 ground measurements (*Betula pendula*) for the SoS and EoS. The SPIRITS percentile method was used to extract the phenology using 30% of LAI amplitude for the SoS and 40% for the EoS. * Significant correlations with p<0.05 (**p<0.001).

Metric	Method	RMSE (d)	Bias (d)	Abs. Bias (d)	*R*	Slope
SoS	WHITTAKER	23.80	-8.16	16.76	0.41	0.76
"visible	BISE	27.22	-7.52	19.84	0.43*	0.89
leaves"	MEAN	23.98	-5.84	18.43	0.39	0.74
(n=359)	**SWETS**	**16.44**	**-1.38**	**17.39**	**0.49****	**0.67**
EoS	WHITTAKER	44.56	13.51	31.65	-0.19	-0.12
"colored	BISE	49.45	19.50	37.25	-0.03	-0.10
leaves"	MEAN	44.10	13.18	30.54	-0.08	-0.01
(n=359)	**SWETS**	**34.28**	**12.01**	**28.96**	**-0.15**	**-0.19**

2.3.2. Sensitivity analysis of the vegetation variable

The best agreement with ground measurements for the timing of SoS was found for the 30% threshold of LAI amplitude, 40% of FCOVER, 50% of FAPAR and 50% of NDVI. The best metric definitions for the EOS were based on 40% of LAI and FCOVER amplitudes and 50% for FAPAR and NDVI. Phenological metrics derived from V2 time series improved over V1 for all variables (compare V1 and V2 statistics in Table 2.3).

Table 2.3: Statistics of comparisons between the derived phenologies from LAI, FCOVER, FAPAR V1 and V2 and NDVI V2.1 time series and PEP725 ground measurements (*Betula pendula*) for the start of the season (SoS) and end of the season (EoS). The SPIRITS percentile method was used to extract the phenology with specific thresholds per vegetation variable and phenological metric. *mark indicates significant correlations with p<0.05 (** indicates p<0.001).

Metric	Index	Version	Definition	RMSE (d)	BIAS (d)	Abs. BIAS (d)	*R*	Slope
SoS	LAI	V1	30%	16.44	-1.38	17.39	0.49**	0.67
(n=359)		**V2**	**30%**	**12.49**	**1.65**	**10.22**	**0.62****	**0.78**
	FCOVER	V1	40%	17.25	-4.44	23.54	0.52**	0.74
		V2	40%	13.95	-4.46	11.21	0.54**	0.95
	FAPAR	V1	50%	31.40	-18.35	31.23	0.48**	0.85
		V2	50%	23.01	-14.26	13.94	0.57**	0.88
	NDVI	V2.1	50%	20.70	-13.18	15.38	0.25	0.82
EoS	LAI	V1	40%	34.28	12.01	28.96	-0.15	-0.19
(n=359)		V2	40%	32.72	-6.18	21.12	0.05	0.11
	FCOVER	V1	40%	30.69	-14.33	42.25	-0.13	-0.20
		V2	**40%**	**25.35**	**6.42**	**20.34**	**0.26**	**0.38**
	FAPAR	V1	50%	44.06	18.75	45.87	-0.23	-0.65
		V2	50%	39.99	18.61	37.97	-0.04	-0.51
	NDVI	V2.1	50%	48.35	14.75	34.58	0.02	-0.25

The best performances for SoS were obtained using the LAI and FCOVER V2 time series (Figure 2.4a), with RMSEs of ~12 and 14 d, respectively (Table 2.3). In contrast, RMSEs were ~21 and 23 d for NDVI V2.1 and FAPAR V2, respectively (Table 2.3), and contained many outliers (Figure 2.4a). SoS was slightly underestimated for all cases, except when using LAI (Figure 2.4a). EoS had a higher RMSE (25-48 d) and a lower *R* (<0.3) (Table 2.3). The estimates of EoS from the LAI and FCOVER V2 time series also agreed best with ground data although no significant correlations were found (Table 2.3, Figure 2.4b).

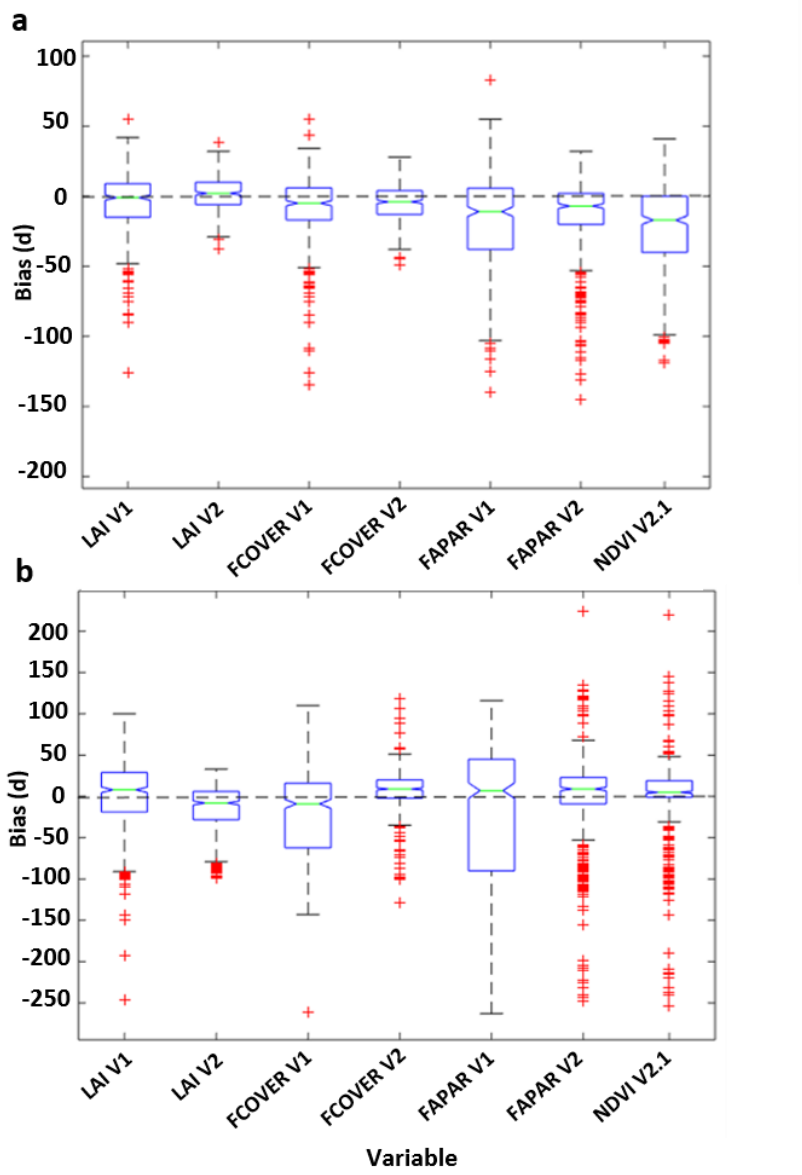

Figure 2.4: Boxplots of the bias errors for (a) SoS and (b) EoS estimated from the LAI, FCOVER, FAPAR V1 and V2 and NDVI V2.1 time series minus the PEP725 ground measurements. An elongated boxplot indicates a greater dispersion of the average bias.

2.3.3. Sensitivity analysis of the method to extract phenological metrics

The 30th percentile and SPIRITS applied to LAI V2 provided the best performances among the different analyzed methods when compared both with USA-NPN and Europe-PEP725 measurements of the SoS (Figure 2.5, Table 2.4). The results for the 30th percentile and SPIRITS were similar because both methods use the same definition of SoS based on the 30% threshold of annual amplitude but the 30th percentile method slightly improved SPIRITS in terms of precision (c.f. Figure 2.6a-6b, 2.7a-7b) and accuracy (RMSE of 9 vs 14 d for USA-NPN "leaves", 9 vs 10 d for USA-NPN "increasing leaf size" and 11 vs 12 d for PEP725 "first visible leaves" (Table 2.4)) because of the daily interpolation applied to the input 10 d data. The logistic function also performed well (RMSE from 13 to 18 d) but provided slightly advanced SoS as compared to ground measurements (bias from -5 to -9 d). The derivative method provided showed higher RMSE (up to 28 d) and positive bias (up to 19 d). The moving-average method performance the worst (RMSE from 30 to 59 d) and systematically advanced the timing of SoS as compared to ground measurements (bias from -24 to -51d).

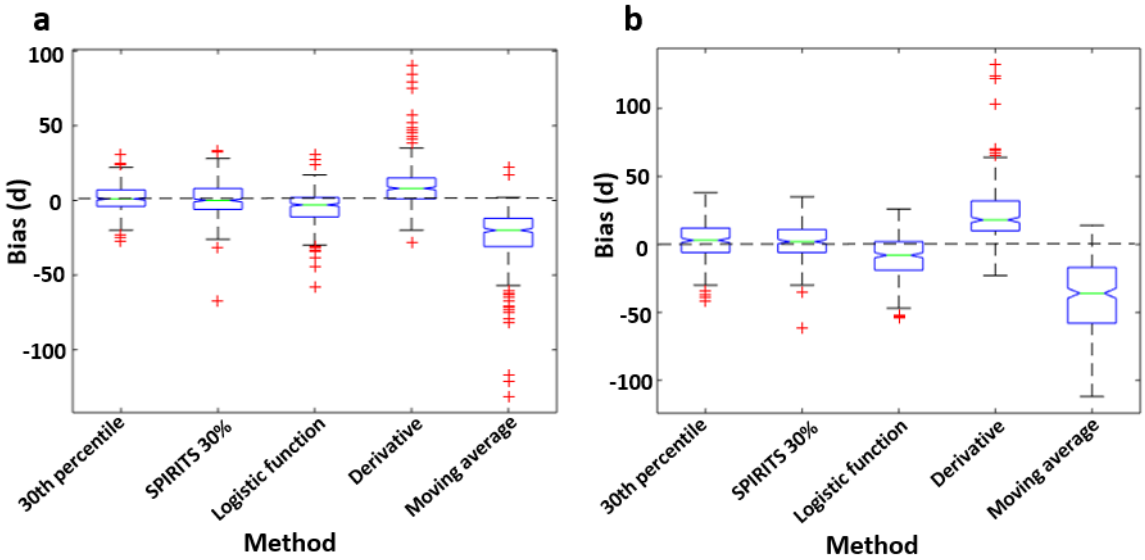

Figure 2.5**:** Boxplots of the bias error for the SoS estimated from LAI V2 minus the ground measurements at the USA-NPN (a) and PEP725 (b) sites. An elongated boxplot indicates a greater dispersion of the average bias in each method.

Table 2.4: Statistics of comparisons between LAI V2 derived phenology for the start of the season (SoS) and end of the season (EoS), and the ground measurements for the various methods (percentiles, logistic function, derivative and moving average). *mark indicates significant correlations with p<0.05 (** indicates p<0.001).

Validation source	Metric	Method	RMSE (d)	Bias (d)	Abs. Bias (d)	*R*	Slope
USA-NPN	SoS	**30th percentile**	**9.19**	**1.59**	**6.77**	**0.81****	**0.73**
(n=462)	"Leaves"	SPIRITS 30%	13.75	0.58	7.05	0.60**	0.58
		Logistic	14.14	-5.25	8.66	0.63**	0.60
		Derivative	16.82	9.63	12.01	0.68**	0.82
		Moving average	30.06	-24.33	23.95	0.59*	0.82
USA-NPN	SoS	**30th percentile**	**8.87**	**-2.20**	**6.11**	**0.83****	**0.67**
(n=158)	"Increaising	SPIRITS 30%	10.40	-3.46	6.18	0.78**	0.67
	leaf size"	Logistic	12.81	-7.24	6.86	0.74**	0.63
		Derivative	10.04	4.22	7.73	0.83**	0.84
		Moving average	34.49	-28.07	27.86	0.49*	0.70
PEP725	SoS	**30th percentile**	**11.50**	**1.69**	**9.84**	**0.60****	**0.90**
(n=359)	"visible	SPIRITS 30%	12.49	1.65	10.22	0.62**	0.78
	leaves"	Logistic	17.96	-9.22	14.21	0.53*	0.71
		Derivative	28.31	19.19	20.42	0.49*	0.88
		Moving average	56.24	-51.35	54.27	0.50*	1.14
USA-NPN	EoS	**40th percentile**	**25.61**	**6.39**	**17.60**	**0.14**	**0.10**
(n=241)	"Colored	SPIRITS 40%	30.79	-3.69	20.17	0.06	0.07
	leaves"	Logistic	30.70	21.80	23.66	0.10	0.15
		Derivative	40.40	-10.11	26.70	0.02	0.01
		Moving average	58.75	50.35	44.26	0.13	0.01
PEP725	EoS	**40th percentile**	**27.69**	**-5.15**	**18.89**	**0.11**	**0.15**
(n=359)	"Colored	SPIRITS 40%	32.72	-6.18	21.12	0.05	0.11
	leaves"	Logistic	30.15	11.91	24.29	0.03	0.28
		Derivative	64.93	-43.96	48.49	0.00	-0.11
		Moving average	54.95	37.81	52.55	0.01	0.21

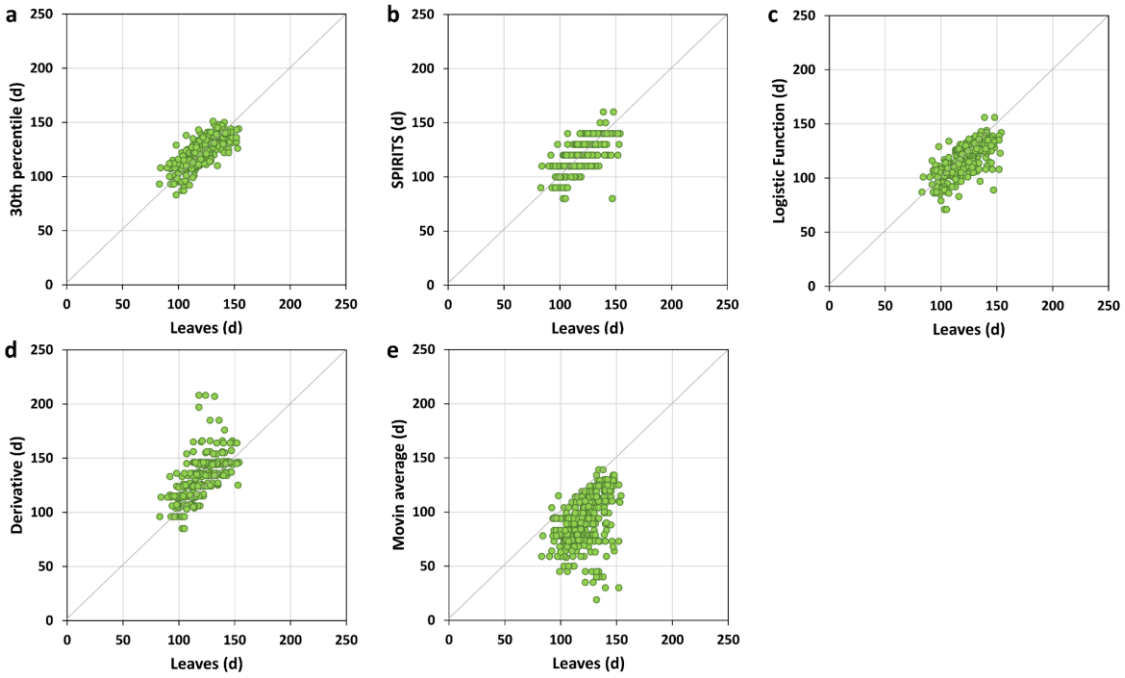

Figure 2.6: Scatterplots between the SoS predicted from LAI V2 by the percentile method (a), SPIRITS (b), logistic function (c), derivative (d) and moving average (e) compared with the ground phenology (USA-NPN "leaves"). Values are given in DoY. Statistics of the comparison are indicated in Table 2.4.

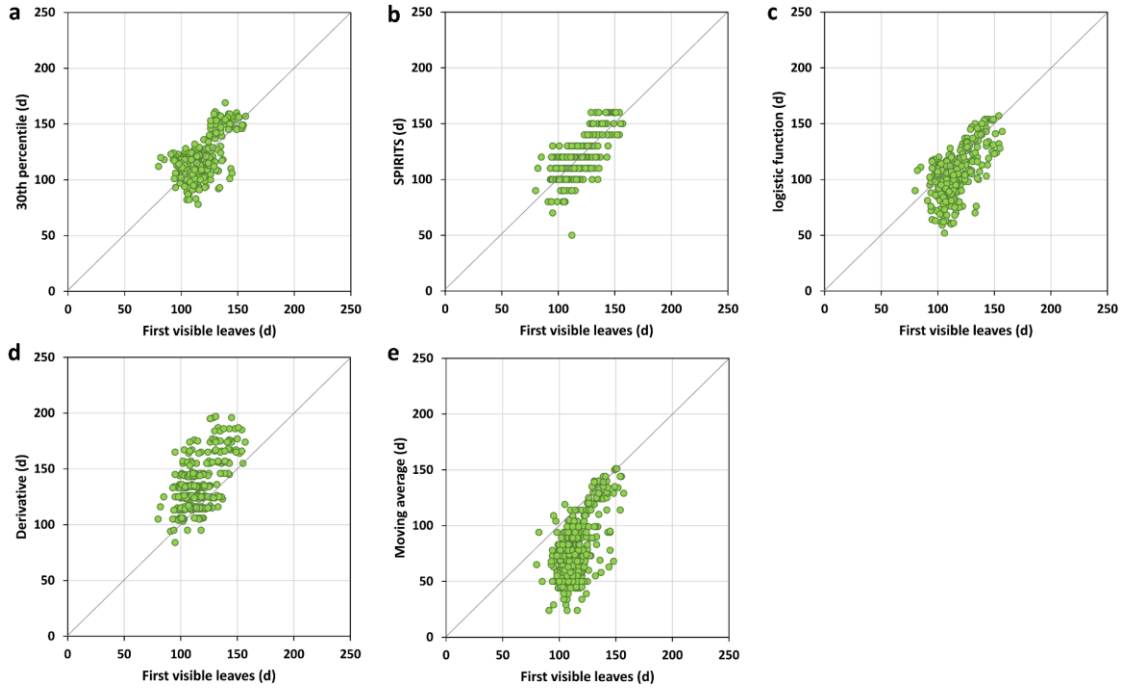

Figure 2.7: Scatterplots between SoS predicted from LAI V2 by the percentile (a), SPIRITS (b), logistic function (c), derivative (d) and moving average (e) methods and ground phenology (PEP725 "first visible leaves"). Values are given in DoY. Statistics of the comparison are indicated in Table 2.4.

The different methods provided poorer performances for the EoS (Table 2.4, Figure 2.8). The best agreement with ground measurements was found for the 40th percentile method (RMSE of 25 d for USA-NPN and 28 d for PEP725 "colored leaves" measurements). The logistic function provided similar performances in terms of RMSE but slightly overestimated ground measurements (bias from 12 to 22 d). The derivative method showed higher scattering (RMSE from 40 to 65 d) and lower correlation than other methods (Table 2.4, Figure 2.9 and Figure 2.10). The moving average retrievals showed a positive delay as compared to ground data (bias of 38 d for PEP725 and 50 d for USA-NPN).

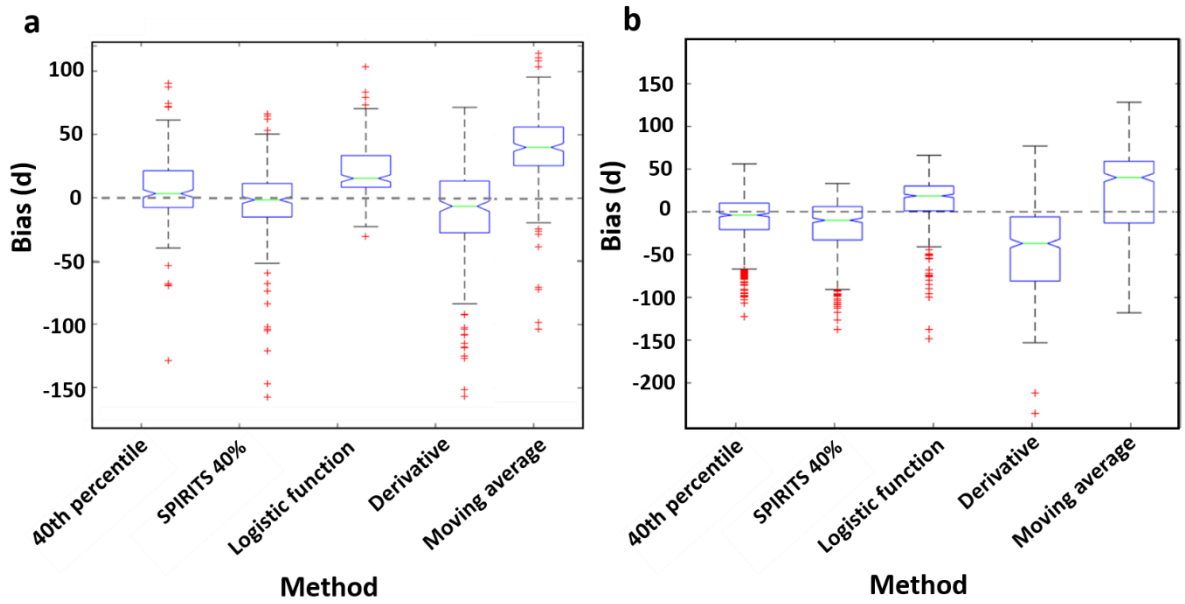

Figure 2.8: Boxplots of the bias error for the EoS estimated from LAI V2 minus the ground measurements at the USA-NPN (a) and PEP725 (b) sites. An elongated boxplot indicates a greater dispersion of the average bias in each method.

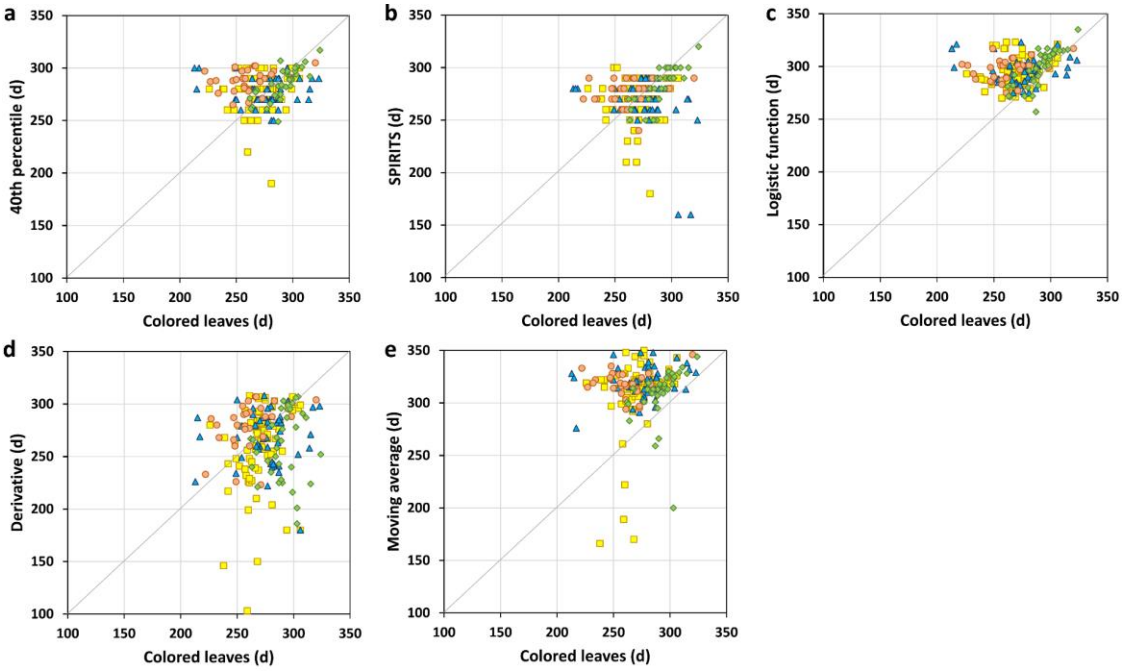

Figure 2.9: Scatterplots between the EoS predicted from LAI V2 by the percentile (a), SPIRITS (b), logistic function (c), derivative (d) and moving average (e) methods and ground phenology (USA-NPN "colored leaves") for *Acer rubrum* (green), *Betula alleghaniensis* (orange), *Fagus grandifolia* (blue) and *Quercus rubra* (yellow). Values are given in DoY. Statistics of the comparison are indicated in Table 2.4.

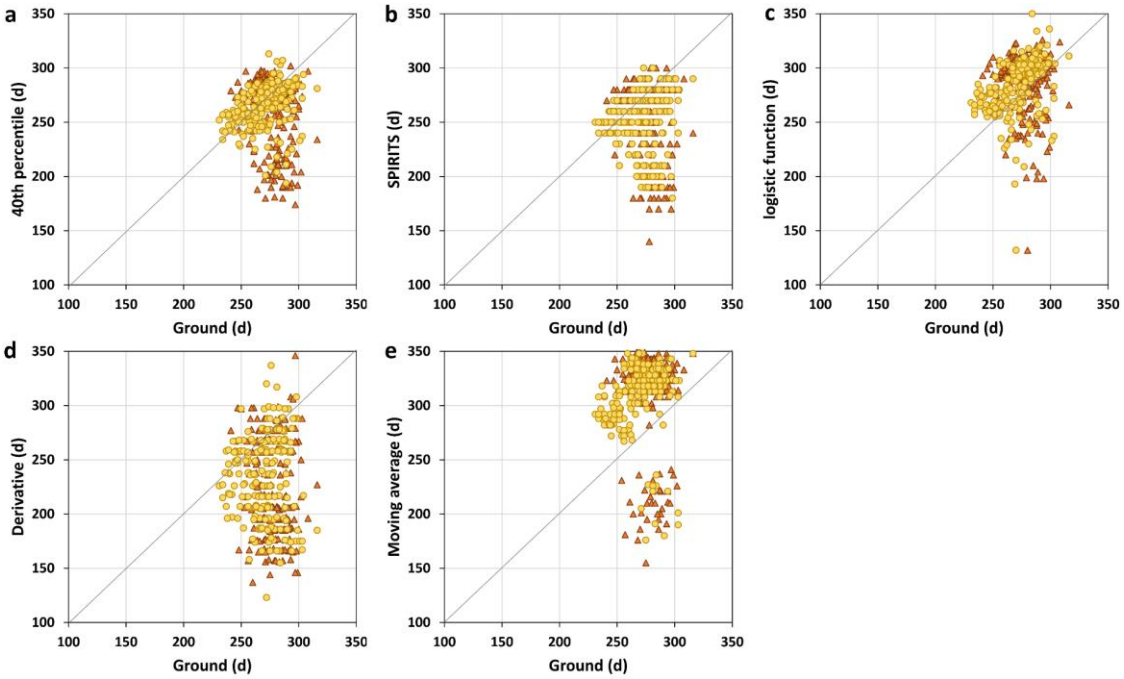

Figure 2.10: Scatterplots between the EoS predicted from LAI V2 by the percentile (a), SPIRITS (b), logistic function (c), derivative (d) and moving average (e) methods and ground phenology (PEP725 "colored leaves"). Brown for heterogeneous sites (forest cover <50%) and yellow for homogeneous sites (forest cover >50%). Values are given in DoY. Statistics of the comparison are indicated in Table 2.4.

2.3.4. Spatial patterns of land surface phenology

Figure 2.11 shows the average timing of SoS, EoS and LoS phenophases at the global scale by using the percentile method (30th and 40th percentiles for SoS and EoS, respectively) and time series of V2 LAI (1999-2017). The LoS is estimated as the length of time between the SoS and the EoS. The derived maps show consistent spatial patterns of the seasonality of vegetation at the global scale which is driven by the distribution of latitudinal climatic patterns, type of vegetation and topographic elements, among other factors (Verger et al., 2015; Zhang et al., 2004). The timing of SoS (Figure 2.11a) and EoS (Figure 2.11b) reflected a broad variation in the range of values and their spatial pattern at the middle and high latitudes of the Northern Hemisphere strongly depend on the thermal and photoperiod latitudinal gradient (Verger et al., 2016).

The LoS (Figure 2.11c) in some ecoclimatic and biogeographic regions of transition such as Sahel shows a broad range of variation from 10 to 200 d following the positive north-south gradient of rainfall (Verger et al., 2016). On the contrary, in northern latitudes >50º the LoS showed a limited range of variation from 10 to 60 d with shorter days at higher latitudes following the latitudinal gradient of temperature and radiation (Verger et al., 2016).

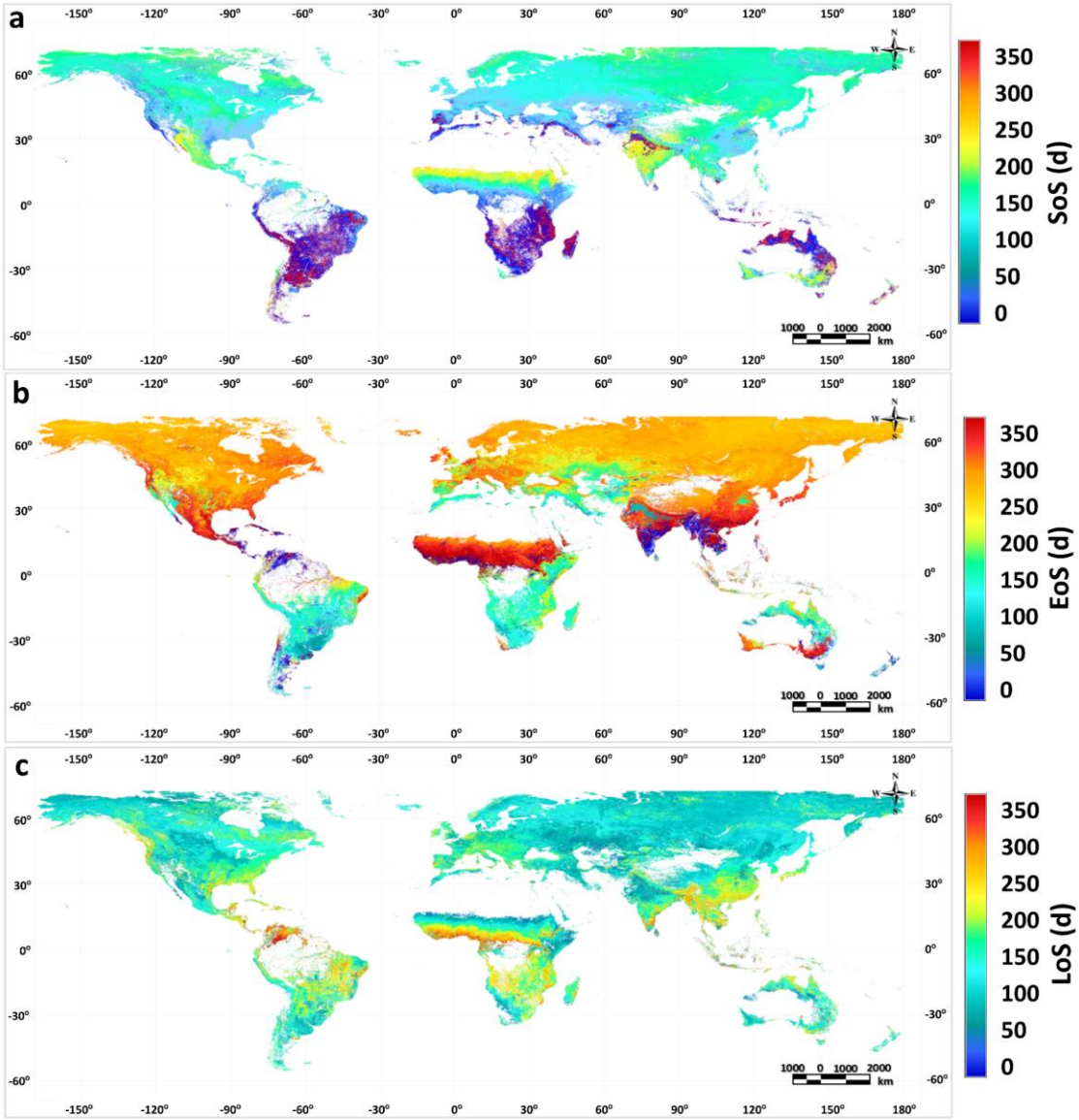

Figure 2.11: Global Map of average SoS (a), EoS (b) and LoS (c) derived from the LAI V2 time series (1999-2017) and the threshold-based method. The continental areas in white are deserts and evergreen forests with limited seasonality where phenology was not computed.

2.4. Discussion and conclusions

Land surface phenology (LSP) provides a synoptic view of vegetation dynamics and it can substantially improve our macroecological knowledge and the representation of phenology in earth-system models. Unlike previous studies limited to NDVI, we used three additional biophysical variables: LAI, FAPAR and FCOVER generated within CGLS from SPOT-VEGETATION (1999-2013) and PROBA-V (2014-2017) satellite imagery. We found that the phenology derived from LAI (or FCOVER) was more closely related to actual ground observation than the NDVI-derived phenology (Table

2.3). LAI-phenology is based on leaf development rather than on proxies provided by vegetation indices which are not driven solely by the amount of leaves but also by the canopy structure and the leaf biochemical properties (Richardson et al., 2009). LAI is more sensitive than vegetation indices such as NDVI to larger amounts of vegetation (Myneni and Williams, 1994). In addition, NDVI V2.1 is affected by variations in solar zenith and viewing angles and surface reflectance bidirectional effects (Tote et al., 2017).

In addition to the vegetation variable, the derived phenology was found to be highly sensitive to the retrieval algorithm and processing chain. We found that the retrieved phenology performed the best using LAI V2 (Table 2.3) due to the improved continuity (no missing data in V2) and smoothness as compared to V1. In V1 products and in NDVI time-series, the noise primarily due to cloud contamination and atmospheric effects is an important shortcoming in the study of land surface phenology. To overcome this limitation, smoothing methods were applied in SPIRITS approach as a pre-processing step to phenological retrieval. The choice of the smoothing method introduced differences of up to 50% in the performance of the phenology derived from LAI V1 (Table 2.2). These conclusions agree with previous literature studies highlighting the importance of the temporal reconstruction methods (Kandasamy et al., 2013; Verger et al., 2013). However, the phenology derived from original LAI V2 (smoothing and gap filling was already included in the retrieval algorithm) outperforms the phenology derived from the seasonal trajectories derived after smoothing LAI V1 (Table 2.3).

We tested four state of the art methods to extract phenological metrics: thresholds, logistic function, derivative and moving average. Each method has its own strengths and limitations (de Beurs and Henebry, 2010). The threshold approach based on a percentage of the annual amplitude is simple and robust but it is sensitive to the minimum and maximum values that may be affected by noise in the signal. The logistic function approach has been widely used (e.g. Zhang et al., 2003) but it is limited to the performance of the model fitting (Beck et al., 2006) and it may fail when the curvature function is too flat to determine the phenophases (de Beurs and Henebry, 2010). The derivative approach based on the maximum increase and decrease of the vegetation variable is very sensitive to the noise in the signal and the temporal smoothing and composition approach and it cannot represent short growing seasons well, especially

when the increase and decrease in the annual time series occur rapidly and abruptly (Beck et al., 2006). The moving average approach is based on the assumption that vegetation growth follows a well-defined temporal profile and it may fail in cases of disturbances and abrupt changes. Further, the selection of the time lag is arbitrary.

We found that the choice of the extraction method introduced differences >150% and > 85% in the performance of the SoS and EoS, respectively, derived from LAI V2 when compared to ground observations (PEP725 and USA-NPN) (Table 2.4). The percentile method agreed the best with ground measurements. The validation over ground observations indicated that the 30% threshold of the LAI amplitude was optimal for detecting SoS but that a 40% threshold was more suitable for detecting EoS in agreement with Verger et al. (2016). The accuracy for SoS using ground observations produced overall RMSEs of 9 and 11 d for the date of increasing leaf size and leaf unfolding, respectively, for the forests in Europe and the USA. The biases were <2 d (~10 d of standard deviation). We found poorer performances for EoS, than SoS, with higher RMSE of 25 d (28 d) and a bias of 8 d (-6 d) in USA (Europe). The lower performances for the EoS as compared to the SoS is associated to higher uncertainties of both satellite (atmospheric effects, snow and poor illumination conditions) (Delbart et al., 2005) and ground (the timing of leaf colouring is more subjective and difficult to identify than spring phenophases like leaf unfolding) (Estrella and Menzel, 2006) phenology for autumn. Richardson et al. (2009) also reported higher variabilities across the canopy of the timing and rate of foliar development in autumn than spring.

The validation of land surface phenology with ground observations presented some difficulties, such as the spatial distribution and the spatial representability of the data. The ground measurements represent the phenology for a limited number of individual plants that are not necessarily the most representative species of the 1-km satellite pixels. Conversely, satellite phenology at 1-km resolution represented an integrated response across landscapes with diverse species and phenological behaviors. The phenology of each species and their characteristics (sizes, ages, homogeneity), though, influenced the satellite signal, depending on its abundance within the pixel sampling area and on the timing of their phenophases (Delbart et al., 2015). Statistics of the comparison between LAI V2 derived EoS using the percentile method and ground measurements improved significantly when the analysis is restricted to *Acer rubrum* in USA-NPN (RMSE of 10

d, bias of -6 d and significant correlation ($p<0.001$) of 0.8 (c.f. Table 2.4)) and to homogeneous sites (forest cover>50% based on GEE high resolution imagery) in PEP725 (RMSE of 22 d, bias of 6 d and significant correlation ($p<0.05$) of 0.4 (c.f. Table 2.4)).

The differences in the definition of the ground phenophases and satellite metrics hamper the comparison. The logistic function and, specially, the moving-average approaches systematically advanced the SoS as compared to ground measurements since these methods determine the SoS as the timing when the vegetation variable starts to increase (Table 2.4). On the contrary, the derivative approach based on the most rapid increase of the signal introduces positive delays in the SoS. The opposite trend is observed for the EoS (Table 2.4): the logistic function and moving-average show a delay in the detection of the EoS while the derivatives advances the timing of EoS. On the other hand, ground measurements are subjective and some ambiguity exists in the definition of phenophases. In this sense, we found positive bias of 2 d for the SoS retrieved with the 30th percentile of LAI amplitude when comparing with USA-NPN "leaves" phenophase but negative bias of -2 d when comparing to "increasing leaf size". Further studies will focus on the comparison of the retrieved land surface phenology with continuous ground observations from PhenoCam (Zhang et al., 2018). This should ultimately lead to propose a standardization in the definition of phenological metrics.

This research is expected to contribute for the development of a dedicated algorithm for the operational retrieval of land surface phenology within CGLS. Validation using ground observations was limited to deciduous broadleaf forests. Further studies should extend the analysis to other vegetation types. The methods may need to be adapted to handle multiple and irregularly occurring vegetation growing cycles. Finally, forecasting approaches need to be developed for near-real time land surface phenology retrieval.

3

Evaluation of VEGETATION and PROBA-V phenology using PhenoCam and eddy covariance data

Kevin Bórnez, Andrew D. Richardson, Aleixandre Verger, Adrià Descals, Josep Peñuelas

Published in *Remote Sens* (2020), Vol. 12 (18), 3077. https://doi.org/10.3390/rs12183077

Scan this code to download the published version

Abstract

High-quality retrieval of land surface phenology (LSP) is increasingly important for understanding the effects of climate change on ecosystem function and biosphere–atmosphere interactions. We analyzed four state-of-the-art phenology methods: threshold, logistic-function, moving-average and first derivative based approaches, and retrieved LSP in the North Hemisphere for the period 1999–2017 from Copernicus Global Land Service (CGLS) SPOT-VEGETATION and PROBA-V leaf area index (LAI) 1km V2.0 time series. We validated the LSP estimates with near-surface PhenoCam and eddy covariance FLUXNET data over 80 sites of deciduous forests. Results showed a strong correlation ($R^2 > 0.7$) between the satellite LSP and ground-based observations from both PhenoCam and FLUXNET for the timing of the start (SoS) and $R^2 > 0.5$ for the end of season (EoS). The threshold-based method performed the best with a root mean square error of ~9 d with PhenoCam and ~7 d with FLUXNET for the timing of SoS (30th percentile of the annual amplitude), and ~12 d and ~10 d, respectively, for the timing of EoS (40th percentile).

3.1. Introduction

The study of vegetation phenology and its patterns on a global scale have become more important since the late twentieth century for analyzing the effects of climate change (Chimielewski and Rotzae, 2001; Peñuelas and Filella, 2001). Remote sensing is a useful tool for characterizing land surface phenology (LSP) (Baumann et al., 2017) and global changes of vegetation (Wu and Chen, 2013; White et al., 2014; Zhang et al., 2018). De Beurs and Henebry (2010) analyzed a broad range of statistical methods designed to extract phenological metrics from satellite time series based on threshold percentiles (Atzberger et al., 2013; Reed et al., 2003; Verger et al., 2016), moving averages (Reed et al., 1994), first derivatives (Tateishi and Ebata, 2004; White et al., 2009), smoothing functions (Piao et al., 2006) and fitted models (de Beurs and Henebry, 2005).

Most literature on LSP has focused on the use of time series of vegetation indices mainly derived from MODIS data (Ganguly et al., 2010; Zhang et al., 2006; Zhang et al., 2018). In previous studies, we showed the added value of using Copernicus Global Land Service (CGLS) leaf area index (LAI) time series derived from VEGETATION and PROBA-V data (Bórnez et al., 2020a; Verger et al., 2016). Bórnez et al. (2020a) found that the phenological metrics extracted from the CGLS LAI Version 2 (V2) time series agreed best with the available human-based ground observations of phenological transition dates for deciduous broadleaf forest in Europe (PEP727) and United States of America (USA-NPN) as compared to other biophysical variables and NDVI vegetation index or previous version V1 of the CGLS products.

Validating LSP is challenging due, in part, to the differences in the definition of satellite metrics and ground phenophases (Schwartz and Hanes, 2009; White et al., 2009). Volunteer observers have traditionally collected data for the timing of specific phenophases of individual plants Menzel (2002). Human observations of phenology, however, are not uniform and may induce uncertainties, despite efforts to establish protocols for monitoring phenophases (Denny et al., 2014; Templ et al., 2018; Tierney et al., 2013).

Near-surface remote sensing using conventional red-green-blue (RGB) digital cameras provides an alternative to human observations to monitor vegetation phenology (Hufkens et al., 2018; Jacobs et al., 2009; Keenan et al., 2014; Richardson et al., 2007,

2009) because of their low cost, ease of set up and capacity to collect detailed spectral information at high temporal frequencies (Hufkens et al., 2012) of individual plants, species or canopies (Bater et al., 2011) across broad spatial scales (Brown et al., 2016; Laskin and McDermid, 2016; Morisette et al., 2009). PhenoCam (https://daac.ornl.gov/VEGETATION/guides/PhenoCam_V1.html) is a network of digital cameras that currently includes >600 site-years of imagery, with high-quality and high temporal resolution providing data of vegetation phenology. Deciduous broadleaved forests (68 sites) are the dominant vegetation type within the PhenoCam Network (Richardson et al., 2018), and the focus of this study. A growing number of studies have compared transition dates derived from the PhenoCam time series of green chromatic coordinates (GCC) with satellite phenological metrics derived mainly from MODIS data (Hufkens et al., 2012; Klosterman et al., 2014; Melaas et al., 2016; Richardson et al., 2018).

Continuous flux measurements from eddy covariance technique also started to be used as a new perspective for estimating LSP at the landscape level (Ahrends et al., 2009; Gonsamo et al., 2012, 2013; Noormets et al., 2009; Richardson et al., 2010; Wu and Chen, 2013). The flux measurements sites are organized as a confederation of regional networks around the world, called FLUXNET. Until the last updated of February 2020, the most recent dataset produces was the FLUXNET2015 dataset (https://fluxnet.org/data/fluxnet2015-dataset/) which includes data from 212 sites (Joiner et al., 2018).

In this study, we build on our previous work (Bórnez et al., 2020a) and take advantage now of PhenoCam and FLUXNET capability of continuous monitoring of vegetation seasonal growth at very high temporal resolution, with data every 30 minutes (Hollinger and Richardson, 2005, 2009; Xiao et al., 2005, 2009; Yan et al., 2019). This allows a more robust and accurate comparison with LSP derived from satellite time series avoiding problems related to the differences in the definition of phenology metrics. We evaluated four methods for estimating phenology: the threshold method based on percentiles (Verger et al., 2016), the derivative method (Tateishi and Ebata, 2004), the autoregressive moving-average method (Reed et al., 1994) and the logistic-function method (Zhang et al., 2003). These methods were applied both to satellite CGLS LAI

V2 time series and ground observations from PhenoCam GCC and eddy covariance flux towers over deciduous forests to assess the accuracy of LSP retrievals.

3.2. Materials and Methods

3.2.1. Study area

The study was conducted over the North Hemisphere in pixels classified as deciduous forests or mixed vegetation according to the annual C3S Global Land Cover for the year 2018 (http://maps.elie.ucl.ac.be/CCI/viewer/download.php). The validation was done over PhenoCam sites distributed across North America and one in Europe, and FLUXNET towers sites both in North America and Europe and one in Japan. We selected only deciduous forests sites with at least 2 years of available observations. This resulted in 64 sites from PhenoCam, and 16 towers of FLUXNET covering a broad range of latitudes (30–60°N) and elevations (1-1870 m a.s.l.) (Figure 3.1 and Table A1).

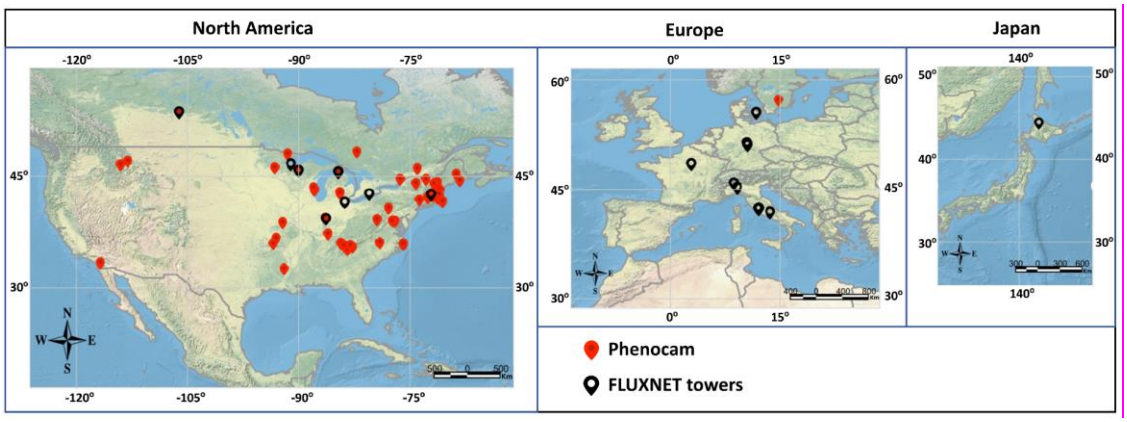

Figure 3.1**:** Locations of the selected PhenoCam sites (red) and FLUXNET towers (black) over deciduous forests.

3.2.2. Satellite Data: CGLS LAI

We used Copernicus land surface products (CGLS LAI V2) derived from SPOT-VEGETATION (1999–2013) and PROBA-V (2014-2017) data. The spatial resolution is 1 km and the temporal frequency is 10 d (https://land.copernicus.eu/global/themes/vegetation).

The algorithm for LAI V2 product (Verger et al., 2014, 2019) capitalizes on the development and validation of already existing products (CYCLOPES version 3.1 and MODIS collection 5 products) and the use of neural networks (Verger et al., 2008). The

inputs of the neural networks are daily top of the canopy reflectances from VEGETATION and PROBA-V in the red, near-infrared and shortwave infrared spectral bands and the sun and view geometry. A multi-step procedure for filtering, temporal smoothing, gap-filling and compositing is then applied to the daily estimates to generate the final 10 d products (Verger et al., 2014).

3.2.3. PhenoCam Data

We used PhenoCam Dataset V1.0 (https://daac.ornl.gov/VEGETATION/guides/PhenoCam_V1.html; Richardson et al., 2017). It provides digital images every 30 min. In each image, a "region of interest" was defined manually based on the dominant vegetation type in the camera field of view (Richardson et al., 2018) (Figure 3.2). The size of the ROI typically ranges from ~50 to ~500 m^2 (Richardson et al., 2018). The green chromatic coordinate (GCC) index (Richardson et al., 2018) was calculated from the red (R), green (G) and blue (B) digital numbers (DN) as:

$$G_{CC} = \frac{G_{DN}}{R_{DN}+G_{DN}+B_{DN}} \quad (1)$$

We used the 90th percentile G_{CC} value and 1 d high quality composites to avoid noise from variations in meteorological, atmospheric or illumination conditions (Sonnentag et al., 2012). We manually filtered the poor-quality G_{CC} observations and then gap-filled the missing data with a locally weighted scatter-plot smoother (lowess)-based filter (Richardson et al., 2018).

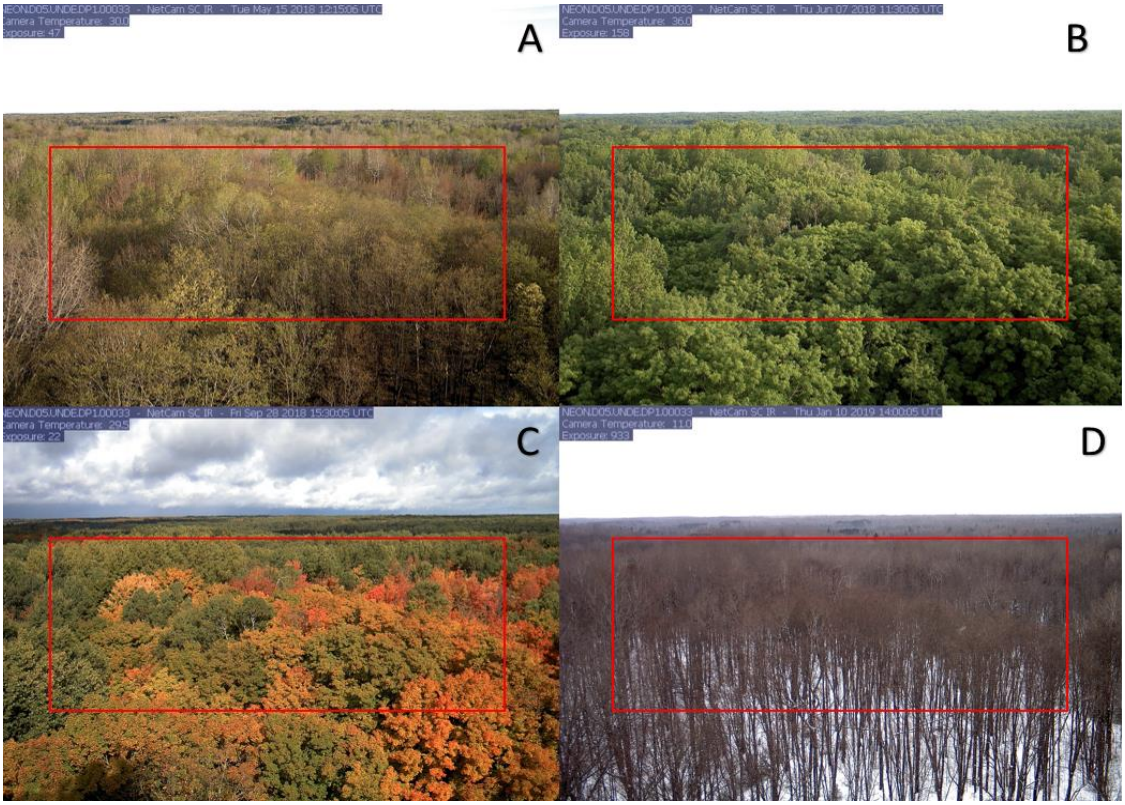

Figure 3.2: PhenoCam images captured in (a) spring, (b) summer, (c) autumn and (d) winter over the NEON.D05.UNDE.DP1.00033 site (46.23°N, 89.54°W). The red rectangle indicates the borders of the selected region of interest.

3.2.4. FLUXNET data

We used FLUXNET 2015 collection of gross primary production (GPP) flux data over 16 forest tower sites (Figure 3.1) for the period 2003–2014 (110 site-years) (https://fluxnet.org/data/fluxnet2015-dataset/). We used the daily GPP (g C m-2 d-1) derived from half-hourly eddy covariance flux measurements using the night time based approach (Reichstein et al., 2005; Vuichard and Papale, 2015). We smoothed the series of the daily GPP by using a Savitzky–Golay filter based on a second degree polynomial and a 30-day smoothing window (Chen et al., 2004; Savitzky and Golay, 1964; Wu et al., 2017).

3.2.5. Methods for Estimating Vegetation Phenology

We tested four methods for estimating phenology (Table 3.1 and Figure 3.3, (Bórnez et al., 2020a) from satellite (CGLS LAI time series) and ground-based data (PhenoCam GCC, FLUXNEX GPP) (e.g., Figure A2). The phenological metrics are the timing of the start of the growing season (SoS), the end of the growing season (EoS) and the length

of the growing season (LoS). LoS was estimated as the length of time between the EoS and the SoS. The CGLS LAI 10 d time series were linearly interpolated at daily steps before phenological retrieval.

Table 3.1: Description of the evaluated methods for the extraction of phenology metrics.

Method.	Reference	Principles and parameters
Threshold based on percentiles	Verger et al., 2010	SoS is defined as the first day of the year (DoY) when the vegetation variable exceeds a particular threshold. EoS is defined as the DoY when an index descends below a threshold. We established dynamic thresholds per pixel based on a percentile (10th, 25th, 30th, 40th and 50th) of the annual amplitude
Logistic function	Zhang et al., 2003	SoS is defined as the DoY with the first local maximum rate of change in the curvature of a logistic function fitted to the time series. EoS is defined as the DoY with the first local minimum rate of change in the curvature
First derivative	Tateishi and Ebata, 2004	SoS is defined as the DoY of the maximum increase (maximum first derivative) in the curve. EoS is defined as the DoY of the maximum decrease in the curve
Autoregressive moving average	Reed et al., 1994	A moving average is first computed at a given time lag (we tested 10–50 d and selected a 30 d time lag). SoS and EoS are then defined as the DoY when the moving-average curves cross the original time series of the vegetation index

3.2.6. Validation Approach

The LSP derived from VEGETATION and PROBA-V LAI V2 time series was compared with the LSP estimates using ground data from PhenoCam and FLUXNET when the same phenological extraction method was applied (Section 3.1). The statistical metrics used for assessing the performance are the root mean square error (RMSE), the mean error (bias); the coefficient of determination (R^2), slope and intercept of the Reduced Major Axis regression (RMA). Further the spatial patterns and latitudinal gradients of LSP estimates were assessed in Section 3.2. We used RStudio for the statistical analysis, Google Earth Engine (GEE, https://earthengine.google.org) for the retrieval of LSP over the North Hemisphere, and ESRI ArcGIS 10.5 and gvSIG-desktop-2.3.1 for the graphs and maps.

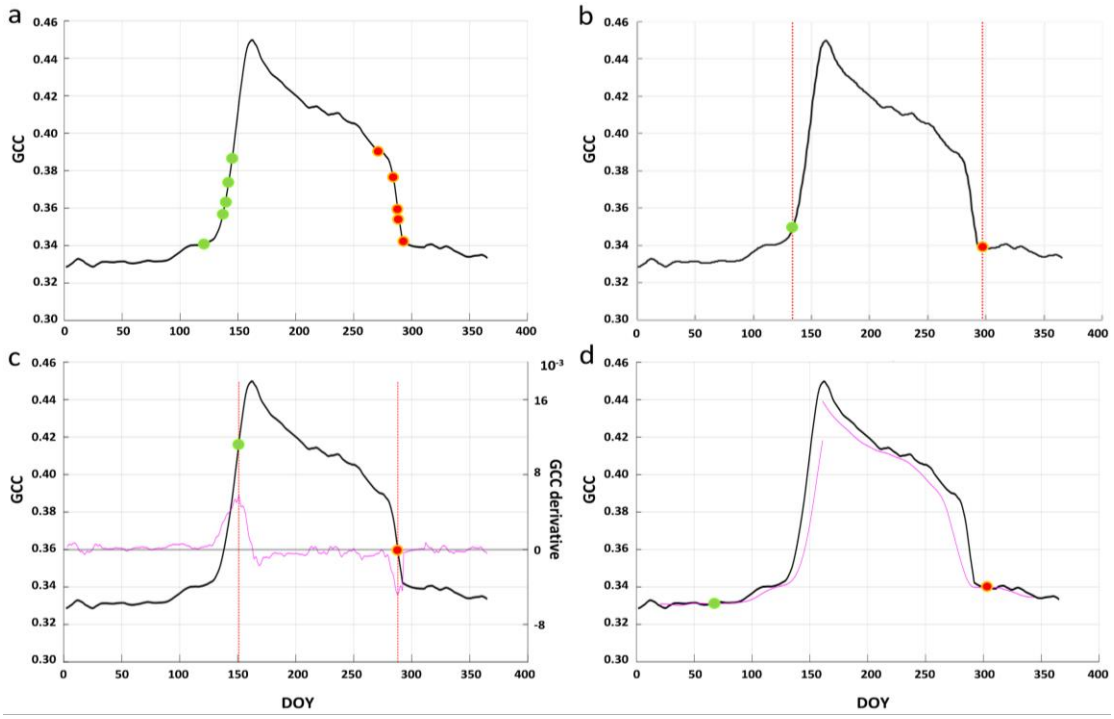

Figure 3.3: Illustration of the threshold (a), logistic-function (b), derivative (c) and moving-average (d) phenological extraction methods applied to PhenoCam G_{CC} time series of Acadia site (44.37ºN, 68.26ºW) for 2014. The green and red points correspond to SoS and EoS, respectively. The different points in panel *a* correspond to the percentiles 10th, 25th, 30th, 40th and 50th. The purple line corresponds to the first derivative in *c*, and to the moving average in *d*.

3.3. Results

3.3.1. Comparison of Satellite and Ground Phenologies

The coefficient of determination, R^2, between the satellite- and ground-based estimates from PhenoCam and FLUXNET phenology ranges from 0.01 to 0.81 ($p < 0.001$) (Table 3.2). The threshold-based method provided the best performances. The 30th percentile of annual amplitude was the best threshold for the SoS (RMSE <9 d, bias <2 d and R^2 = 0.74 with $p < 0.001$ for CGLS LAI V2 estimates compared to PhenoCam; and RMSE <7 d, bias <4 d and R^2 = 0.81 with $p < 0.001$ when compared to FLUXNET) and the 40th percentile for the EoS (RMSE = 12 d, bias <1 d and R^2 = 0.51 with $p < 0.001$ compared to PhenoCam; RMSE < 10 d, bias < 5 d and R^2 = 0.53 with $p < 0.001$ compared to FLUXNET).

Table 3.2: Statistics of the comparison between the SOS and EOS dates retrieved using the LAI, GCC, and GPP estimates for the four methods: thresholds, logistic function, derivative and moving average. * indicates significant correlations at $p < 0.05$; **, significant correlations at $p < 0.001$. The bold type highlights the best method. Evaluation over the 64 PhenoCam sites (356 samples (sites × years)) and 16 FLUXNET towers (110 samples (sites × years)) over deciduous forests in the North Hemisphere (Figure 3.1).

Metric	Validation	Method	RMSE	BIAS	R2	Slope	Intercept
SoS	PhenoCam	Threshold (10th percentile)	17.80	-0.53	0.29	1.07	-8.57
		Threshold (25th percentile)	9.92	1.29	0.61**	1.02	-2.11
		Threshold (30th percentile)	**8.82**	**1.96**	**0.74****	**1.01**	**0.7**
		Threshold (40th percentile)	9.05	2.61	0.67**	1.02	-0.39
		Threshold (50th percentile)	9.45	3.74	0.65**	1.00	2.98
		Logistic function	10.79	1.21	0.58**	0.99	1.18
		Derivative	19.27	2.40	0.18	0.93	11.12
		Moving average	15.49	0.48	0.42*	1.24	-30.9
SoS	FLUXNET	Threshold (10th percentile)	16.50	3.54	0.31	0.90	14.03
		Threshold (25th percentile)	7.91	-2.08	0.7**	1.00	-2.91
		Threshold (30th percentile)	**6.77**	**-3.56**	**0.81****	**1.03**	**-8.02**
		Threshold (40th percentile)	7.21	-3.91	0.80**	0.99	-3.24
		Threshold (50th percentile)	8.42	-5.65	0.77**	1.04	-11.8
		Logistic function	8.05	-0.42	0.69**	0.94	6.06
		Derivative	23.63	-14.31	0.19	0.61	41.66
		Moving average	16.09	1.99	0.37*	0.79	30.13
EoS	PhenoCam	Threshold (10th percentile)	15.33	5.59	0.33*	0.88	40.86
		Threshold (25th percentile)	12.90	2.27	0.45*	0.91	28.12
		Threshold (30th percentile)	13.49	1.36	0.39*	0.92	22.75
		Threshold (40th percentile)	**12.07**	**0.65**	**0.51****	**0.95**	**13.51**
		Threshold (50th percentile)	29.31	7.23	0.09	0.49	142.16
		Logistic function	17.64	-0.93	0.26	0.82	52.52
		Derivative	50.74	-1.50	0.03	0.33	179.59
		Moving average	27.40	2.15	0.01	1.46	-140.06
EoS	FLUXNET	Threshold (10th percentile)	10.84	6.25	0.5**	1.00	5.93
		Threshold (25th percentile)	9.80	5.29	0.55**	1.04	-5.93
		Threshold (30th percentile)	9.99	4.90	0.44*	1.06	-12.38
		Threshold (40th percentile)	**9.67**	**4.67**	**0.53****	**1.18**	**-46.54**
		Threshold (50th percentile)	17.39	9.88	0.18	0.76	71.9
		Logistic function	10.26	2.97	0.41*	1.10	-26.47
		Derivative	48.06	32.40	0.01	-0.09	289.18
		Moving average	31.50	-14.30	0.04	0.53	114.78

Figures 4 and 5 show the scatter plots of the comparison of satellite and ground-based SoS and EoS retrievals for the four methods. The points were very close to the 1:1 line using the percentile and logistic-function methods while the derivative and moving-average methods produced worse results with more widely dispersed points, especially for the timing of EoS.

The satellite SoS (Figure 3.4, Figure 3.5 and Figure A1) retrieved with threshold and logistic-function methods showed RMSE <11 d and bias <2 d compared to PhenoCam, and RMSE <8 d and bias <4 d with FLUXNET (Table 3.2). Higher discrepancies for the SoS were found with the derivative and moving-average methods: RMSE of 19 d and 15 d, and bias of 2 d and <1 d, respectively using PhenoCam estimates, and RMSE of 24 d and 16 d, and bias of –14 d and 2 d, respectively with FLUXNET estimates (Table 3.2).

The EoS can be also robustly estimated using remote sensing observations (Figure 3.4, Figure 3.5 and Figure A1) although we observed a degradation of performances for all the methods for the estimation of the EoS as compared to the SoS: higher dispersion of points, higher RMSE and lower correlation for EoS (Table 3.2). The EoS estimates from satellite time series of LAI agreed the best with GCC and GPP derived phenology metrics using the threshold method followed by the logistic function: RMSE of 12 d and 18 d, respectively, and biases <1 d compared to PhenoCam, and RMSE of 10 d and bias <5 d with FLUXNET (Table 3.2). The performance highly decreased for the derivative and moving average methods with RMSE of 50 d and 27 d, respectively, compared to PhenoCam, and RMSE of 48 d and 31 d with FLUXNET, and no significant correlation (R^2<0.2) (Table 3.2).

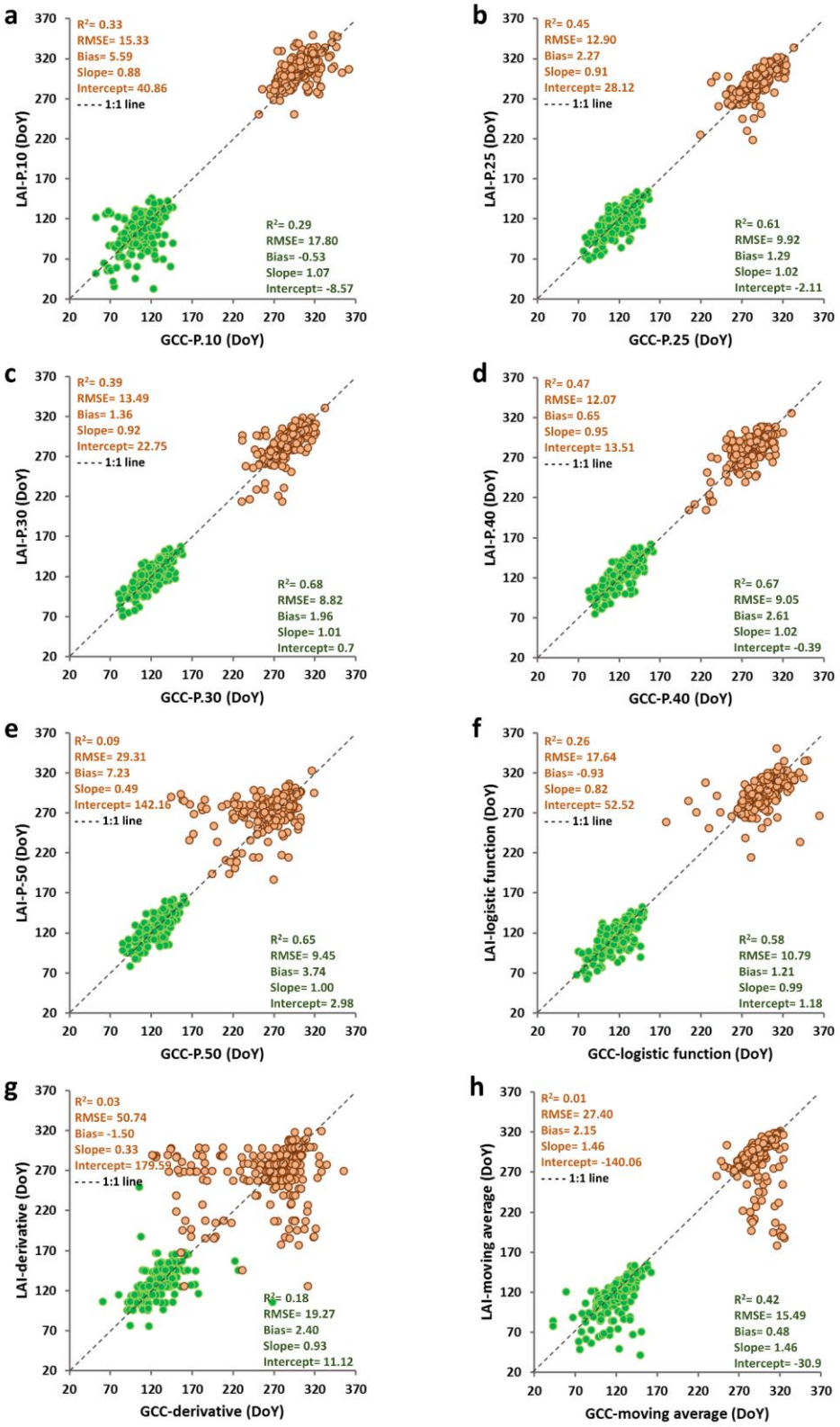

Figure 3.4**:** Scatterplots for SoS (in green) and EoS (in orange) estimated from CGLS LAI V2 and PhenoCam GCC time series by the threshold (10th (a), 25th (b), 30th (c), 40th (d) and 50th (e) percentiles of LAI amplitude), logistic-function (f), derivative (g) and moving-average (h) methods. Statistics of the comparison are presented in Table 3.2.

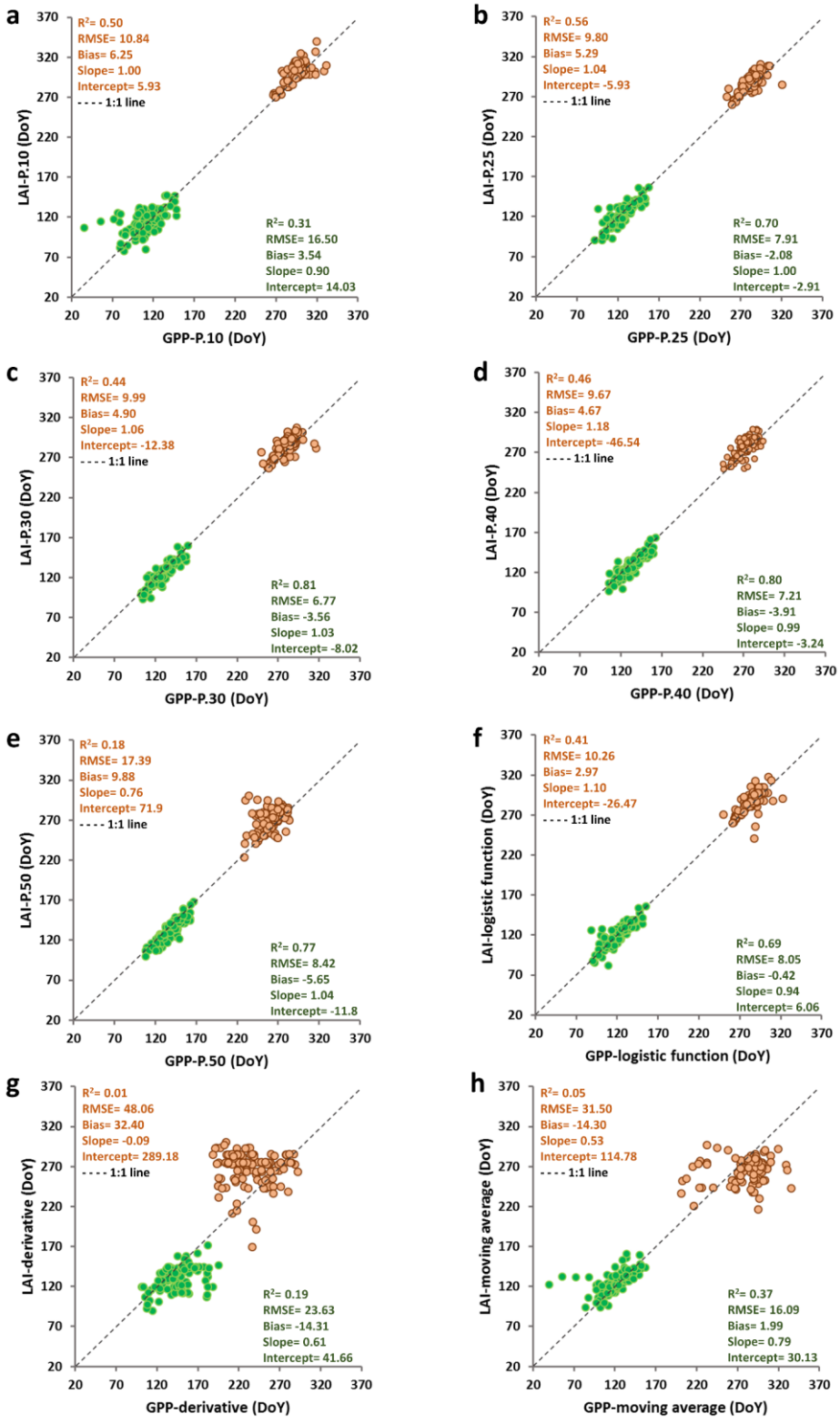

Figure 3.5: Scatterplots for SoS (in green) and EoS (in orange) estimated from CGLS LAI V2 and FLUXNET GPP time series by the threshold (10th (a), 25th (b), 30th (c), 40th (d) and 50th (e) percentiles of LAI amplitude, logistic-function (f), derivative (g) and moving-average (h) methods. Statistics of the comparison are presented in Table 3.2.

3.3.2. Latitudinal Gradients of Satellite and Ground-Based Phenology

Figure A3 shows the spatial distribution of the GCLS LAI phenological estimates (SoS, EoS, and LoS) from 2000 to 2017 over the North Hemisphere using the threshold method. The length of the vegetation cycles regularly decreases from 220 days to 80 days when latitude increases from temperate to boreal regions. The SoS ranges widely from late march in the south to approximately mid-July in the north. The SoS is slightly earlier in central Europe than in North America for the same latitude. The EoS date ranges from early August to December.

The latitudinal patterns of the timings of SoS and Eos derived from CGLS LAI V2 (Figure A3) and PhenoCam GCC over deciduous forests from 30ºN to 53ºN in North America showed a very good agreement with a gradual decrease in the length of growing season of approximately five days per degree of latitude which resulted from symmetric variations of 2.5 days per degree of latitude in the start and end of season (Figure 3.6). We found a correlation R^2 of 0.92 for the timing of SoS and 0.88 for the EoS when comparing the average satellite and PhenoCam phenology per latitude.

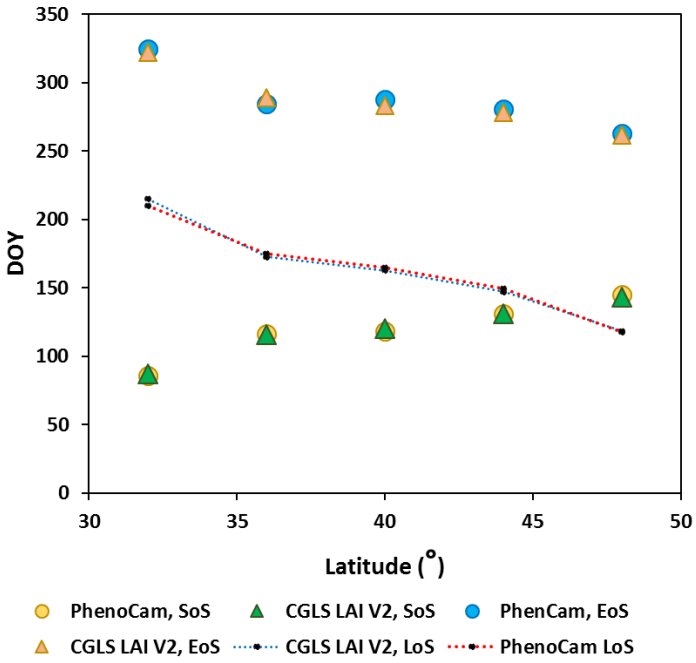

Figure 3.6: Latitudinal gradients of average phenological metrics for the start (SoS), end (EoS) and length of season (LoS) extracted from CGLS LAI V2 and PhenoCam GCC time series over the PhenoCam deciduous sites in North America (Figure 3.1). Data was aggregated in five groups of latitude, taking into account the number of sites: 30–34ºN, 34–38ºN, 38–42ºN, 42–46ºN and 46–53°N.

3.4. Discussion

We assessed the agreement of the phenological metrics derived from satellite LAI (CGLS LAI V2 from VEGETATION and PROBA-V time series, 1999-2017) with those derived from PhenoCam (GCC) and FLUXNET flux towers (GPP) across 80 sites of deciduous forests mainly located in North America and Europe. The agreement between satellite and ground-based estimates depends on the method used to extract the transition dates. We compared four phenology methods: thresholds based on percentiles of the annual amplitude (Verger et al., 2016), first derivatives (Tateishi and Ebata, 2004), autoregressive moving average (Reed et al., 1994) and a logistic function fitting approach (Zhang et al., 2003). Thresholds and logistic function resulted the most robust methods and the phenological metrics extracted from CGLS LAI V2 time series were strongly correlated with those derived from PhenoCam GCC and FLUXNET GPP. On the contrary the derivative and moving average methods showed higher discrepancies between satellite and ground estimates specifically for the timing of the EoS.

The threshold-based method performed the best in terms of accuracy of satellite estimates for the timing of the SoS and EoS: RMSE ~ 9 d and bias < 2d for the SoS, RMSE ~12 d and bias < 1d for the EoS, and correlation of R^2~0.7 compared to PhenoCam data; and RMSE <7d and bias < 4d for the SoS, RMSE <10 d and bias < 5d for the EoS, and correlation R^2~0.8 compared to FLUXNET data. In both PhenoCam and FLUXNET comparison, the 30th percentile of the annual amplitude provided the best performances for the timing of the SoS and the 40th percentile for the EoS, confirming our previous findings (Bórnez et al., 2020a; Verger et al., 2016). These thresholds slightly outperformed 10th, 25th and 50th percentiles of the amplitude as proposed in PhenoCam Dataset V1.0 for the extraction of the phenological transition dates (Richardson et al., 2018). For the sites with concomitant measurements from the 3 sources of data: satellite LAI, PhenoCam GCC and FLUXNET GPP, we observed that the phenology derived from LAI V2 using percentiles 30 and 40 accurately reproduce the interannual variation of the SoS and EoS and usually provides an intermediate solution between PhenoCam and FLUXNET estimates with differences lower than 10 days (Figure 3.7). The latitudinal gradient in the northern hemisphere of the CGLS LAI V2 phenophases highly agree with PhenoCam observations with an advance (delay) of

2.5 days per degree of latitude from low to high latitudes in response to the South-North gradient of temperature and photoperiod (Richardson et al., 2013; Schwartz et al., 2006). These results are comparable to other studies (Zhang et al., 2004). The spatial variability in phenophases can be explained not only by the difference in climatic patterns but also by the elevation and soil conditions (Rodriguez et al., 2015).

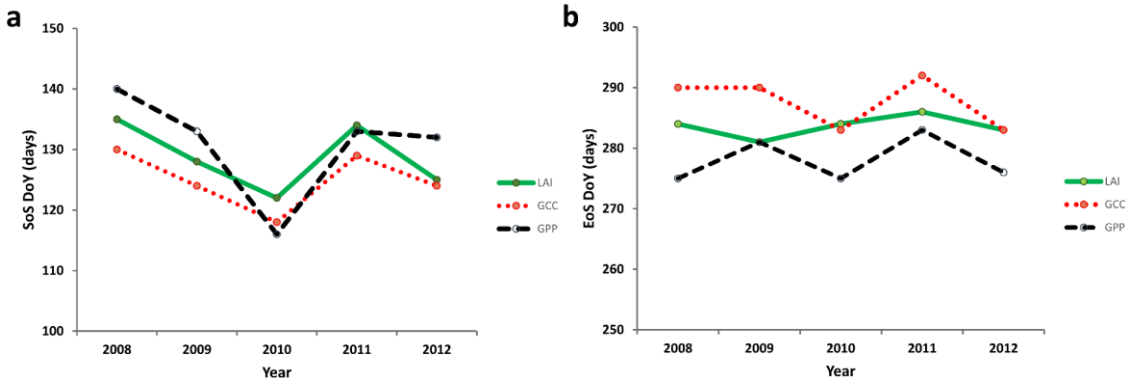

Figure 3.7: Interannual variation of the (a) start of the growing season (SoS), and (b) end of season (EoS) estimated from the CGLS LAI V2, PhenoCam GCC and FLUXNET GPP with the threshold method (percentile 30 for the timing of SoS, and percentile 40 for the timing of EoS) over the Harvard Forest (Latitude 42.54º, Longitude –72.17º).

Detecting phenology from carbon flux and PhenoCam data also faces some challenges (Hollinger and Richardson, 2005; Richardson et al., 2009). The flux measurements are potentially ~20% biased due to the lack of energy balance closure, instrument response time, pathlength averaging and incomplete measurement of nocturnal CO2 exchange (Hollinger and Richardson, 2005; Massman and Lee, 2002; Morgenstern et al., 2004) which can lead uncertainties in phenology estimates. However, these errors are difficult to quantify and correct (Richardson et al., 2009). Furthermore, for some FLUXNET sites, there are substantial data gaps due to instrument malfunction or bad data quality (Hollinger and Richardson, 2005). In these cases, the gap-filling may lead to uncertainty in GPP time series and, consequently, in the phenological estimates (Baldocchi, 2003).

The scale difference between ~1km VEGETATION and PROBA-V satellite pixels and the deca-/hectometric footprints of PhenoCam cameras and flux towers may introduce some difficulties for the comparison. This is partially minimized because our validation is limited to deciduous forests which tend to form large patches of the same vegetation type, reducing the influence of mixed or border pixels (Richardson et al., 2006, 2009; Ryu et al., 2014). The mixed signal due to multi-canopy layers may also introduce confounding effects since the understorey may have a different phenological cycle (Ryu

et al., 2014). The emergence of forest understorey is interpreted in both ground-based and satellite observations as an increase in the greening signal.

The agreement between the PhenoCam, FLUXNET and remotely sensed phenological metrics showed generally a higher accuracy for SoS than EoS, consistent with previous studies (Bórnez et al., 2020a; Garrity et al., 2011; Hufkens et al., 2012; Liang et al., 2011; Melaas et al., 2013; Nijland et al., 2016; Richardson et al., 2013). Differences in the structure, ecophysiology and dynamics of the vegetation canopy at the start and end of the growing season (Klosterman et al., 2014) may partially explain this. The phenological dynamics for the timing of EoS tend to vary with species, age, dispersion and homogeneity, and can also differ across the same species, with differences of up to two weeks within the same ROI (Delbart et al., 2005; Richardson et al., 2006, 2009, 2010, 2019). Further studies will use high resolution satellite data from Sentinel-2 to mitigate these issues and capture the spatial variability of EoS (Snyder et al., 2019). Note, however, that monitoring EoS is affected by the intrinsic uncertainties of satellite remote sensing at northern latitudes in autumn: atmospheric effects, snow and poor illumination conditions (Luquez et al., 2007).

3.5. Conclusions

Phenological data from PhenoCam, FLUXNET and satellite remotely sensed data have become a broad resource for analyzing the relationships between global change and vegetation (Hufkens et al., 2012; Richardson et al., 2018). The network of PhenoCam webcams and eddy covariance towers cover only small areas around the camera or flux tower (Churkina et al., 2005; Gonsamo et al., 2012). Satellite imagery has the advantage of providing continuous spatio-temporal coverage at the global scale. Near-surface digital cameras and flux towers have nevertheless become a good tool for characterizing local phenology and validate satellite estimates (Klosterman et al., 2014; Migliavacca et al., 2011; Richardson et al., 2009; Sonnentag et al., 2012). The high temporal frequency of PhenoCam and flux measurements provide continuous time series for applying the same phenology extraction methods to ground and satellite time series. This way, we avoid some of the issues identified in our previous research (Bórnez et al., 2020a) related to the differences in the definition of satellite phenology metrics and ground phenophases when PEP725 and USA-NPN data were used for the validation (e.g.; the

representativity and spatial distribution of the data as well as the gaps in the time series of ground measurements).

Results validate the land surface phenology estimated from CGLS LAI V2 time series, as well as the robustness of PhenoCam and FLUXNET data to analyze vegetation phenology. This study has put bounds on the uncertainty in satellite-derived phenological transitions, which should allow to analyze changes in the phenological distribution pattern and serve as a starting point for other studies that characterize anomalies and trends over vegetation phenology, as well as its possible relationship with changes in the climate pattern as a result of climate change.

4

Monitoring the responses of deciduous forest phenology to 2000-2018 climatic anomalies in the Northern Hemisphere

Kevin Bórnez, Aleixandre Verger, Adrià Descals, Josep Peñuelas

Article (in press) *Remote Sens.* 2021, 13,xxx

Abstract

Monitoring the phenological responses of deciduous forests to climate is important due to the increasing frequency and intensity of extreme climatic events associated with climate change and global warming, which will in turn affect vegetation seasonality. We investigated the spatiotemporal patterns of the response of deciduous forests to climatic anomalies in the Northern Hemisphere using satellite-derived phenological metrics from the Copernicus Global Land Service Leaf Area Index and multi-source climatic data sets for 2000–2018 at resolutions of 0.1°. Thereafter, we assessed the impact of extreme heatwaves and droughts on this deciduous forest phenology. We assumed that changes in the deciduous forest phenology in the Northern Hemisphere for the period 2000-2018 were monotonic and temperature and precipitation were the main climatic drivers. Analyses of partial correlations of phenological metrics with the timing of the start of the season (SoS), end of the season (EoS), and climatic variables indicated that changes in preseason temperature played a stronger role than precipitation in affecting the interannual variability of SoS anomalies: the higher the temperature, the earlier the SoS in most deciduous forests in the Northern Hemisphere (mean correlation coefficient of -0.31). Correlations between SoS and temperature were significantly negative in 57% of the forests and significantly positive in 15% of the forests ($P<0.05$). Both temperature and precipitation contributed to the advance and delay of EoS. A later EoS was significantly correlated with a positive standardized precipitation-evapotranspiration index (SPEI) at the regional scale (~30% of deciduous forests). The timings of EoS and SoS shifted by >20 d in response to heat waves throughout most of Europe in 2003 and in the United States of America in 2012. This study contributes to improve our understanding of the phenological responses of deciduous forests in the Northern Hemisphere to climate change and climate extreme events.

4.1. Introduction

Interest in understanding the interactions between phenology and climate has increased in the last few decades (Ceccherini et al., 2014) because vegetation phenology plays an important role in balancing biogeochemical cycles, such as the exchange of water, energy, and carbon (He et al., 2018; Peñuelas et al., 2009; Richardson et al., 2013; White et al., 2005). Changes in the timing of phenology provide the first signals of adjustments in the responses of species to climatic anomalies (Walther et al., 2002).

Changes in the pattern of distribution of temperatures and precipitation as a consequence of global climate change, and the interactions with other cues such as photoperiod, could strongly alter vegetation phenology (Bradley et al., 2011; Cleland et al., 2017; IPCC, 2007, 2012, 2013). Investigating the interactive effects of temperature and precipitation on phenology to understand and anticipate the effects of climate change on vegetation is therefore crucial (Du et al., 2019). Many previous studies have investigated the changes in vegetation phenology as a result of the climate change and the associated global warming (de Beurs and Henebry, 2005; Jeong et al., 2011; Piao et al., 2007; Zhou et al., 2001). In this sense, the analysis of the sensitivity of vegetation to hydroclimatic anomalies is increasingly studied (Ceccherini et al., 2014; Shen et al., 2015), especially the role of the temperature on phenology (Cong, et al., 2017; Forrest and Miller, 2010; Forzieri et al., 2014; Thackeray et al., 2016; Wang et al., 2007). Previous studies have demonstrated that temperature has been one of the most decisive factors affecting phenology in the last four decades, with strong correlations between deciduous forest phenology and temperature (R^2>0.5) in central Europe, China (Estrella and Menzel, 2006; Lu et al., 2016), and the Mediterranean region, especially with temperatures in the months prior to the phenophases (Peñuelas et al., 2002). Phenology is changing in response to global warming, leading to an earlier SoS and a later EoS during the last few decades in some areas of the Northern Hemisphere (Peñuelas and Filella, 2001; Piao et al., 2019), such as North America (Richardson et al., 2013), China (Piao et al., 2006; Kang et al., 2018), and Eurasia (Menzel, 2003; Piao et al., 2011). Droughts also play an important role where humidity determines vegetation growth (Piao et al., 2015; Ramos et al., 2015).

Global warming has increased the intensity, frequency, and spatial distribution of extreme climatic events at global and regional scales (Chen and Sun, 2017; Held and

Soden, 2006; Javed et al., 2021; Sheffield and Wood, 2008). Extreme climatic events are often accompanied by anomalies of temperature and precipitation (He et al., 2018; Ma et al., 2015). These events are characterized by being severe and unique compared to average conditions over a particular time series (Butt et al., 2015; Menzel et al., 2011). Understanding the responses of phenology to climatic extremes is therefore crucial and challenging, because future climatic anomalies will become more intense and frequent relative to those in past decades (IPCC, 2007 2013; Jentsch et al., 2009; Reichstein et al., 2013; Tang et al., 2017; Zhao et al., 2018; Zheng et al., 2018). Climatic extremes early in the 21st century have affected most regions of the Northern Hemisphere, such as Europe (Ivits et al., 2014; Reichstein et al., 2007) and North America (Ponce-Campos et al., 2013), where heat waves were more common than in previous decades (Fischer and Schär, 2010; Trumbore et al., 2015). Some previous studies have also focused on assessing the vegetation phenological responses to climate extreme events in Europe (Ciais et al., 2005; Gobron et al., 2005; Lorenz et al., 2013) and North America (Diffenbaugh, 2005; Ellwood et al., 2013; Karl et al., 2012).

Remotely sensed data have been widely used to analyze vegetation dynamics and estimate phenological metrics at hemispherical and global scale (Bórnez et al., 2020a, 2020b; Richardson et al., 2009; Verger et al., 2014., 2019). Several phenological metrics, including the start of the growing season (SoS) and the end of the season (EoS), have been estimated from time series of vegetation indices derived from medium resolution satellite instruments such as the Moderate Resolution Imaging Spectroradiometer (MODIS), the Advanced Very High-Resolution Radiometer (AVHRR), VEGETATION on board the Satellite Pour l'Observation de la Terre (SPOT-VGT) and PROBA-V (Atkinson et al., 2012; Bórnez et al., 2020a; Delbart et al., 2005; Verger et al., 2016; Zhang et al., 2004). Estimates of land-surface phenology (LSP) using remotely sensed data play an important role in monitoring terrestrial responses to climate change (White et al., 2005). Numerous LSP studies e.g. (Beaubien and Freeland, 2000; Chmielewski and Rotzer, 2002; Menzel and Fabian, 1999; Schwartz et al., 2006) have been focused on the northern hemisphere. These studies commonly use the NDVI for detecting phenological trend and interannual variation (de Beurs and Henebry, 2005;

Julien and Sobrino, 2009; White et al., 2009), and mainly focus on determining trends and investigating the advance for the timing of SoS during the last decades.

This is the first study analyzing the response of vegetation phenology to climate anomalies by using phenological metrics derived from leaf area index (LAI) time series from both SPOT-VGT and PROBA-V sensors that were demonstrated to outperform NDVI time series for phenology detection (Bórnez et al., 2020a). Our study focusses on understanding the changes and the sensitivity of deciduous forest phenology to the anomalies of temperature, precipitation and drought for 2000–2018 in the Northern Hemisphere. We assumed that changes in the deciduous forest phenology in the Northern Hemisphere for the period 2000-2018 were monotonic and temperature and precipitation were the main climatic drivers. Our specific objectives were to: (1) quantify the spatial patterns of correlations of the anomalies of deciduous forest phenology with precipitation and temperature, (2) identify the main causes of phenological change, (3) determine the impact of drought on phenology, (4) quantify the sensitivity of phenology to climate, and (5) assess the effects of some climate extreme events (e.g. heat wave) on phenology. This study contributes to improve our understanding of the phenological response to climate change and climate extreme events in the Northern Hemisphere.

4.2. Materials and Methods

4.2.1. Data sources and processing

4.2.1.1. Study area

Our study is focused on deciduous forests in the Northern Hemisphere (Figure 4.1) where the used LSP retrievals were validated (Bradley et al., 2011; Cleland et al., 2017). According to the Intergovernmental Panel on Climate Change (IPCC) predictions (de Beurs and Henebry, 2005; Zhou et al., 2001), these northern regions are highly sensitive to climate change.

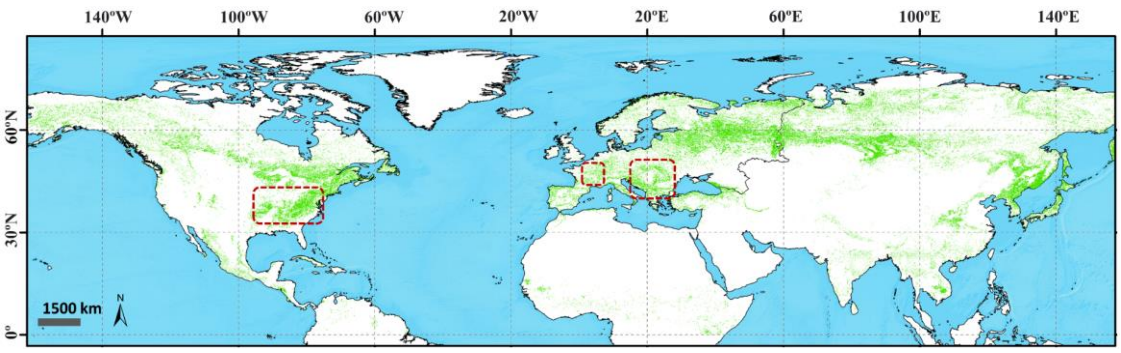

Figure 4.1: Map showing the study area with the distribution of the deciduous forests analyzed (in green). The red dashed lines show the regional areas assessed in section 3.2.

4.2.1.2. Land – cover / vegetation map

Because we focused on deciduous forests, we used a land-cover (LC) map that identified this type of vegetation: the Climate Change Initiative (CCI-LC) map series for 2015 at a spatial resolution of 300 m, available from the European Space Agency (ESA) (http://maps.elie.ucl.ac.be/CCI/viewer/download.php). CCI-LC discriminates 38 classes of land cover. We resampled the map to 0.1° and analyzed only pixels containing deciduous forest.

4.2.1.3. Vegetation phenology from SPOT VEGETATION and Proba-V data

SoS and EoS during 2000–2018 were estimated using the time series of Copernicus Global Land Service LAI 1km version 2 derived from SPOT VEGETATION (VGT) and Prova-V data (Verger et al., 2014) (https://land.copernicus.eu/global/themes/vegetation). These metrics were based on previous protocols and research (Bórnez et al., 2020a; Bórnez et al., 2020b; Verger, et al., 2016) that used dynamic thresholds. This method is based on the percentage of the LAI amplitude in each pixel, in which SoS is defined as the day of the year (DoY) when LAI exceeds the 30% threshold and EoS is defined as the DoY when LAI overpasses the 40% threshold after the growing season.

4.2.1.4. Rainfall and temperature data sets

The data for temperature and precipitation were collected from the ERA5 hourly gridded data sets from 2000 to 2018 with a spatial resolution of 0.25° (https://cds.climate.copernicus.eu/). To achieve higher resolution, we interpolated all

climatological data from the spatial resolution of 0.25 to 0.1° using a cubic convolution that calculated the value of each pixel by fitting a smooth curve based on the surrounding 16 pixels. Temperature was the air temperature at a height of 2 m, and precipitation was the accumulated amount of liquid or frozen water that fell, calculated as the sum of large-scale and convective precipitation in millimeters.

We used the mean temperature and accumulated precipitation for the preseason using time lags of 1, 3, and 6 months prior to the timings of SoS and EoS.

4.2.1.5. SPEI

Drought indices have become useful tools for analyzing, assessing, and estimating the dry and humid periods that may impact on phenology (Javed et al., 2021). Various drought indices are available, such as the standardized precipitation index (SPI) or the Palmer drought severity index (Palmer, 1965) (PDSI), and several recent studies have analyzed drought conditions using the standardized precipitation-evapotranspiration index (SPEI) (Chen et al., 2015; Wang et al., 2017). SPEI is based on precipitation and potential evapotranspiration, which includes the role of temperature in drought severity (Beguería et al., 2013; Vicente-Serrano et al., 2010., 2013). SPEI considers drought timescales, which represent the cumulative water balance over the previous 1–48 months. It is based on the Standardized Precipitation Index (SPI) calculation method but with improvements to include the potential evapotranspiration (PET). The SPEI uses the weekly (or monthly) difference between precipitation and PET (based on Thornthwaite method), and it is calculated as a standardized variable, which allows the comparison with other SPEI values and climatic variables over time and space (Vicente-Serrano et al., 2010). Unlike SPI, SPEI includes the effects of temperature variability on drought estimation and therefore, it takes into account the effect of warming processes on drought severity (Vicente-Serrano et al., 2010., 2013).

SPEI data set Version 2.6 was downloaded from the Global SPEI database (https://spei.csic.es/database.html) at a spatial resolution of 0.5° and was resampled to 0.1° for the analysis. This data set is based on the United Nations Food and Agriculture Organization (FAO)-56 Penman-Monteith estimation of potential evapotranspiration. The complete procedure for calculating SPEI is provided by Vicente-Serrano et al. (2010).

We determined drought severity for the timings of SoS and EoS using different SPEI timescales (1, 3, 6, and 12 months), representing the cumulative water balance for the timings of preseason and presenescence. Positive SPEI values indicate that humidity is higher than the historical median, and negative values indicate a water deficit (Vicente-Serrano et al., 2010., 2013). The SPEI data were classified into seven categories (Table 4.1) based on the World Atlas of Desertification (Cherlet et al., 2018) for analyzing conditions of wetness or dryness.

Table 4.1: Classification of drought based on SPEI data.

Range	Condition
SPEI ≤ -2	Extremely dry
-2 < SPEI ≤ -1.5	Severely dry
-1.5 < SPEI ≤ -1	Moderately dry
-1 < SPEI ≤ 1	Near normal
1 < SPEI ≤ 1.5	Moderately wet
1.5 < SPEI ≤ 2	Severely wet
SPEI ≥ 2	Extremely wet

4.2.2. Methodology and statistical analysis

We first estimated the significant trends in the time series of the estimates (SoS and EoS). Secondly, we explored the impacts of anomalies in hydroclimatic variables, such as temperature, precipitation, and drought on deciduous phenology throughout the Northern Hemisphere for 2000–2018. We applied spatiotemporal response analysis to determine the relationships of phenology and climate variables. Moreover, we investigated the spatial pattern of the sensitivity of phenology to climate and its relationship with preseason and presenescence temperature, precipitation, and drought. We thereafter focused on some of the extreme events, including high temperatures, low temperatures and severe drought, that have occurred in the last two decades.

We used different software to calculate and evaluate the effects of climatic variables on vegetation phenology. We first used Google Earth Engine (Gorelick et al., 2017) to

download and process the time series of the hydroclimatic variables and for estimating land-surface phenological metrics in the Northern Hemisphere (Bórnez et al., 2020a; 2020b). We then used RStudio, XLSAT and Idrisi TerrSet for processing and statistically analyzing all data. Finally, we used ESRI ArcGIS 10.5 for generating the graphs and maps.

4.2.2.1. Trend analysis

We calculated the trends in the estimated time series of SoS and EoS before analyzing the relationships between phenology and climate. Temporal trends in the data sets were

calculated by applying the Theil-Sen (TS) median-slope trend analysis, which is an effective method for analyzing the rate of change in observations over a period of time (2000–2018 in our study) and is similar to linear least squares regression. TS is based on nonparametric statistics (Mann-Kendall) and is independent of the assumptions of linear regression. Medians are used to calculate the trend, which is consequently less susceptible to noise and outliers (Kang et al., 2018; Sen, 1968; Theil, 1992). The equation used to estimate TS slope is:

$$\text{TS Slope} = \text{Median}\left(\frac{x_j - x_i}{t_j - t_i}\right) \quad (1)$$

where xj and xi are values in years i and j, respectively. We estimated the significance of the TS slope using a nonparametric test (Mann-Kendall significance test), which provided a standardized Z and the corresponding probability (p). Positive and negative slopes indicated that SoS or EoS had delayed and advanced trends, respectively, during the study period. The Mann Kendall significance (Z and P) was calculated as:

$$z = \begin{cases} \frac{S-1}{\sqrt{\text{Var}(S)}} & \text{for } S > 0 \\ 0 & \text{for } S = 0 \\ \frac{S+1}{\sqrt{\text{Var}(S)}} & \text{for } S < 0 \end{cases} \quad (2)$$

and

$$P = 2[1 - \phi(|z|)] \quad (3)$$

where

$$\Phi(|z|) = \frac{2}{\sqrt{\pi}} \int_0^{|z|} e^{-t^2} \, dt \quad (4)$$

We also used the nonparametric Pettitt test method (Pettitt, 1979) to detect the possible abrupt change points in the phenological time series. This test allows to identify shifts in the average and their significance. The null hypothesis of the Pettitt test is the absence of a change point. The empirical significance level (p value) was computed using XLSTAT statistical and data analysis software 2021 v.3.1 at a significance level of 5%. The non-parametric Pettitt statistical test is defined as:

$$K_\tau = \max\left|U_{t,T}\right|, \quad (5)$$

*w*here

$$U_{t,T} = \sum_{i=1}^{t} \sum_{j=i+1}^{n} \operatorname{sgn}\left(xj - x_j\right) \quad (6)$$

where t is the period length and n is the number of data in the statistical series. p-value and an interval around the p-value was evaluated by using a Monte Carlo method.

4.2.2.2. Standardized anomalies

We calculated standardized anomalies in the interannual time series (2000–2018) of phenology, temperature, and precipitation. Standardized anomalies were calculated by dividing anomalies by the standard deviation. The equation is (Funk et al., 2019):

$$Z = \frac{X-\mu}{\sigma} \quad (7)$$

where Z is a standardized anomaly, X is the annual value, and μ and σ are the interannual mean and standard deviation, respectively, for each variable analyzed (i.e. the timings of SoS and EoS, the mean preseason or presenescence temperature, or the accumulated preseason or presenescence precipitation).

Note that we estimated the anomalies in the time series of temperature and precipitation using the mean temperature and the accumulated precipitation for different timescales (1, 3, and 6 months) before estimating the timings of SoS and EoS (see section 2.1.3).

4.2.2.3. Correlations and partial correlation analyses

We calculated the coefficients for the correlations between the estimated time series of phenology (SoS and EoS), temperature, precipitation, and SPEI for different preseason lengths. We used two types of correlation analysis to quantify the response of vegetation to climatic drivers. We first calculated the linear correlation (Pearson's correlation) between the interannual anomalies of phenology (y) and hydroclimatic variables (x) at a significant level of 95%:

$$r_{xy} = \frac{n\,\Sigma x_i y_i - \Sigma x_i \Sigma y_i}{\sqrt{n\sum x_i^2 - (\Sigma x_i)^2}\,\sqrt{n\sum y_i^2 - (\Sigma y_i)^2}} \quad (8)$$

where rxy is the Pearson correlation coefficient between x and y, n is the number of observations, xi is the value of x for observation i, and yi is the value of y for observation i. A multivariate linear regression model was used for multivariate cases.

We correlated SoS and EoS anomalies with the climatic variables (temperature and precipitation) for timescales of 1, 3, and 6 months prior to the dates of SoS and EoS and summarized the climatic variables for the preseason periods in which the correlation was highest. For SPEI, we used timescales from 1 to 12 months (Vicente-Serrano et al., 2013).

We then applied a partial correlation analysis of SoS and EoS using the preseason and presenescence climatic variables for the three-time lags (1, 3, and 6 months). The precipitation data for the same timescale were used as a constant factor for calculating the partial correlation between phenology and temperature. Similarly, the influence of temperature was considered a constant for calculating the correlation with accumulated precipitation. The partial correlation coefficient between vegetation and mean temperature and its significance were tested as:

$$r_{vt.p} = \frac{r_{vt} - r_{vp}r_{tp}}{\sqrt{(1-r^2_{vp})(1-r^2_{tp})}} \quad (9)$$

where v is the vegetation phenology, t is temperature, p is precipitation, and r_{vt} and r_{vp} are the simple correlation coefficients of the phenology (SoS or EoS) with the mean preseason or presenescence temperature and accumulated precipitation, respectively. Eq. (8) is also valid for calculating the partial correlation between phenology and precipitation by changing the order in which the data are entered. The significance of the partial correlation coefficients at the 95% level was evaluated using the Student's t-test.

The Pearson's correlation and partial correlation analysis produced similar maps, so the results obtained by partial correlation will be taken into account in subsequent sections for analyzing the correlations between phenology, temperature, and precipitation.

4.2.2.4. Sensitivity analysis

We used multiple linear regression and sensitivity analysis to further investigate the interactions of phenology with temperature, precipitation, and SPEI. The responses of the sensitivity of vegetation phenology to the climatic variables corresponded to the slopes of the linear regressions between the phenological metrics and the climatic variables, representing the unit change in phenological date divided by the unit change in temperature, precipitation, or SPEI.

4.3. Results

4.3.1. Analysis of trends and correlations in the 2000–2018 time series

4.3.1.1. Trends in the time series of estimated phenology

The Pettitt test confirmed that phenological time series were monotonic and any statistically significant change points was detected (p values of 0.74 and 0.86 for SoS and EoS, respectively). The temporal trends in SoS for 2000–2018 (Figure 4.2a) were significant ($P<0.05$) for 20.5% of the deciduous forests in the Northern Hemisphere. Negative trends, representing an advance in the timing of SoS, and positive trends, representing a delay in the timing of SoS, accounted for 61.5 and 38.54% of these pixels, respectively (Table B1). Northeastern Europe mainly had negative SoS trends, and Russia and North America mainly had positive trends (Figure 4.1a). EoS changed significantly in 23.8% of the deciduous forests (Figure 4.5a), with 40.5 and 59.49% of these forests having a delayed and advanced EoS, respectively (Table B1). Our results indicated that SoS and EoS advanced by 0.08 and 0.1 d/y, respectively. Positive significant trends were mainly in northeastern Europe, and negative trends were mainly in eastern North America (Figure 4.5a).

4.3.1.2. Correlation and sensitivity of phenology with climatic variables

The correlation between SoS anomalies and preseason temperature (Figure 4.3 and Figure B1a) indicated that 72.13% of all pixels had significant correlations at $P<0.05$, with negative correlations accounting for 57% of all pixels (Table 4.2). An earlier SoS tended to be associated with higher temperatures in 35% of the pixels, and a later SoS was associated with lower temperatures in 21% of the pixels (Table B2). Temperature and SoS were negatively correlated in Eurasia and eastern North America, with coefficient correlations (r) of ~-0.7 and -0.6, respectively (Figure B1).

The spatial pattern of the distribution of the partial correlations between SoS and precipitation was more heterogeneous than the correlation between SoS and temperature. The correlation between SoS and precipitation was positive in most pixels, accounting for 42% of them (Table 4.2; Figure 4.3b and Figure B1b), which led to significant positive correlation advance or delay (20.9% and 21.4%) in the SoS with precipitation decrease or increase respectively (Table B2).

Table 4.2: Percentage of pixels with significant correlations (P<0.05) between the anomalies of phenological events (SoS and EoS) and climatic variables (temperature, precipitation, and SPEI) in the Northern Hemisphere for 2000–2018.

Phenological event	**Climatic variable**	**Positive (%)**	**Negative (%)**
SoS	Temperature	14.94	57.19
	Precipitation	42.30	20.07
	SPEI	17.57	9.87
EoS	Temperature	23.57	20.75
	Precipitation	34.44	28.42
	SPEI	28.78	9.04

The mean sensitivities of SoS to temperature and precipitation were -2.45 d/°C and 0.8 d/10 mm, respectively (Figure 4.4). The sensitivity to temperature was highest (~-5 d/°C) in Eurasia and southeastern North America (Figure 4.2b), and the sensitivity to precipitation was highest (3 d/10 mm) at latitudes >60°N (Figure 4.2c).

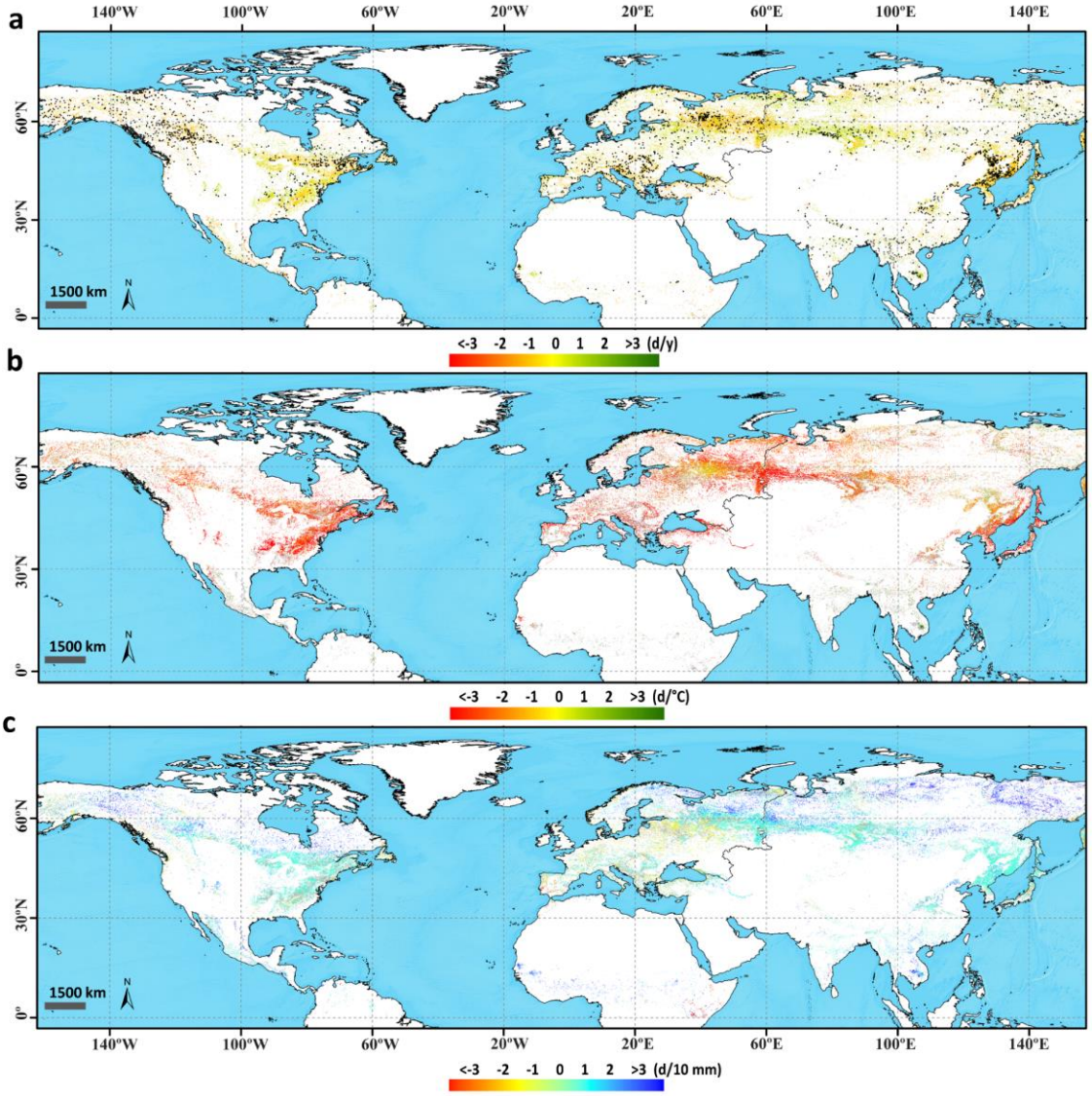

Figure 4.2: (a) Distribution of trends for the SoS time series in the Northern Hemisphere between 2000 and 2018 in pixels with significant correlations between phenology and climate (a positive trend indicates a delayed SoS, and a negative trend indicates an advanced SoS). Regions with black dots indicate significant trends (Mann-Kendall test, $P<0.05$). For visualization purposes, the size of black dots has been increased. (b) Distribution of sensitivity coefficients between SoS and mean preseason temperature (d/°C). (c) Distribution of sensitivity coefficients between SoS and preseason accumulated precipitation (d/10 mm). White indicates unvegetated areas and areas with no deciduous forests, and light gray (in b and c) indicates vegetated areas with nonsignificant correlations ($P>0.05$).

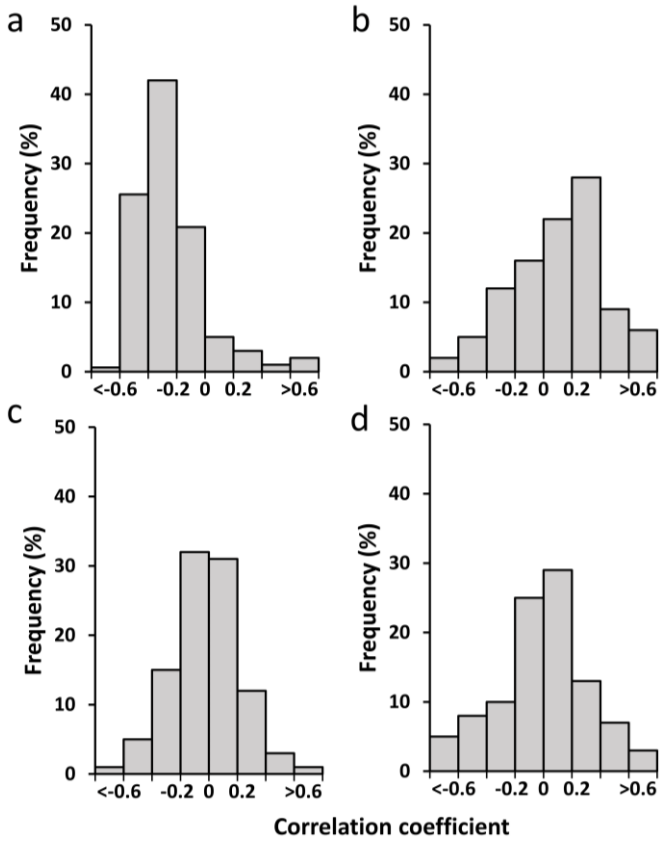

Figure 4.3**:** Frequencies of the correlations between phenology and the climatic variables. Panels a and b show the correlations between SoS and temperature and precipitation, respectively. Panels c and d show the correlations between EoS and temperature and precipitation, respectively.

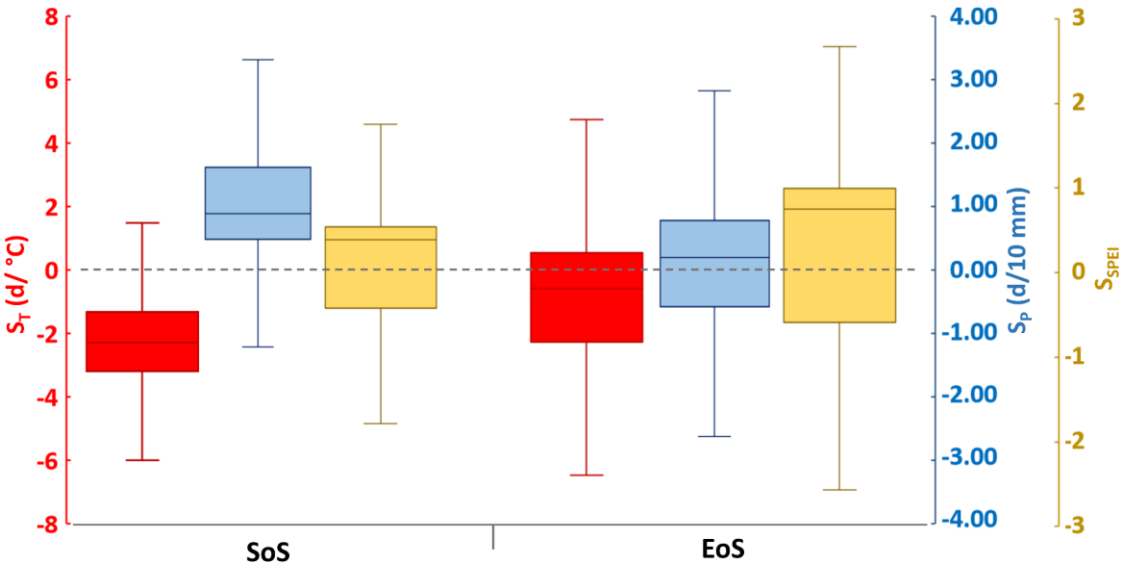

Figure 4.4: Boxplots of the sensitivities of the timings of SoS (left) and EoS (right) to temperature (ST, red), precipitation (SP, blue), and SPEI (SPEI, yellow) before SoS and EoS. Only significant (*P<0.05*) correlation coefficients are shown.

The sensitivity analysis (Figure 4.4 and Figure 4.5) indicated that the response of phenology to climatic anomalies was lower for the timing of EoS than the timing of SoS. The pattern of temperature sensitivity was very heterogeneous, with symmetric

distributions of positive and negative correlations between temperature and EoS in 23.57 and 20.75% of the pixels, respectively (Table 4.2, Figure 4.3c). EoS advanced with temperature by an average of ~0.5 d/°C (Figure 4.5b). The sensitivity of EoS to precipitation had the opposite pattern: the timing of EoS was delayed by an average of ~0.5 d/10 mm. Correlations were significantly positive (i.e. a delay in the timing of EoS with an increase in precipitation) in 34.44% of the study area (Figure B2), with sensitivities highest in southern and southwestern Europe (~3 d/10 mm). In contrast, 28.42% of the pixels had negative correlations (i.e. an advance in the timing of EoS with an increase in precipitation), mainly in northeastern Europe and areas of Russia (Figure 4.5c).

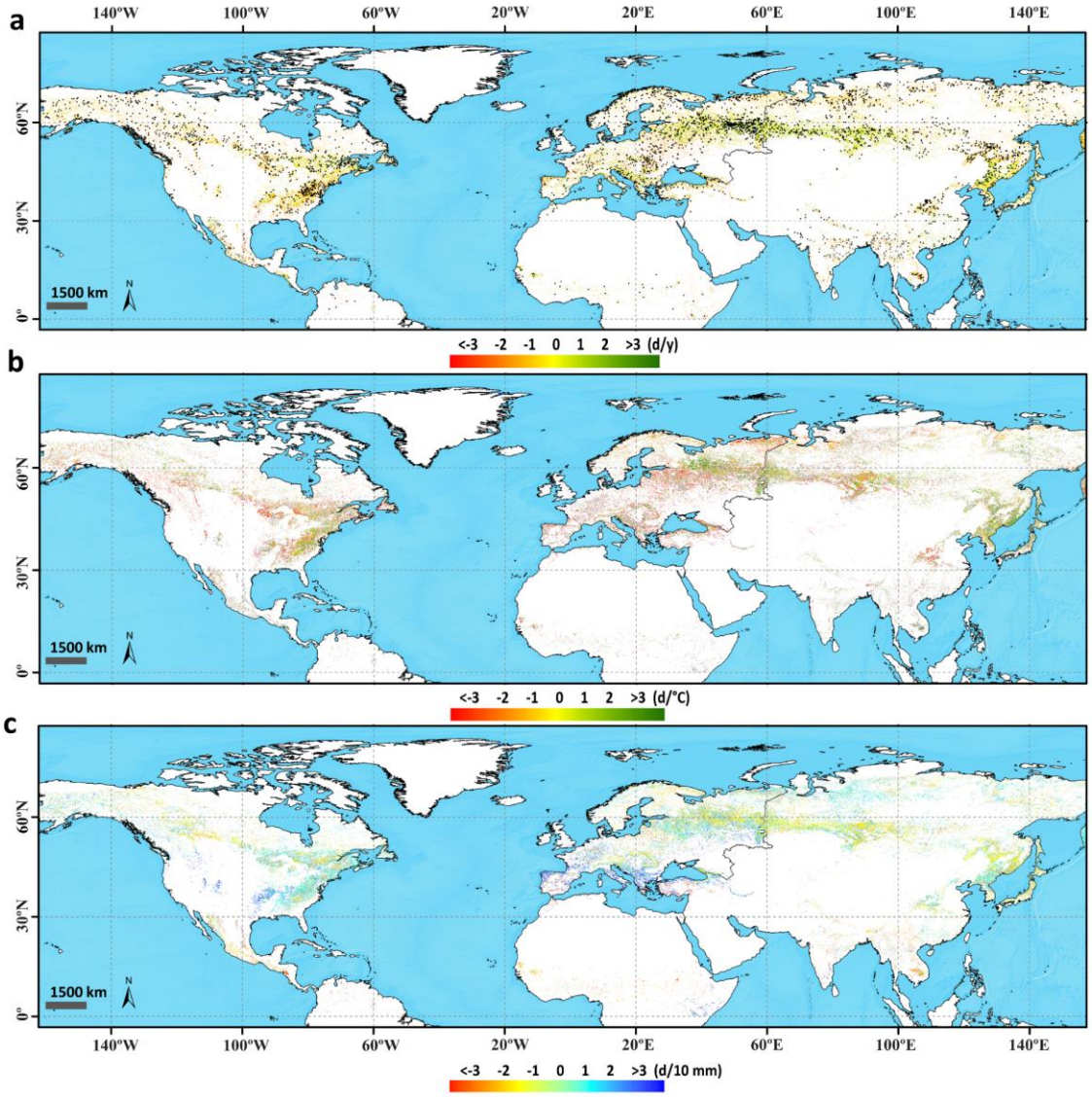

Figure 4.5: (a) Distribution of trends for the EoS time series in the Northern Hemisphere between 2000 and 2018 in pixels with significant correlations between phenology and climate (a positive trend indicates a delayed EoS, and a negative trend indicates an advanced EoS). Regions with black dots indicate significant trends (Mann-Kendall test, P<0.05). For visualization purposes, the size of the black dots has been increased. (b) Distribution of sensitivity coefficients between EoS and mean presenescence temperature (d/°C). (c) Distribution of sensitivity coefficients between EoS and presenescence accumulated precipitation (d/10 mm). White indicates unvegetated areas and areas with no deciduous forests, and light gray (in b and c) indicates vegetated areas with nonsignificant correlations (P>0.05).

4.3.1.3. Response of vegetation phenology to drought using SPEI

When analyzing the influence of drought on vegetation, we found that SPEI calculated using time lags between 1 and 3 months was correlated the best with the timings of SoS and EoS in >50% of the pixels (Table B3).

The Spearman correlations between SoS and SPEI were positive in 52.3% of the Northern Hemisphere and were significant (*P<0.05*) in 17.5% of the pixels (Table 4.2),

mostly >60°N in northeastern Europe and North America (Figure 4.6a). The correlations were negative (47.6% of the pixels, significant in 9.8%) in northeastern Europe (between 50° and 60°) in areas where the sensitivity of SoS to SPEI was highest (Figure B3a).

Correlations between the timings of EoS and SPEI were positive in 58.8% of the study area (Table 4.2), with significant correlations for 28.8% of the pixels (P<0.05). The correlations were particularly strong in southwestern Europe and northeastern North America (Figure 4.6b) in areas where the sensitivity of EoS to SPEI was highest (Figure B3b). Drought weakly affected phenology at high northern latitudes (>60°N), where temperature (Figure 4.5b), not precipitation (Figure 4.5c), was the main variable limiting phenology. The correlations between EoS and SPEI were thus weak.

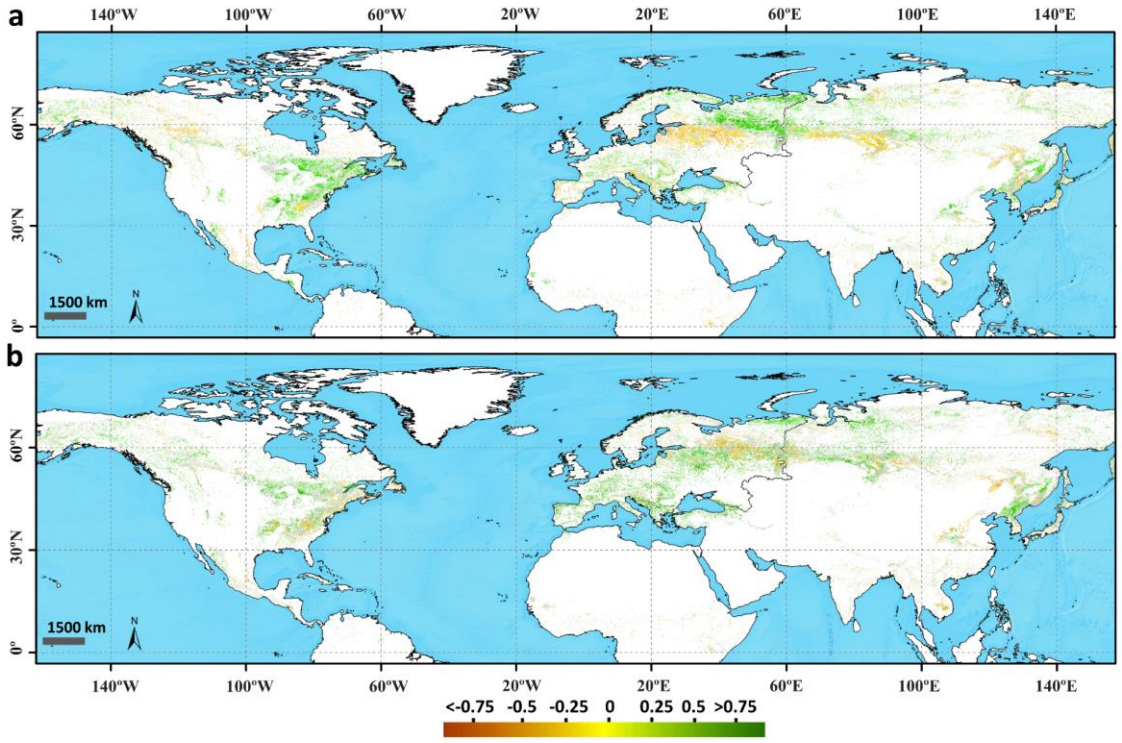

Figure 4.6**:** Spatial patterns of the partial correlations between SPEI and (a) SoS and (b) EoS for 2000–2018 in the Northern Hemisphere. The color scale represents the maximum correlation coefficient for each pixel, independently of the SPEI timescale. White indicates unvegetated areas and areas with no deciduous forests, and light gray indicates vegetated areas with nonsignificant correlations (P>0.05).

4.3.2. Phenological responses to recent climatic extremes

We analyzed the effects of three heat and cold waves on vegetation phenology in Europe and North America.

4.3.2.1. Effect of the 2003 summer heat wave in western Europe

2003 was one of the driest and warmest years recorded in the last 30 years in most of central Europe (Fischer et al., 2007; Stéfanon et al., 2012). The effects of this extreme episode were represented by negative anomalies in the timing of EoS throughout most of western Europe (Figure 4.7a). We highlight a region of southern France and southwestern Germany where an unstandardized anomaly for the timing of EoS had a mean of -22 d.

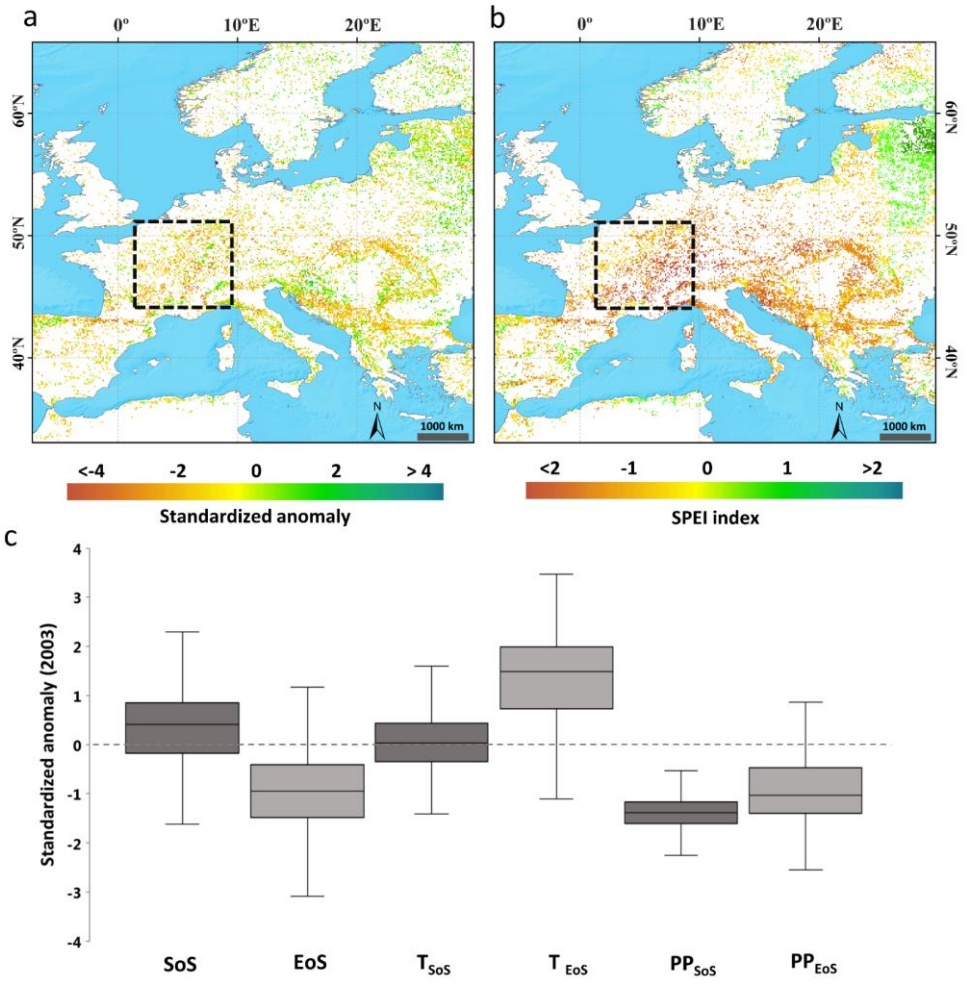

Figure 4.7: Distribution of the anomalies for the timing of EoS (a) and (b) SPEI before EoS in western Europe for 2003. The boxplots (c) show the standardized anomalies between phenology and the climatic variables (SoS in dark gray, and EoS in light gray).

An intense drought also occurred in 2003, which we identified using SPEI (Figure 4.7b, Table 4.3). More than 80% of the pixels indicated an intense drought prior to the timing of EoS. Fischer et al. (2007) observed that an early EoS and stress from the lack of soil moisture contributed greatly to the suppression of evapotranspiration after the summer and that this interaction may have amplified the temperature anomaly by locally increasing the flux of sensible heat. Figure 4.7c shows the standardized anomalies between phenology and the climatic variables, which allows the visualization of the positive temperature anomaly for the timing of EoS and the precipitation deficit for the timings of both SoS and EoS.

Table 4.3: Classification of SPEI data for characterizing drought in the three case studies: Europe, North America, and Balkans for 2003, 2012, and 2005, respectively. Two analytical periods are used: preseason (for the timing prior to SoS) and presenescence (for the timing prior to EoS). The SPEI timescale with the highest correlation in each pixel was considered.

		SoS (area, %)			EoS (area, %)		
Range	**Condition**	**Europe 2003**	**North America 2012**	**Balkans 2005**	**Europe 2003**	**North America 2012**	**Balkans 2005**
SPEI ≤ -2	Extremely dry	0	0.77	0	26.30	3.96	0
-2 SPEI ≤ -1.5	Severely dry	2.88	9.60	0	29.75	5.56	0
-1.5 SPEI ≤ -1	Moderately dry	15.96	16.69	0	23.99	4.68	1.04
-1 < SPEI ≤ 1	Near normal	80.96	72.93	14.44	19.96	52.44	67.56
1 SPEI ≤ 1.5	Moderately wet	0	0	35.13	0	29.57	28.78
1.5 SPEI ≤ 2	Severely wet	0	0	35.08	0	3.81	2.40
SPEI ≥ 2	Extremely wet	0	0	15.35	0	0	0.23

4.3.2.2. Effect of the 2012 spring heat wave in eastern North America

We analyzed the early spring for 2012 in North America, focusing on southeastern of The United States (US). We calculated the interannual anomalies for the phenological metrics and climatic variables for each pixel to assess the spatial patterns of the phenological responses to the climatic extreme. Previous studies (Ellwood et al., 2013; Karl et al., 2012) considered the spring SoS anomaly in 2012 as the earliest spring recorded since 1900 across North America (Figure 4.8a). Karl et al. (2012) reported that

the anomaly was driven by a strong and stable high-pressure anticyclone that remained over much of the northeast from late February to April, causing record high temperatures (Figure 4.8b, c) and phenological advancement.

Spring in many central and eastern areas of North America began between -15 and -30 d (unstandardized anomalies) before mean SoS for the time series analyzed (2000–2018) (Figure 4.8c). The anomalies for the timing of SoS were negative in most of the pixels (96.2%) (Figure 4.8a). Figure 4.8c shows the dominant role of temperature in the phenological advancement of SoS in 2012, with mean standardized anomalies >2 °C. Precipitation was slightly negatively anomalous before the timing of SoS in 2012, but with no water stress, and the majority of the pixels (73%) indicated a normal SPEI between -1 and 1 (Table 4.3).

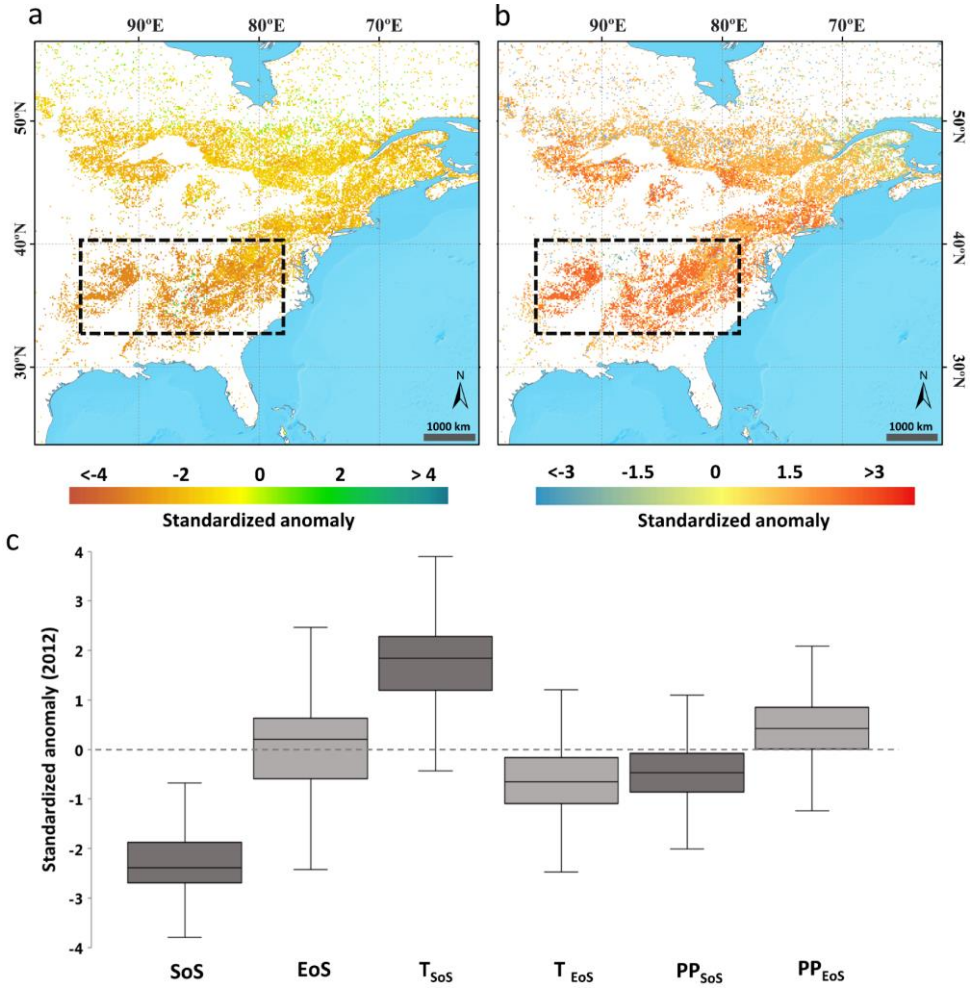

Figure 4.8**:** Distribution of the anomalies for the timing of SoS (a) and (b) preseason mean temperature in eastern USA for 2012. The boxplots (c) show the standardized anomalies between phenology and the climatic variables (SoS in dark gray, and EoS in light gray).

4.3.2.3. Effect of the late 2005 cold wave in the Balkans

Unlike the two previous analyses, this third case refers to a delayed SoS due to a negative temperature anomaly for the timing of the preseason. Figure 4.9a and b shows the SoS anomaly and preseason mean temperature for 2005, respectively. The positive anomalies of SoS affected much of central and eastern Europe, especially the northern Balkan Peninsula and Carpathian Mountains, where positive anomalies were 10 d in most of the pixels (80.3%) (Figure 4.9a, c). The average standardized temperature anomaly was ~-1 °C (Figure 4.9b,c), which greatly delayed the timing of SoS (~10 d). This delay also coincided with a positive SPEI. Eighty percent of the pixels represented moderate or very high humidities prior to SoS (Table 4.3).

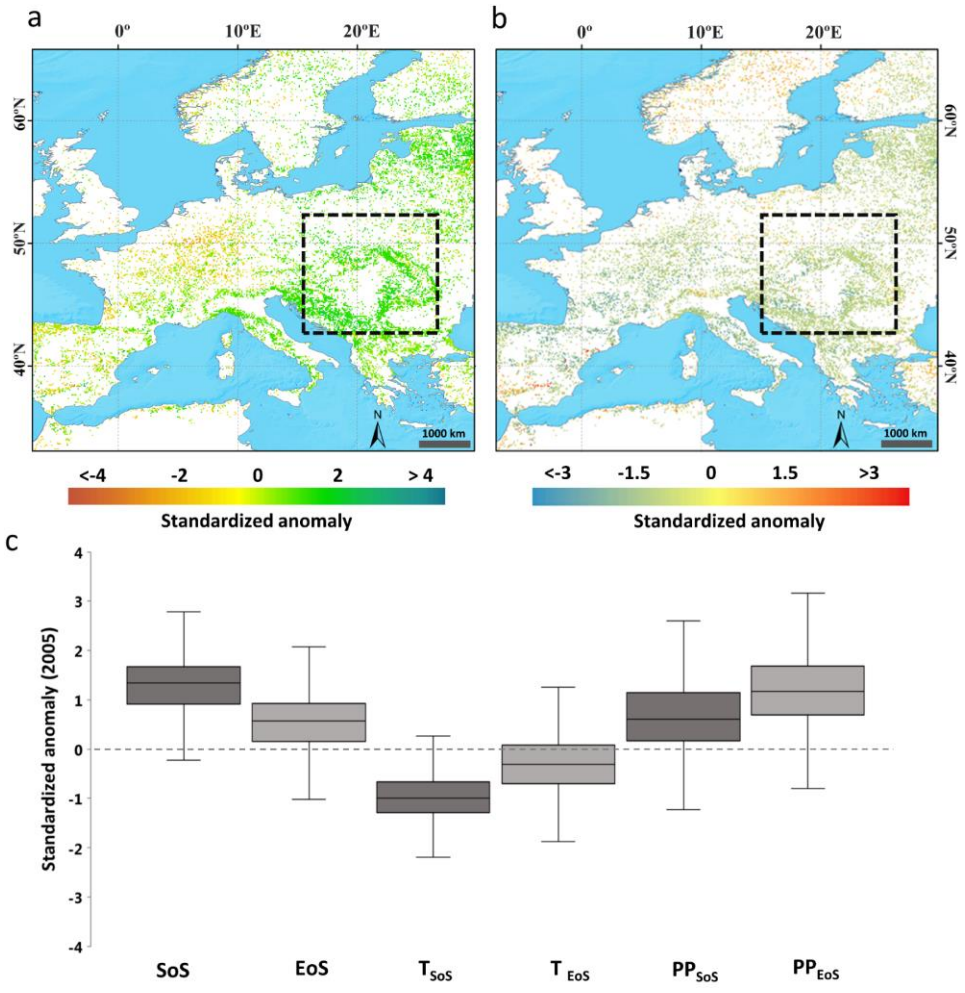

Figure 4.9**:** Distribution of the anomalies for the timing of SoS (a) and (b) preseason mean temperature in the Balkans for 2005. The boxplots (c) show the standardized anomalies between phenology and the climatic variables (SoS in dark gray, and EoS in light gray).

4.4. Discussion

Climatic projections indicate a likely increase in temperatures in much of the world, especially at the higher latitudes of the Northern Hemisphere (IPCC, 2007, 2012). Recent studies (Du et al., 2019; Lin et al., 2017) have also found that extreme climatic events have increased in frequency, intensity, and duration, consistent with IPCC projections, which will affect many ecosystems, particularly vegetation. Climatic variability adds uncertainty in analyzing and predicting the impacts of climate change on vegetation phenology (Ma et al., 2015; Peñuelas et al., 2009; Siegmund et al., 2016).

Previous studies have attributed the recent shifts in phenology to climate change and the effects of variations in temperature and precipitation (de Beurs and Henebry, 2005; Shen et al., 2015; Vitasse et al., 2009; Zhou et al., 2001). Assessing the pattern of distribution, the variability of phenology, and the correlations between phenology and climatic variables is crucial for understanding the potential effects of future climate change (Miao et al., 2017). Remotely sensed data have been widely used to assess trends in phenological time series and their responses to climatic variability. Numerous studies have reported that the phenological trends from 2000 to 2018 were lower than the rates of change from 1980 to 1999 (Jeong et al., 2011; Wang et al., 2015; Zeng et al., 2011; Zhao et al., 2015). De Beurs et al. (2005) and Piao et al. (2006) reported that SoS advanced by 6.6 and 7.9 d/decade in North America and China, respectively, between 1982 and 1999. Jeong et al. (2011) and Zeng et al. (2011), however, found that phenological trends declined significantly after 2000, with an advanced for the timing of SoS of 0.1–0.2 d/decade, respectively, consistent with our results. Some studies have even reported delays of 1 d/decade in the timing of SoS after 2000, specifically in western North America (Wang et al., 2015; Zhao et al., 2015).

In our study we used land-surface phenological metrics at the continental scale derived from LAI time series (2000–2018) of the SPOT-VGT and PROBA-V sensors (Bórnez et al., 2020a, 2020b). Since the time series start in 2000, the detected trends are limited to reduced areas. For this reason, we mainly target on analyzing the correlations between phenology and climatic variables and analyzing the responses of phenological anomalies to recent climatic events.

Most previous studies have only emphasized the role of preseason temperature in determining SoS, because an increase in the advance of SoS is a consequence of global warming (Cleland et al., 2017; Kang et al., 2018; Monahan et al., 2016; Peng et al., 2017; Piao et al., 2006; Zhang et al., 2007). Other studies focusing on EoS have recorded a delay in senescence, which led to longer growing seasons in some areas of Eurasia and North America (Jeong et al., 2011; Liu et al., 2016). We focused on analyzing the responses of phenology to mean preseason and presenescence temperatures, accumulated precipitation, and drought across the deciduous forests in the Northern Hemisphere. Our results indicated that anomalies of temperature and precipitation controlled the changes in phenological metrics in the deciduous forests, consistent with previous studies (He et al., 2018; Zhou et al., 2016), particularly the anomalies of SoS strongly associated with the changes in mean preseason temperature, so this climatic variable may have been the main cause of the advance or delay in the start of the growing season, affecting 72.1% of the study area (mean r of -0.31) ($P<0.05$). Correlations were significantly negative in 57% of the pixels ($P<0.05$), i.e. an advance or delay in SoS due to higher or lower temperatures, respectively.

The effects of the relationships between the climatic variables and vegetation on the timing of EoS were more complex. The timing of the end of the growing season in response to temperature was generally delayed in most pixels. Water stress associated with droughts during summer, however, advanced EoS in some regions such as southern Europe (Figure B2 and Figure 4.6) with negative anomalies longer than -20 d for the timing of EoS throughout most of Europe (in 2003), consistent with other studies (Angert et al., 2005; Hmimina et al., 2013; Li et al., 2019; Wang et al., 2011).

The influence of drought on the timing of EoS was lower in humid and cold regions (such as those pixels located between 55 and 80°N) than drier regions, such as areas with a Mediterranean climate (Figure. S3). The availability of water in Mediterranean areas was the primary limiting resource for the timing of EoS, but temperature and other variables such as photoperiod may have a larger role at higher latitudes.

The distribution of the regression coefficients between the anomalies in phenology and the climatic variables were highly spatially heterogeneous, due to the spatial and latitudinal heterogeneity in climate and to the biological characteristics of the species,

which could account for the variable responsiveness to climate (Hou et al., 2015; Peñuelas et al., 2002). The responses of phenology to climate, especially to climatic extremes, also vary with climatic gradients, type of event, and biome, and even among individuals of the same species (Ma et al., 2015; Siegmund et al., 2016).

These phenological changes may affect climate change by the feedbacks between vegetation and climate (Beer et al., 2010; Bonan et al., 2015; Ceccherini et al., 2014; Lian et al., 2020; Peñuelas et al., 2009). For example, climatic anomalies or extremely high temperatures (such as during heatwaves) alter vegetation growth due to both the high temperatures and lower amounts of soil moisture (Ciais et al., 2005; Reichstein et al., 2007; Seneviratne et al., 2006). Altered vegetation growth greatly affects the uptake of CO_2, depending on the availability of soil water, regional characteristics, and plant species (Peñuelas et al., 2009). Deficits in soil moisture lead to lower water evaporation, which lowers the release of latent heat from the land, prevents the development of clouds, and may consequently intensify droughts because precipitation is reduced (Berg et al., 2016; Buermann et al., 2013, 2018), which could also involve teleconnections between areas (Lian et al., 2020).

4.5. Conclusions

This study comprehensively analyzed the response of vegetation to climatic anomalies in the Northern Hemisphere and assessed the impact of extreme climatic events on deciduous phenology. Our results suggest that deciduous phenology in the Northern Hemisphere is very sensitive to shifts in temperature, especially for the timing of SoS, but also indicate the importance of water availability to the timing of EoS as the increase in drought stress contribute to its advance throughout some regions (e.g., southern Europe). Results also revealed that climate extremes events exert severe impacts on vegetation phenology both for the timing of SoS and EoS. These findings highlight the need to develop strategies focused on mitigating future climate changes on vegetation and their monitoring. The interactions of temperature, precipitation, drought, and phenology with other variables such as solar radiation, soil type, soil moisture, and the coupling between variables and feedbacks between vegetation and climate warrant future research.

5

General discussion and conclusions

5.1. Discussion

My doctoral thesis is framed within the increasing interest in the retrieval of Land Surface Phenology (LSP) from remote sensing and in the study of their changes and interactions with climate change (Ceccherini et al., 2014; Peñuelas et al., 2009; Richardson et al., 2013). I aimed to (i) improve estimation of Land surface Phenology (LSP) from satellite time series, (ii) evaluate the uncertainty associated to its estimation, and (iii) assess phenology-climate relationships in a climate change context.

5.1.1. Ground based phenological estimation techniques and challenges of LSP validation

Validating LSP is challenging due, in part, to the differences in the definition of satellite metrics and ground phenophases (White et al., 2009, Schwartz and Hanes, 2009). The timing of vegetation seasonality has traditionally been recorded by researchers and volunteers from in situ measurements by observing the leaf growth from bud to fall. These observations have proven to be useful to validate the satellite estimates. However, human-based ground observations of phenological transition dates are not uniform and depend on the criterion used for visual inspection which may induce uncertainties, despite efforts to establish protocols for monitoring phenophases (Denny et al. 2014, Tierney et al. 2013). Some studies have reported differences of ~7 days among different observers for the same place and species (Klosterman et al., 2014).

In recent years near-surface remote sensing techniques have emerged, providing an alternative to human observations to monitor vegetation phenology (Hufkens et al., 2012; Richardson et al., 2009; Sonnentag et al., 2012), including digital cameras and continuous flux measurements from eddy covariance towers. Near-surface remote sensing provides a new perspective for estimating phenology at the landscape level, becoming an advanced technique to validate remote sensing estimates by using consistent and continuously measurements at high temporal frequencies (e.g. PhenoCam imagery) across broad spatial scales. In particular, in this work I used PhenoCam Network and the existing eddy covariance flux data from FLUXNET, and the results

were significantly more robust compared to those observed with PEP725 or USA-NPN, especially for the timing of EoS, with a RMSE of 10 d and 12 d (FLUXNET and PhenoCam) compared with 25 d and 27d (USA-NPN and PEP725) when the threshold method was used.

The validation of land surface phenology with ground observations presented also some difficulties associated to the spatial distribution and the spatial representability of the data. The ground measurements represent the phenology for a limited number of individual plants that are not necessarily the most representative species of the 1-km satellite pixels. Conversely, satellite phenology at 1-km resolution represented an integrated response across landscapes with diverse species and phenological behaviors. The phenology of each species and their characteristics (sizes, ages, homogeneity), though, influenced the satellite signal, depending on its abundance within the pixel sampling area and on the timing of their phenophases (Delbart et al., 2015). Chapter 2 showed that statistics of the comparison between LAI V2 derived EoS using the percentile method and ground measurements improved significantly when the analysis was restricted to homogeneous forest sites. The scale difference between ~1km VEGETATION and PROBA-V satellite pixels and the deca-/hectometric footprints of PhenoCam cameras and flux towers may also introduce some difficulties for the comparison in Chapter 3. This is partially minimized because our validation is limited to deciduous forests which tend to form large patches of the same vegetation type, reducing the influence of mixed or border pixels (Richardson et al., 2006, 2009; Ryu et al., 2014).

5.1.2. Sensitivity of LSP to the satellite time series

Unlike ground observations and near-surface measurements, which only cover a small area for a reduced number of trees, the development of satellite remote sensing has allowed phenological dates to be estimated from local to global scale at different temporal periods, using time series of vegetation indices and biophysical variables (e.g. Verger et al., 2016; Zhang et al., 2006). Traditionally, the most used index for estimate phenology from satellite has been the Normalized Difference Vegetation Index (NDVI) (Rouse et al., 1974). However, NDVI is sensor dependent and saturates for high amounts

of vegetation. In Chapter 2 I derived land surface phenology from Copernicus Global Land time series not only from NDVI time series but also using three biophysical variables: LAI, FAPAR and FCOVER (version I and version II products) to determine the variable that best allows to estimate LSP. Comparison with ground data showed that phenological metrics extracted from the CGLS LAI Version 2 (V2) time series performed the best as compared to other biophysical variables and NDVI vegetation index or previous version V1 of the CGLS products. For this reason, I used LSP derived from LAI V2 CGLS in Chapter 2 and Chapter 3.

The estimation of LSP from VI or biophysical variables presents several challenges. Firstly, the presence of clouds has been a major difficulty for acquiring high temporal resolution image time series of vegetation over the same location. Therefore, data smoothing approaches are employed as a necessary procedure in image preprocessing (Reed et al., 1994; Bradley et al., 2007), and the method selected for this purpose can influence the performance of the phenology extraction from the reconstructed time series (Atkinson et al., 2012; Kandasamy et al., 2013; Verger et al., 2016). Several studies have used existing software tools to analyze and reconstruct time series data (Heumann et al., 2007; Jia et al., 2014; Rodrigues et al., 2013) that include TIMESAT (Jönsson and Eklundh, 2004), SPIRITS (Bórnez et al., 2020; Rembold et al., 2015), Phenosat (Rodrigues et al., 2012), Hants (Zhou et al., 2015), Crop Phenology (Araya et al., 2018) and QPhenoMetrics (Duarte et al., 2018). In chapter 2, I used SPIRITS software proving the functionalities for the reconstruction of time series data and extraction of phenology for V1 time series (e.g. SoS, EoS) by using the threshold method. However, it is still limited for applying other methods. I found the choice of the smoothing method (Whittaker, BISE or Swets) in SPIRITS software introduced differences of up to 50% in the performance of the phenology metrics.

5.1.3. Sensitivity of LSP to the phenological extraction method

The second challenge for satellite estimates relates to the variety of methods available to derive LSP estimates, which can lead to very different results (de Beurs and Henebry, 2010; Zeng et al., 2020). This includes thresholds (Myneni et al., 1997; White et al., 1997), moving averages (Reed et al., 1994), first derivatives (Tateishi and Ebata, 2004;

White et al., 2009], and curvature of piecewise logistic functions (Zhang et al., 2003). The choice of the most appropriate approach is important to establish a robust, quantitative method that best estimates the phenology, especially when the goal is the comparison with climate variables (de Beurs and Henebry, 2010). However, it is difficult to determine the best method for all datasets, vegetation types or spatial scales as each method has its own strengths and limitations (Atkinson et al., 2012; de Beurs and Henebry, 2010).

White et al. (2009) analyzed different methods to derive LSP from satellite time series across North America using 8 km 15-day composite AVHRR NDVI data for 1982–2006, and found that the differences between the methods were up to ±60 days and none of the methods performed uniformly well across the different regions and species. In this sense, by focusing on deciduous forest in the Northern Hemisphere, I tested four state of the art methods to extract phenological metrics: thresholds, logistic function, derivative and moving average, and found (1) that threshold method bears a closer resemblance to ground observations than the other methods, and (2) that the differences between methods were up to ±40 days when comparing with ground observation and near-surface estimates over deciduous broadleaf forests in the Northern Hemisphere for the period 1999-2017 (Bórnez et al., 2020a, 2020b).

5.1.4. Monitoring the responses of vegetation phenology to climate change

The phenology estimated from LAI time series offered an approach to connect vegetation growth to its climate drivers, providing a quantitative description of vegetation variation as a consequence of climate change. Global change has significantly affected vegetation and it is reflected as anomalies in the phenological and climatic time series (Ceccherini et al., 2014; Keenan et al., 2014; Mu et al., 2011). Therefore, the study of LSP and the analysis of changes in the climatic variability is serving the scientific community to analyze vegetation and climate from local to global scale (White et al., 2009).

Remote sensing plays an important and increasing role in the assessment of LSP, especially important because the changes in phenology can also be used as a sensitive indicator of climatic changes (Chmura et al., 2019; Inouye, 2008; Moore et al., 2015).

Numerous studies have reported shifts in vegetation phenology as a response to climate anomalies, especially related to changes in temperature in various areas of the Northern Hemisphere (e.g. Cleland et al., 2007; Fitchett et al., 2015, Piao et al., 2019; Shen et al., 2014). Thompson and Clark (2008) reported phenological advances of 3–8 days per 1ºC increase in temperature analyzing data for the period 1772–2006 in England. In Europe, Menzel et al. (2006) reported an advancement of ~2.5 days for the timing of SoS, and a delay of ~1 day for the timing of EoS associated with 1ºC increase in temperature. Significant phenological changes have also been found in areas of the USA advanced ~8 days in the period 1885–2002 (Primack et al., 2004).

Assessing the pattern of distribution, the variability of phenology, and the correlations between phenology and climatic variables is crucial for understanding the potential effects of future climate change. In this sense, the results (Chapter 4) showed that the climatic drivers play a strong role on regulating vegetation phenology. Temperature anomalies had the greatest impact on the SoS. This finding agrees with other studies which indicate that the SoS was mainly driven by temperature (Miao et al., 2017; Ramos et al., 2015; Wang et al., 2015).

Chapter 4 also focused on understanding the responses of vegetation ecosystem to climate extreme events. A better understanding of the sensitivity of vegetation to climate change and to the extreme climate events, as well as its feedback at different spatial scales is one of the major research challenges over the next few years (Peñuelas et al., 2009; Richardson et al., 2013). This sensitivity is particularly relevant because the frequency and intensity of climate extreme events have increased across a wide range of spatial scales in recent decades (Trumbore et al., 2015). Among these extreme events, droughts and heat waves stand out for their adverse effects on vegetation over large areas of the Northern Hemisphere, and the IPCC reports indicate that future extreme events (Brown et al., 2008; Meroni et al., 2013) will become more intense than those experienced in the past century (IPCC, 2007, 2012, 2014). In chapter 4, I report that these extreme climate events, especially heat waves, cause abrupt changes in vegetation phenology (e.g. advanced of ~20 days for the timing of SoS (2012) over large areas of North America).

5.1.5. Future research directions

The results of my PhD thesis show a consistent correspondence between the phenology estimated from SPOT-VGT and PROBA-V LAI and the continuous monitoring from near-surface observations, despite the mismatch between the camera/tower field of view and the satellite pixels. However, satellite LSP still has limitations regarding the accurate monitoring of phenology shifts, at least in terms of specific plant species, and it is even more challenging in heterogeneous forests. To analyze small areas or regions, an alternative approach to bridging in situ phenology with LSP could be attempted using Landsat TM/TME data at high spatial resolution (30 m), and a repeat coverage of 16 days (Fisher et al. 2006; Fisher and Mustard 2007). Recent studies (Descals et al., 2020; Lange et al., 2017; Jonsson et al., 2018; Vrieling et al., 2018) have also demonstrated the potential of Sentinel-2 for vegetation phenology due to the improvement in spatial (10-60 m) and temporal resolution (<5d). In addition, the use of new sensors onboard unmanned aerial vehicles (UAVs) to monitor LSP is continually increasing. The use of these remote sensing tools for vegetation monitoring, in combination with other sensors with greater spatial and temporal coverage, would bring new opportunities to assess satellite LSP at local scale (Berra et al., 2021; D'Odorico et al., 2020), leading to greater utility of phenological estimates.

Long term data records from the combination of Landsat and Sentinel-2 high spatial resolution data are expected to contribute to a better understanding of phenology-climate relationship at local and regional scales. A better interpretation of shifts in the sensitivity of vegetation to climate change will result from the improvements in Earth observation data and land surface models, as well as the analysis of the interactions of temperature, precipitation, drought, solar radiation, and phenology with other variables such as soil type or soil moisture, and the coupling between variables and feedbacks.

5.2. Conclusions

Chapter 2

- The phenology derived from Copernicus Global Land Service (CGLS) products derived from 1km VEGETATION and PROBA-V data improved other existing

- products including MODIS-EVI (MCD12Q2) when compared with available ground observations from PEP725 and USA National Phenology Network (NPN). The phenology derived from the Leaf Area Index (LAI) or the Fraction of Vegetation Cover (FCOVER) was more closely related to actual ground observation than the Fraction of Absorbed Photosynthetically Active Radiation (FAPAR) or the Normalized Difference Vegetation Index (NDVI) derived phenology.

- Noise and missing data in satellite time series can introduce significant uncertainties in the estimation of phenological metrics. The choice of the method for data filtering, smoothing and gap filling can have a large impact on the accuracy of the phenology extracted from the reconstructed time series.

- The LSP was found to be highly sensitive to the retrieval algorithm and processing chain. The retrieved phenology performed the best using LAI Version 2 (V2) due to the improved continuity (no missing data in V2) and smoothness as compared to Version 1 products.

- The threshold method agreed the best with ground measurements. The validation over ground observations indicated that the 30% threshold of the LAI amplitude was optimal for detecting Start of Season (SoS) but that a 40% threshold was more suitable for detecting End of Season (EoS). The logistic function and, specially, the moving-average approaches showed lower accuracy and higher bias: systematic advance in the timing of the SoS as compared to ground measurements of leaf out.

- The lower performances for the EoS as compared to the SoS is associated to higher uncertainties of both satellite (atmospheric effects, snow and poor illumination conditions) and ground (the timing of leaf colouring is more subjective and difficult to identify than spring phenophases like leaf unfolding) phenology for autumn.

- Ground observations of vegetation phenology provide a large volume of data across diverse ecosystems. However, there still exists an enormous challenge in

- quantifying its uncertainties relating the definition of the phenophases and the spatial distribution.

Chapter 3

- Near-surface digital cameras (PhenoCam) and flux measurements (FluxNet) have been shown to be valuable tools to interpret, evaluate and validate the phenology results derived from time series of LAI, as a support of traditional ground observations.

- PhenoCam and FluxNet provide continuous time series and agree with the estimated LSP when the same method is used to extract the phenology metrics both to ground and satellite time series. This avoids some of the issues identified in Chapter 2 related to the differences in the definition of satellite phenology metrics and ground phenophases. It allows a more straightforward comparison with satellite derived phenology.

- Thresholds and logistic function resulted the most robust methods and the phenological metrics extracted from CGLS LAI V2 time series were strongly correlated with those derived from PhenoCam and FLUXNET, showing generally a higher accuracy for SoS than EoS.

- LAI V2 using percentiles 30 and 40 accurately reproduced the interannual variation of the SoS and EoS, and usually provided an intermediate solution between PhenoCam and FLUXNET estimates with differences lower than 10 days.

- Results validate the land surface phenology estimated from CGLS LAI V2 time series, as well as the robustness of PhenoCam and FLUXNET data to analyze vegetation phenology.

Chapter 4

- Phenological estimates from the LAI time series have considerable potential for characterizing and analyzing the response of vegetation to climate variables at large scale.

- Deciduous forest phenology in the Northern Hemisphere is very sensitive to shifts in temperature and precipitation. Especially important is the role of pre-season temperature for the timing of SoS. Temperature anomalies are the main cause of the observed anomalies in the start of the growing season, affecting more than 70% of the study area.

- The response of vegetation to temperature for the timing of EoS were complex, and it was generally delayed in most pixels. However, water stress associated with droughts during summer could advance the EoS in some regions such as Southern Europe.

- The influence of drought on the timing of EoS was lower in humid and cold regions than drier regions, such as areas with a Mediterranean climate. The availability of water in Mediterranean areas was the primary limiting resource for the timing of EoS, where vegetation responds to drought at short time-scales.

- Results also revealed that climate extremes events exert severe impacts on vegetation phenology both for the timing of SoS and EoS, and these findings highlight the need for developing strategies focused on mitigating future climate changes on vegetation and its monitoring

A

Appendix Chapter 3

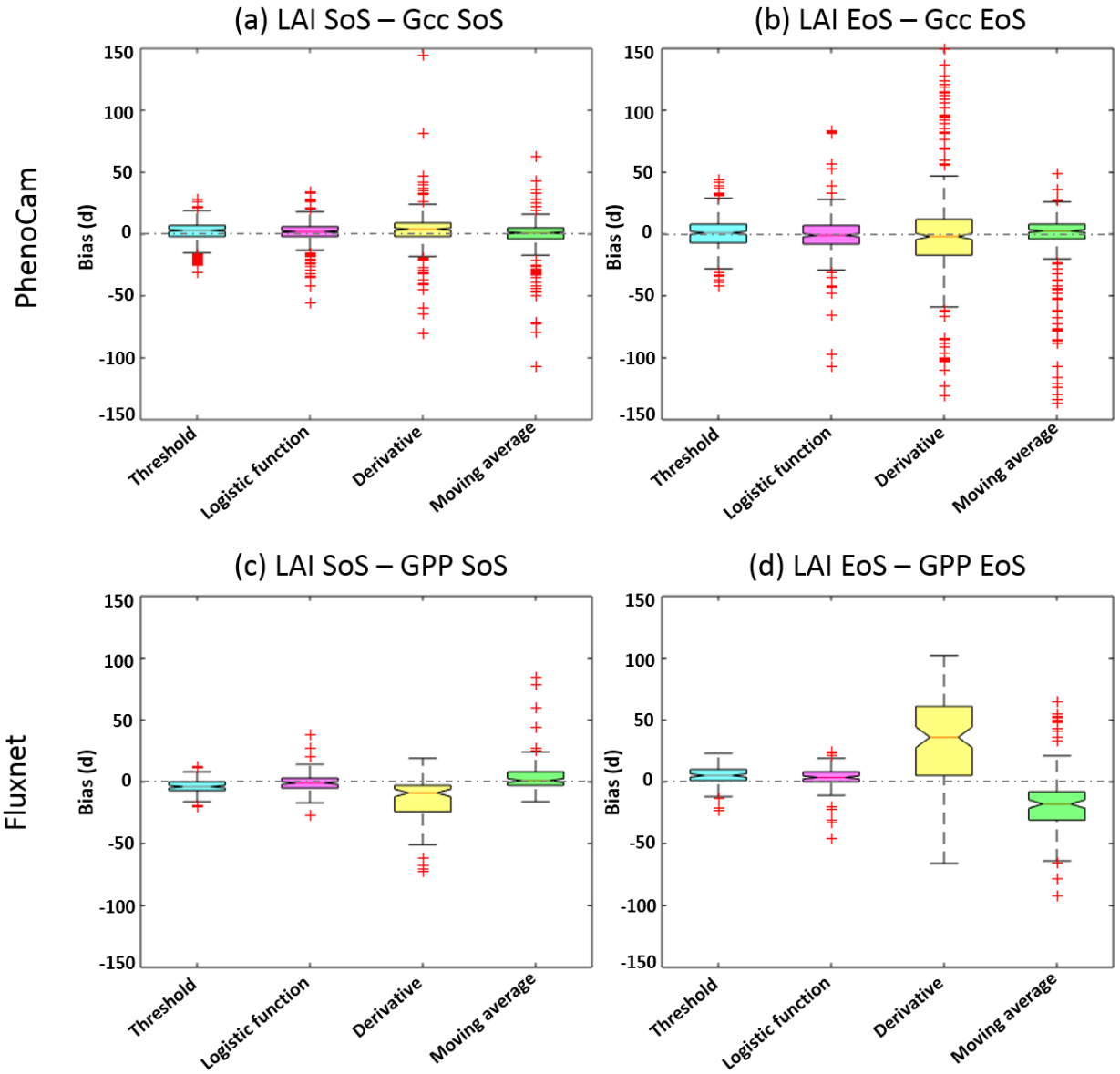

Figure A.1: Boxplots of the bias errors of satellite-based minus the near-surface estimates of SoS (a) and EoS (b) over the 64 PhenoCam sites (a,b) and the 16 FLUXNET towers (c,d) for the four extraction methods: threshold method (the 30th percentile of annual amplitude for the SoS (a, c) and the 40th percentile for the EoS (b, d)), the logistic-function, first derivatives and moving-average. An elongated boxplot indicates a larger dispersion of the average bias.

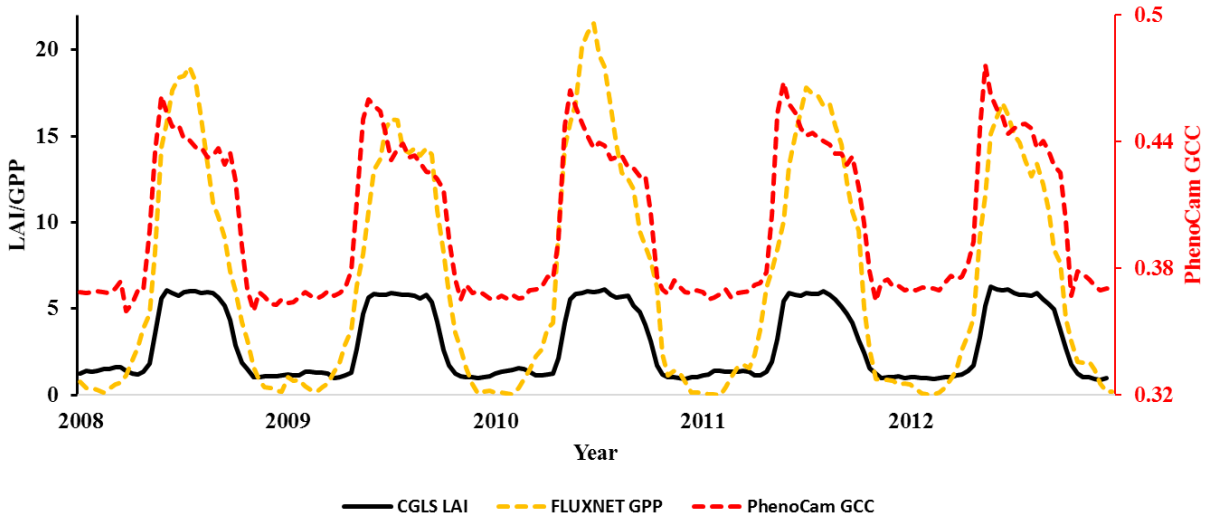

Figure A.2: Time series of CGLS LAI, PhenoCam GCC and FLUXNET GPP for the Harvard Forest site (42.5378N, -72.1715O) over the 2008-2012 period.

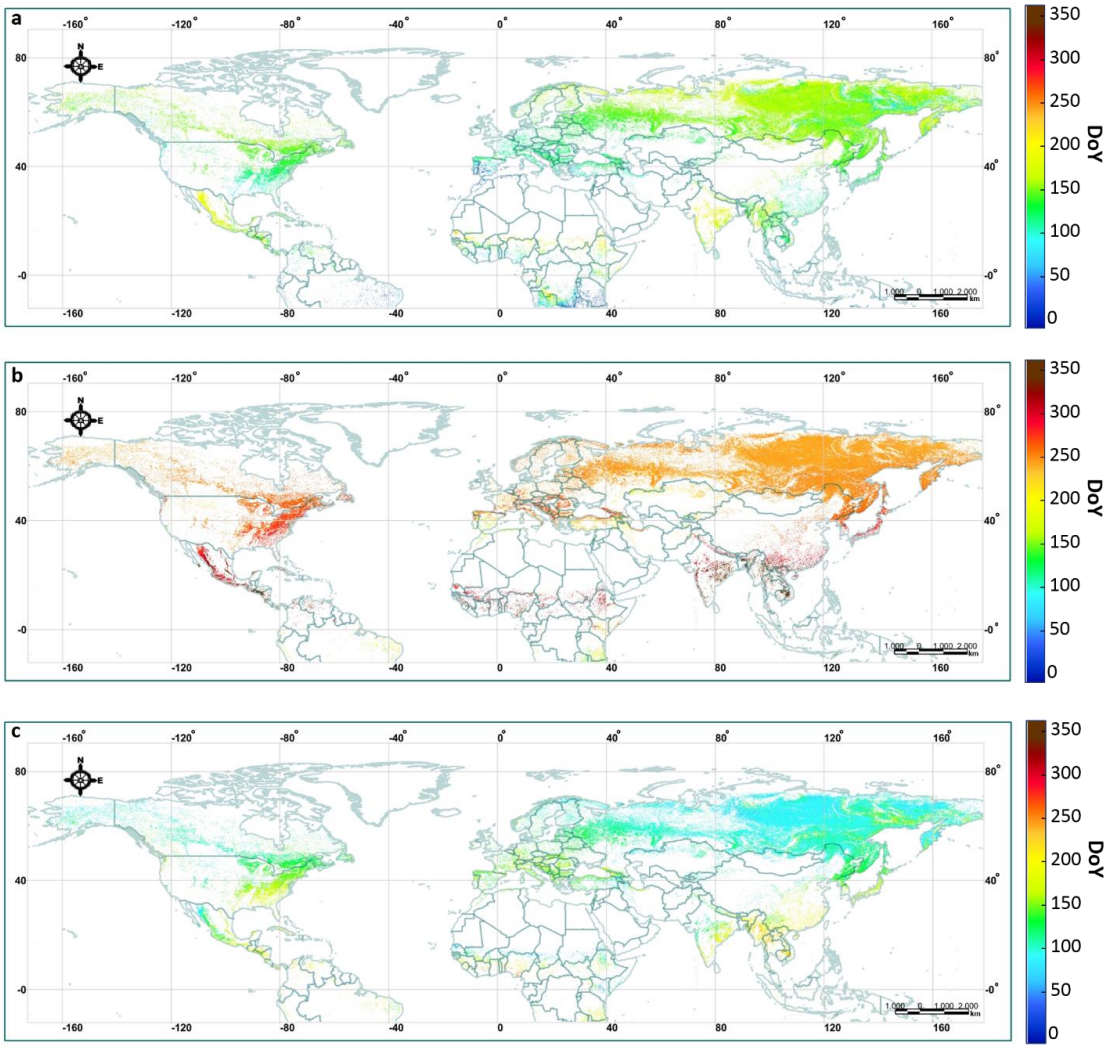

Figure A.3: Maps of average SoS (a), EoS (b) and LoS (c) derived from CGLS LAI V2 time series (1999-2017) using the threshold method (30th percentile of annual LAI amplitude for SoS and 40th percentile for EoS). The maps show the estimated phenology in deciduous or mixed forest based on the annual C3S Global Land Cover for the year 2018 (http://maps.elie.ucl.ac.be/CCI/viewer/download.php). The continental areas in white are lakes, deserts, agricultural areas and evergreen forests. The phenology was not computed for pixels with very limited seasonality: when the annual amplitude ((max (LAI) – min (LAI)) was lower than the 30% of the median value in the time series (0.3 * $LAI_{50^{th}}$). For pixels with multiple growing seasons, we computed the phenological metrics for the growing season having the highest LAI amplitude.

Table A.1: Characteristics of PhenoCam (Richardson et al., 2018) and FLUXNET (fluxnet.fluxdata.org) sites. The Start date and End date indicates the period of available data. MAT is mean annual temperature and MAP is mean annual precipitation based on climate data are from WorldClim. Primary and secondary vegetation types are as follows: AG = agriculture; DB = deciduous broadleaf; DN = deciduous needleleaf; EB = evergreen broadleaf; EN = evergreen needleleaf; GR = grassland; MX = mixed vegetation (generally EN/DN, DB/EN, or DB/EB); SH = shrubs; TN = tundra (includes sedges, lichens, mosses, etc.); WL = wetland.

Dataset	Site name	Site Description	Latitude (°)	Longitude (°)	Elevation (m ASL)	Start date	End date	MAT (°C)	MAP (mm)	Primary Veg.	Secondary Veg.	IGBP Landcover	Acknowledgements
PhenoCam	acadia	Acadia National Park, McFarland Hill, near Bar Harbor, Maine	44.3769	-68.2608	158	15/03/2007	31/12/2015	6.5	1303	DBF	EN	5	Camera images from Acadia National Park are provided courtesy of the National Park Service Air Resources Program.
	alligator river	Alligator River National Wildlife Refuge, North Carolina	35.7879	-75.9038	1	03/05/2012	31/12/2015	16.4	1312	DBF	WL	5	Research at the Alligator River flux site is supported by DOE NICCR (award 08-SC-NICCR-1072), DOE-TES (awards 11-DE-SC-0006700 and 7090112), USDA Forest Service (award 13-JV-11330110-081) and USDA-NIFA (award 2014-67003-22068).
	arbutuslake	Arbutus Lake, Huntington Wildlife Forest, Newcomb, New York	43.9821	-74.2332	535	12/06/2008	23/08/2014	4.8	1051	DBF	EN	4	Research at the Huntington Wildlife Forest sites is supported by the New York State Energy Research and Development Authority and the State University of New York, College of

													Environmental Science and Forestry.
	asa	Asa, Sweden	57.1645	14.7825	180	28/10/2010	31/12/2015	6.3	639	DBF	GR	5	Research at the SITES Asa Research Station, Sweden, is jointly supported by the Swedish University of Agricultural Science and the Swedish Research Council (Vetenskapsradet).
	ashburnham	Ashburnham State Forest / Overlook Middle School, Ashburnham, Massachusetts	42.6029	-71.926	292	13/09/2011	31/12/2015	7.1	1147	DBF	EN	5	
	bartlett	Bartlett Experimental Forest, Bartlett, New Hampshire	44.0646	-71.2881	268	04/10/2005	31/12/2015	5.5	1224	DBF	EN	5	Research at the Bartlett Experimental Forest tower is supported by the National Science Foundation (grant DEB-1114804) and the USDA Forest Service's Northern Research Station.
	bartlettir	Bartlett Experimental Forest, Bartlett, New Hampshire	44.0646	-71.2881	268	18/04/2008	31/12/2015	5.5	1224	DBF	EN	5	Research at the Bartlett Experimental Forest tower is supported by the National Science Foundation (grant DEB-1114804) and the USDA Forest Service's Northern Research Station.

	bitterootvalley	Bitterroot Valley, Stephensville, Montana	46.507	-114.091	1017	18/04/2002	31/12/2015	7.2	318	DBF		13	Camera images from the Bitterroot Valley are provided courtesy of the USDA Forest Service Air Resources Management Program.
	bostoncommon	Boston Common, Boston, Massachusetts	42.3559	-71.0641	10	06/05/2010	31/12/2015	9.8	1127	DBF		13	Research at the Boston Common is supported by an Emerson College Faculty Advancement Funds Grant.
	bostonu	Boston University, Charles River Esplanade, Boston, Massachusetts	42.3504	-71.1044	10	14/09/2012	31/12/2015	9.7	1121	DBF		13	
	boundarywaters	Boundary Waters Canoe Area Wilderness, Superior National Forest, Minnesota	47.9467	-91.4955	519	16/12/2005	31/12/2015	2.8	719	DBF	EN	5	Camera images from Superior National Forest are provided courtesy of the USDA Forest Service Air Resources Management Program.
	bullshoals	Bull Shoals Field Station, Missouri State University, Drury-Mincy Conservation Area, M	36.5628	-93.0666	260	20/11/2013	31/12/2015	13.9	1084	DBF	GR	4	
	canadaOA	BERMS Old Aspen Site, Prince Albert National Park,	53.6289	-106.1978	601	16/06/2011	31/12/2015	0.1	445	DBF		5	Research at the Old Aspen Flux Tower site is supported through the Changing Cold Regions Network, with funding from the National

		Saskatchewan, Canada											Science and Engineering Research Council of Canada (NSERC), Greg Neufeld/Eagle Bay Resort
	caryinstitute	Cary Institute of Ecosystem Studies, Millbrook, NY	41.7839	-73.7341	127	08/01/2001	31/12/2015	8.9	1084	DBF		4	
	cedarcreek	Cedar Creek Ecosystem Science Reserve (LTER), East Bethel, Minnesota	45.4019	-93.2042	276	01/12/2009	10/08/2010	6.3	750	DBF		14	Research at Cedar Creek Ecosystem Science Reserve is supported by the National Science Foundation LTER program and the Minnesota Agriculture Experiment Station.
	columbiamissouri	University of Missouri, Ashland Wildlife Research Area, Missouri	38.7441	-92.1997	232	23/01/2009	12/01/1900	12.4	974	DBF	EN	4	
	coweeta	Coweeta Hydrologic Laboratory, USDA Forest Service, Southern Research Station, Otto, N	35.0596	-83.428	680	08/04/2011	31/12/2015	12.5	1722	DBF		5	Research at the Coweeta flux tower is funded through the USDA Forest Service, Southern Research Station; USDA Agriculture and Food Research Initiative Foundational Program, award number 2012-67019-19484; EPA agreement number 13-IA-11330140-044; and the National Science Foundation, Long-Term

													Ecological Research (LTER) program, award #DEB-0823293.
	dollysods	Canaan Valley / Dolly Sods Wilderness, Monongahala National Forest, West Virginia	39.0995	-79.427	1133	21/11/2003	31/12/2015	7.6	1328	DBF		4	Camera images from the Dolly Sods Wilderness, Mononghahela National Forest are provided courtesy of the USDA Forest Service Air Resources Management Program.
	downer woods	UW-Milwaukee Field Station, Downer Woods Natural Area, Milwaukee, Wisconsin	43.0794	-87.8808	213	25/03/2013	31/12/2015	8.2	812	DBF		13	
	dripping springs	Cleveland National Forest, California	33.3	-116.8	400	06/04/2001	26/05/2009	13.2	599	DBF	SH	8	Camera images from Cleveland National Forest are provided courtesy of the USDA Forest Service Air Resources Management Program.
	dukehw	Hardwood Stand, Duke Forest, North Carolina	35.9736	-79.1004	400	31/05/2013	31/12/2015	14.6	1166	DBF		5	
	freeman wood	Woodland Site, Texas State University, Freeman Ranch,	29.94	-97.99	254	27/06/2012	21/03/2014	19.6	862	DBF	EN	8	

		San Marcos, Texas											
	groundhog	Groundhog River, Ontario, Canada	48.2174	-82.1555	350	21/10/2008	17/05/2014	1.2	761	DBF	DB	5	Research at the Groundhog River site was supported by the Natural Sciences and Engineering Research Council (NSERC), the Canadian Foundation for Climate and Atmospheric Sciences (CFCAS), Great Lakes Forestry Centre (GLFC) of the Canadian Forest Service (CFS),
	harvard	EMS Tower, Harvard Forest, Petersham, Massachusetts	42.5378	-72.1715	340	04/04/2008	31/12/2015	6.8	1139	DBF	EN	5	Research at Harvard Forest is partially supported through the National Science Foundation's LTER program (DEB-1237491), and Dept. of Energy Office of Science (BER)
	harvard barn2	Barn Tower, Camera 2, Harvard Forest, Petersham, Massachusetts	42.5353	-72.1899	350	03/08/2011	31/12/2015	6.7	1151	DBF	EN	5	Research at Harvard Forest is partially supported through the National Science Foundation's LTER program (DEB-1237491).
	harvard blo	Below-canopy camera, EMS Tower, Harvard Forest,	42.5378	-72.1715	340	01/04/2009	31/12/2015	6.8	1139	DBF	EN	5	Research at Harvard Forest is partially supported through the National Science Foundation's LTER

		Petersham, Massachusetts											program (DEB-1237491).
	harvardlph	LPH Tower, Harvard Forest, Petersham, Massachusetts	42.542	-72.185	380	15/06/2010	31/12/2015	6.8	1139	DBF	EN	5	Research at Harvard Forest is partially supported through the National Science Foundation's LTER program (DEB-1237491).
	howland2	North Tower (Regrowing clearcut, ca. 1990), Howland Forest, Howland, Maine	45.2128	-68.7418	79	30/03/2008	31/12/2015	5.3	1058	DBF	EN	5	Research at Howland Forest is supported by the Office of Science (BER), US Department of Energy, and the USDA Forest Service's Northern Research Station.
	hubbardbrook	Hubbard Brook Experimental Forest, USDA Forest Service Headquarters, North Woodstock,	43.9438	-71.701	253	16/04/2008	31/12/2015	5.6	1060	DBF		4	Research at the Hubbard Brook Experimental Forest is partially supported by the National Science Foundation's LTER program (grant DEB-1114804) and the USDA Forest Service's Northern Research Station
	hubbardbrooknfws	North Facing Watersheds, Hubbard Brook Experimental Forest, Thornton, New Hampshire	42.958	-71.7762	930	24/09/2012	31/12/2015	7.4	1111	DBF		5	The Hubbard Brook Ecosystem Study is a collaborative effort at the Hubbard Brook Experimental Forest, which is operated and maintained by the USDA Forest Service,

													Northern Research Station, Newtown Square, PA.
	joycekilmer	Joyce Kilmer Slickrock Wilderness, North Carolina	35.257	-83.795	1373	06/06/2006	31/12/2015	9.2	1905	DBF		4	Camera images from the Joyce Kilmer Slickrock Wilderness are provided courtesy of the USDA Forest Service Air Resources Management Program.
	laurentides	Station de biologie des Laurentides, University of Montreal, St-Hippolyte, Quebec	45.9881	-74.0055	350	16/09/2011	31/12/2015	3.7	1066	DBF		5	
	mammothcave	Environmental Learning Center, Mammoth Cave National Park, Kentucky	37.1858	-86.1019	226	01/01/2002	31/12/2015	13.5	1312	DBF		4	Camera images from Mammoth Cave National Park are provided courtesy of the National Park Service Air Resources Program.
	missouriozarks	University of Missouri, Ashland Wildlife Research Area, Missouri	38.7441	-92.2	219	05/03/2012	31/12/2015	12.4	974	DBF		4	Research at the MOFLUX site is supported by the U.S. Department of Energy, Office of Science, Office of Biological and Environmental Research Program, Climate and Environmental Sciences Division. ORNL is managed by UT-Battelle, LLC, for the U.S. Department of

													Energy under contract DE-AC05-00OR22725. U.S. Department of Energy support for the University of Missouri (Grant DE-FG02-03ER63683) is gratefully acknowledged.
	monture	Lolo National Forest, Ovando, Montana	47.0202	-113.1283	1255	08/06/2001	31/12/2015	5	407	DBF	DB	12	Camera images from Lolo National Forest are provided courtesy of the USDA Forest Service Air Resources Management Program.
	morgan monroe	Morgan Monroe State Forest, Indiana	39.3231	-86.4131	275	27/08/2008	31/12/2015	11.2	1087	DBF		4	Research at the Morgan-Monroe Ameriflux site is supported by the US Departement of Energy, Office of Science, Office of Biological and Environmental Research throuth the Ameriflux Management Project administered by Lawrence Berkeley National Lab
	national capital	Park Police Headquarters, National Capital Parks, Washington DC	38.8882	-77.0695	28	25/07/2003	31/12/2015	13.1	1020	DBF		13	Camera images from the National Capital are provided courtesy of the National Park Service Air Resources Program.
	northattleboroma	North Attleboro High School, North Attleboro, Massachusetts	41.9837	-71.3106	60	21/02/2012	31/12/2015	9.4	1202	DBF		14	

	oakridge 1	Chestnut Ridge, Oak Ridge, Tennessee	35.9311	-84.3323	371	12/10/2006	31/12/2015	13.8	1365	DBF		4	Research at Chestnut Ridge is funded by US Dept of Commerce, National Oceanic and Atmospheric Administration, Office of Atmospheric Research, Air Resources Lab, Atmospheric Turbulence and Diffusion Division as part of the Surface Energy Budget Network (SEBN)
	oakridge 2	Chestnut Ridge, Oak Ridge, Tennessee	35.9311	-84.3323	371	12/10/2006	31/12/2015	13.8	1365	DBF		4	Research at Chestnut Ridge is funded by US Dept of Commerce, National Oceanic and Atmospheric Administration, Office of Atmospheric Research, Air Resources Lab, Atmospheric Turbulence and Diffusion Division as part of the Surface Energy Budget Network (SEBN)
	proctor	University of Vermont, Proctor Maple Research Center, Underhill, Vermont	44.525	-72.866	403	11/09/2008	31/12/2015	5	1081	DBF		4	Supported by the Agricultural Experiment Station of the University of Vermont
	queens	Queen's University Biological	44.565	-76.324	126	26/05/2008	31/12/2015	6.4	887	DBF		5	

		Station, Lake Opinicon, Ontario, Canada											
	readingma	Austin Prep School, Reading, Massachusetts	42.5304	-71.1272	100	06/03/2012	31/12/2015	9.3	1107	DBF		13	
	russellsage	Russell Sage State Wildlife Management Area, near Monroe, Louisiana	32.457	-91.9743	20	20/11/2013	31/12/2015	18.1	1341	DBF		5	
	sanford	Sanford Natural Area, Michigan State University, East Lansing, Michigan	42.7268	-84.4645	268	20/12/2013	31/12/2015	8.1	781	DBF		13	
	shalehillsczo	Susquehanna Shale Hills Critical Zone Observatory (CZO), Pennsylvania	40.65	-77.9	310	18/04/2012	31/12/2015	9.8	980	DBF		4	Research at the Penn State Sone Valley Forest is supported by the National Science Foundation EAR 07-25019 (C. Duffy), and EAR 12-39285, EAR 13-31726 (S. Brantley) for the Susquehanna Shale Hills Critical Zone Observatory and the College of Agricultural Sciences, Department of Ecosystem Science and Management.

	shenandoah	Pinnacles Viewpoint, Shenandoah National Park, Virginia	38.6167	-78.35	1037	14/09/2009	31/12/2015	8.4	1222	DBF		4	Funding for the Shenandoah PhenoCam and related research has been provided by the U.S. Geological Survey Land Change Science Program (Shenandoah National Park Phenology Project) with logistical support from the National Park Service in collaboration with the University of Virginia Department of Environmental Sciences.
	shiningrock	Shining Rock Wilderness, Blue Ridge Parkway National Park, North Carolina	35.3902	-82.775	1500	09/08/2000	31/12/2015	9.3	1835	DBF		4	Camera images from the Shining Rock Wilderness are provided courtesy of the USDA Forest Service Air Resources Management Program.
	silaslittle	Silas Little Experimental Forest, New Lisbon, New Jersey	39.9137	-74.596	33	15/03/2011	31/12/2015	11.6	1128	DBF		5	Research at the Silas Little Experimental Forest is supported by the USDA Forest Service, Northern Research Station, NRS-06, Climate, Fire, and Carbon Cycle Sciences.
	smokylook	Look Rock, Great Smoky National Park, Tennessee	35.6325	-83.9431	801	11/02/2000	31/12/2015	12.3	1487	DBF		4	Camera images from Great Smoky National Park are provided courtesy of the National Park Service Air Resources Program.

	smokypurchase	Purchase Knob, Great Smoky National Park, Tennessee	35.59	-83.0775	1550	19/08/2003	31/12/2015	8.7	1786	DBF	GR	4	Camera images from Great Smoky National Park are provided courtesy of the National Park Service Air Resources Program.
	snakerivermn	Hay-Snake State Wildlife Management Area, near Woodland, Minnesota	46.1206	-93.2447	1181	18/11/2009	31/12/2015	4.4	742	DBF		5	
	springfieldma	Academy Hill School, Springfield, Massachusetts	42.1352	-72.586	56	21/02/2012	31/12/2015	9.3	1115	DBF		13	
	thompsonfarm2N	University of New Hampshire, Thompson Farm Observatory, Durham, New Hampshire	43.1086	-70.9505	23	11/01/2009	31/12/2015	8.1	1108	DBF	EN	5	Research at the Thompson Farm Observatory is supported by NH EPSCoR with support from the National Science Foundation's Research Infrastructure Improvement Award (#EPS 1101245) and by the NH Agricultural Experiment Station/USDA NIFA (Hatch project #1006997).
	tonzi	Tonzi Ranch, Amador County, California	38.4309	-120.9659	177	26/10/2011	31/12/2015	15.9	603	DBF	GR	9	Funding for AmeriFlux core site data was provided by the U.S. Department of Energy's Office of Science.

	turkeypointdbf	Mature Deciduous Site, Turkey Point Carbon Cycle Research Project, Ontario, Canada	42.6353	-80.5576	211	10/02/2012	31/12/2015	8	968	DBF		4	
	umichbiological	University of Michigan Biological Station, near Pellston, Michigan	45.5598	-84.7138	230	21/08/2008	31/12/2015	5.9	797	DBF	EN	4	Primary support for the University of Michigan AmeriFlux Core Site (US-UMB) provided by the Department of Energy Office of Science. Infrastructure support provided by the University of Michigan Biological Station.
	umichbiological2	FASET Tower, University of Michigan Biological Station, near Pellston, Michigan	45.5625	-84.6976	240	24/11/2008	31/12/2015	5.9	797	DBF	EN	5	Camera images from Ozark National Forest are provided courtesy of the USDA Forest Service Air Resources Management Program.
	upperbuffalo	Upper Buffalo Wilderness, Ozark National Forest, Arkansas	35.8637	-93.4932	777	02/11/2005	31/12/2015	13	1247	DBF		4	
	usgsreston	USGS Headquarters, Reston, Virginia	38.9471	-77.3676	10	09/03/2012	16/06/2014	12.4	1019	DBF		13	
	uwmfieldsta	University of Wisconsin-Milwaukee Field Station,	43.3871	-88.0229	265	14/03/2013	31/12/2015	7.5	806	DBF		14	Research at the Willow Creek Ameriflux core site is provided by the Dept. Of Energy Office

		Saukville, Wisconsin											of Science to the ChEAS Cluster
	willowcreek	Willow Creek, Chequamegon-Nicolet National Forest, Wisconsin	45.806	-90.0791	521	25/10/2011	31/12/2015	3.9	820	DBF		4	Logistical support is provided by the Woods Hole Research Center.
	woodshole	Woods Hole Research Center, Falmouth, Massachusetts	41.5495	-70.6432	10	14/04/2011	31/12/2015	10	1178	DBF		5	
	worcester	Worcester State University, Worcester, Massachusetts	42.2697	-71.8428	185	13/05/2013	31/12/2015	8.3	1174	DBF	NV	13	
FLUXNET	CA-Oas	Broadleaf tree communities with an annual cycle of leaf-on and leaf-off periods	53.6289	-106.1978	600	1996	2010	0.34	428	DBF		5	
	CA-TPD	The forest is approximately 90 years old. Naturally regenerated on sandy terrain and abandoned agricultural land	42.6353	-80.5577	260	2012	2017	8	1036	DBF			

	DE-Hai	Deciduous Broadleaf Forests	51.0792	10.453	430	2000	2012	8.3	720	DBF			
	DE-Lnf	Leinefelde, deciduous Broadleaf Forests	51.3282	10.3678	451	2002	2012	6.9	895	DBF			
	Dk-Sor	Soroe	55.4858	11.6446	40	1996	2014	8.2	660	DBF			
	IT-CA3	Castel d'Asso3	42.38	12.0222	197	2011	2014	14	766	DBF			
	IT-Col	Collelongo, deciduous forests	41.8494	13.5881	1560	1996	2014	6.3	1180	DBF			
	IT-Isp	Ispra ABC-IS, deciduoust forest	45.8126	8.6336	210	2013	2014	12.2	1300	DBF			
	IT-PT1	Parco Ticino forest	45.2009	9.061	60	2002	2004	12.7	984	DBF			
	JP-MBF	Moshiri Birch Forest Site	44.3869	142.3186		2003	2005			DBF			
	US-Ha1	The Harvard Forest tower is on land owned by Harvard University.	42.5378	-72.1715	240	1991	2012	6.62	1071	DBF			Operation of the US-Ha1 site is supported by the AmeriFlux Management Project with funding by the U.S
	US-MMS	Owned by the Indiana Department of Natural Resources (IDNR), the	39.3232	-86.4131	275	1999	2014	10.85	1032	DBF			AmeriFlux Management Project

		Morgan Monroe State Forest.											
	US-Oho	The Ohio Oak Openings site is located within the Oak Openings Preserve Metropark of northwest Ohio, one of the few remaining oak woodlands/savanna/prairie complexes in the Midwest.	41.5545	-83.8438	230	2004	2013	10.1	849	DBF			USDA FS Southern Global Change Program (cooperative agreements 03-CA-11330147-073 and 04-CA-11330147-238)
	US-UMB	The UMBS site is located within a protected forest owned by the University of Michigan.	45.5598	-84.7138	234	2000	2014	5.83	803	DBF			
	US-UMd	The UMBS Disturbance site is an artificial disturbance site that has recently been created as part of the Forest	45.5625	-84.6975	239	2007	2014	5.83	803	DBF			
	US-WCr	Upland decduous broadleaf forest. Mainly sugar	45.8059	-90.0799	520	1994	2014	4.02	787	DBF			

		maple, also basswood.											

B

Appendix Chapter 4

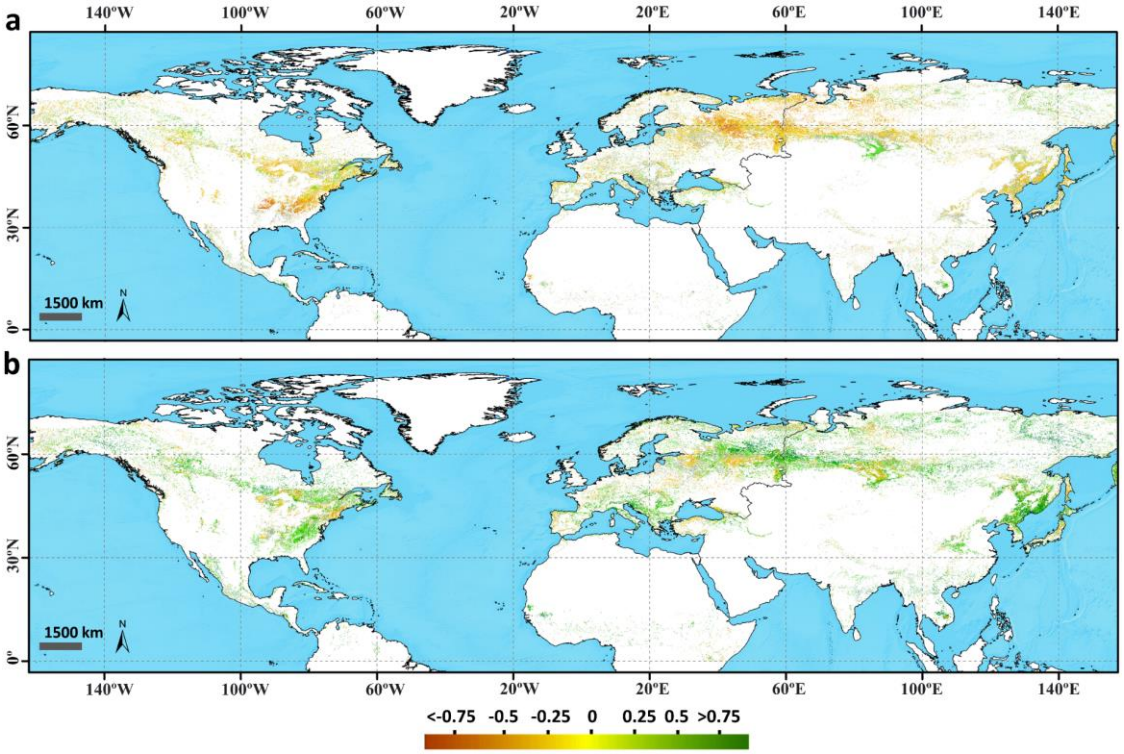

Figure B.1**:** Spatial patterns of partial correlation coefficients between pre-season temperature and (a) SoS and (b) EoS for 2000-2018 in the Northern Hemisphere. The color scale represents the maximum correlation coefficients recorded for each pixel, independently of the SPEI timescale. White indicates unvegetated areas and areas with no deciduous forests, and light gray indicates vegetated areas with nonsignificant correlations (P>0.05).

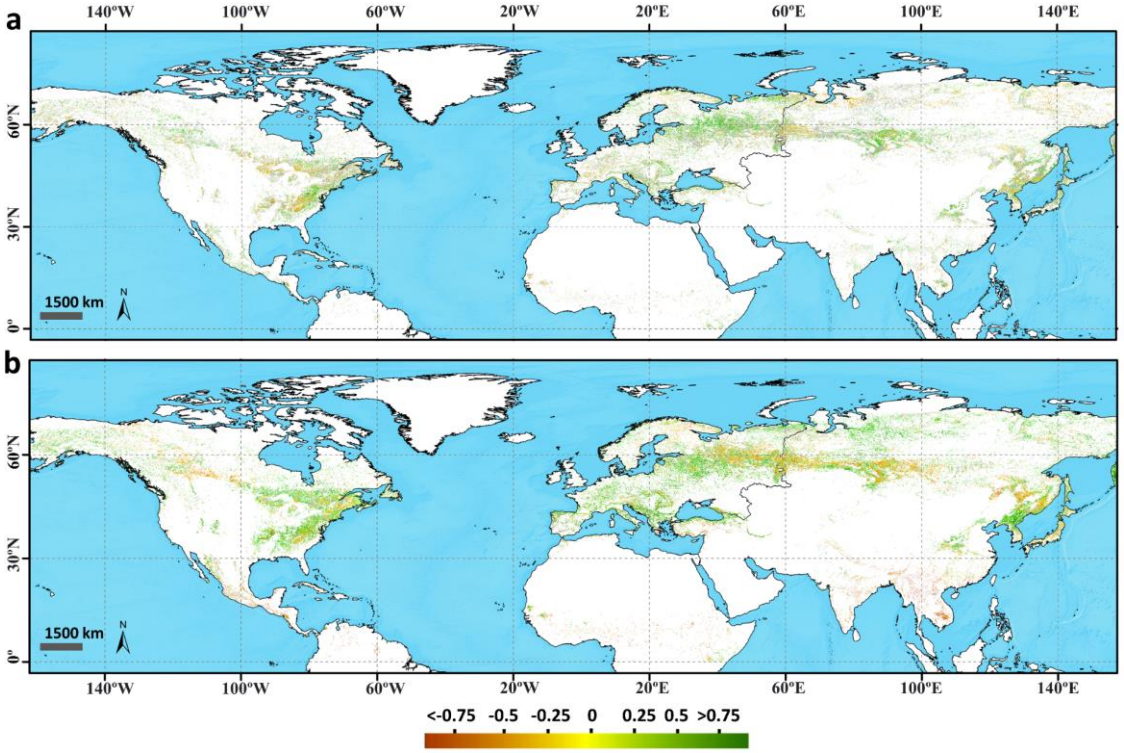

Figure B.2: Spatial patterns of partial correlations between presenescence accumulated precipitation and (a) SoS and (b) EoS for 2000-2018 in the Northern Hemisphere. The color scale represents the maximum correlation coefficients recorded for each pixel, independently of the SPEI timescale. White indicates vegetated areas and areas with no deciduous forests, and light gray indicates vegetated areas with nonsignificant correlations (P>0.05).

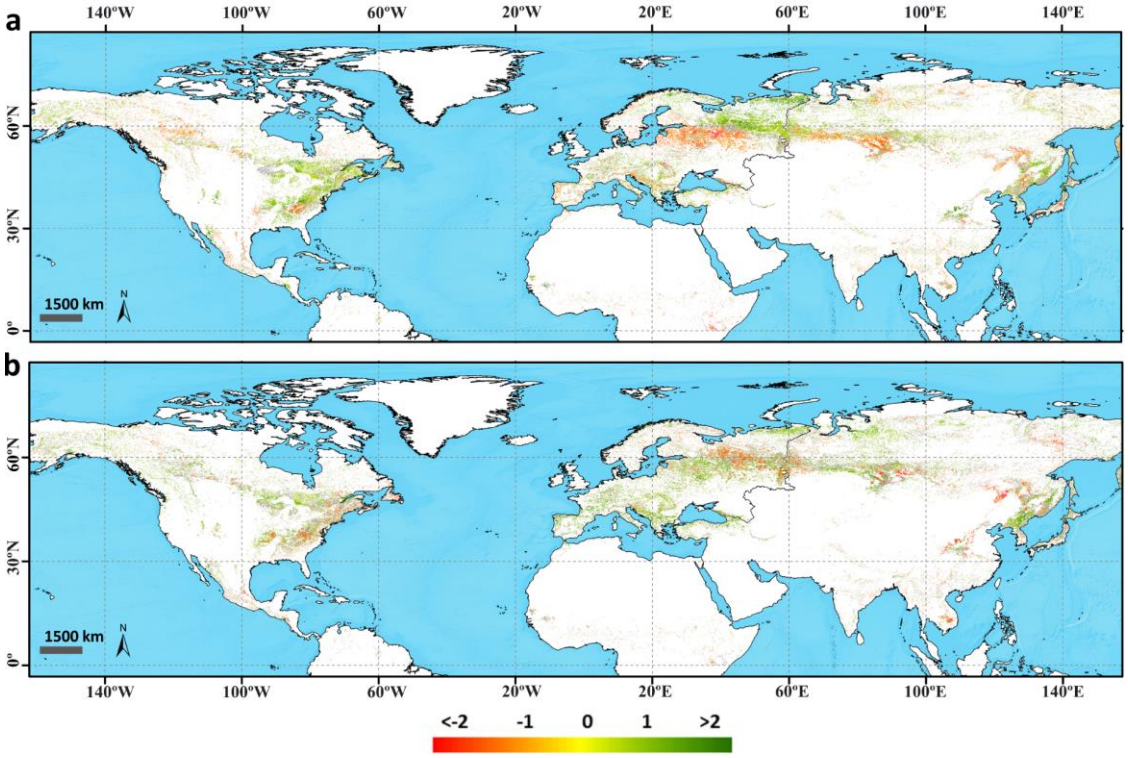

Figure B.3: Spatial distributions of the coefficients (color scale) for the sensitivity of (a) SOS and (b) EoS to pre-season SPEI. White indicates unvegetated areas and areas with no deciduous forests, and light gray indicates vegetated areas with nonsignificant correlations (*P>0.05*).

Table B.1**:** Areas with significant trends (*P≤0.05*) in the time series (2000-2018) for the timing of SoS and EoS. The slope of the regression line is also provided in the table.

Metric	Area (%)	Positive trends (%)	Negative trends (%)	Slope (d/y)
SoS	20.5	38.54	**61.46**	-0.08
EoS	23.8	40.51	**59.49**	-0.1

Table B.2**:** Percentages of pixels with positive and negative correlations (*P≤0.05*) between phenology and climatic variables, indicating whether these correlations represent an advance or delay in phenology. The highest correlation values (positive or negative) are shown in bold.

Metric	Variable	Positive correlation		Negative correlation	
		Advance (%)	Delay (%)	Advance (%)	Delay (%)
SoS	**Temperature**	7.12	**7.82**	**35.8**	21.39
	Precipitation	20.87	**21.43**	**12.36**	7.71
	SPEI	8.65	**8.92**	**6.21**	3.66
EoS	**Temperature**	9.27	**14.3**	7.55	**13.2**
	Precipitation	15.11	**19.33**	13.12	**15.30**
	SPEI	13.2	**15.58**	4.25	**4.79**

Table B.3**:** Percentage of pixels with significant partial correlations between anomalies of phenology, temperature, precipitation, and SPEI at different time lags. Bold values show the timescale in which a higher percentage of significant correlations were found.

Variable	Timescale (months)	SoS (%)	EoS (%)
Temperature	1	47.27	**74.08**
	3	**52.73**	25.92
	6	7.13	5.80
Precipitation	1	**58.69**	31.13
	3	20.77	31.23
	6	20.55	**37.64**
SPEI	1	**33.12**	**30.22**
	3	23.73	27.05
	6	20.99	18.20
	12	22.16	24.53

References

Addabbo, P., Focareta, M., Marcuccio, S., Votto, C., and Ullo, S. (2016). Contribution of Sentinel-2 data for applications in vegetation monitoring. *Acta Imeko*, 5 (2), 44

Ahrends, H., Etzold, S., Kutsch, W., Stoeckli, R., Bruegger, R., Jeanneret, F., Wanner, H., Buchmann, N., and Eugster, W. (2009). Tree phenology and carbon dioxide fluxes: use of digital photography for process-based interpretation at the ecosystem scale. *Clim. Res.*, 39, 261–274

Angert, A., Biraud, S., Bonfils, C., Henning, C.C., Buermann, W., Pinzon, J., Tucker CJ., and Fung, I. (2005). Drier summers cancel out the CO_2 uptake enhancement induced by warmer springs. *Proc Natl Acad Sci USA*, 102 (31), 10823–10827

Aono Y., and Kazui K. (2008). Phenological data series of cherry tree flowering in Kyoto, Japan, and its application to reconstruction of springtime temperatures since the 9th century. *Int J Climatol.*, 28, 905–914

Aono Y., and Tani A. (2014). Autumn temperature deduced from historical records of autumn tints phenology of maple tree in Kyoto, Japan. *Climate in Biosphere.*, 14, 18–28

Araya, S., Ostendorf, B., Lyle, G., and Lewis, M. (2018). CropPhenology: an R package for extracting crop phenology from time series remotely sensed vegetation index imagery. *Ecol. Inf.*, 46, 45–56

Atkinson, C., Brennan, R.M., and Jones, H.G. (2013). Declining chilling and its impact on temperate perennial crops. *Environmental and Experimental Botany*, 91,48–62

Atkinson, P.M., Jeganathan, C., Dash, J., and Atzberger, C. (2012). Inter-comparison of four models for smoothing satellite sensor time-series data to estimate vegetation phenology. *Remote Sens. Environ.*, 123, 400–417

Atzberger, C., and Eilers, P.H. (2011). Evaluating the effectiveness of smoothing algorithms in the absence of ground reference measurements. *Int. J. Remote Sens*., 32, 3689–3709

Atzberger, C., and Eilers, P.H.C. (2011a). A time series for monitoring vegetation activity and phenology at 10-daily time steps covering large parts of South America. *International Journal of Digital Earth*, 4(5), 365–386

Atzberger, C., Klisch, A., Mattiuzzi, M., and Vuolo, F. (2013). Phenological metrics derived over the European continent from NDVI3g data and MODIS time series. *Remote. Sens.*, 6, 257–284

Bajocco, S., Ferrara, C., Alivernini, A., Bascietto, M., and Ricotta, C. (2019). Remotely-sensed phenology of Italian forests: going beyond the species. *Int. J. Appl. Earth Obs. Geoinf*., 74, 314–321

Baldocchi, D. (2003). Assessing the eddy covariance technique for evaluating carbon dioxide exchange rates of ecosystems: Past, present and future. *Glob. Change Biol.*, 9, 479–492

Baret, F., Weiss, M., Lacaze, R., Camacho, F., Makhmara, H., Pacholcyzk, P., and Smets, B. (2013). GEOV1: LAI, FAPAR essential climate variables and FCOVER global time series capitalizing over existing products. Part 1: Principles of development and production. *Remote Sens. Environ*., 137, 299–309

Bater, C.W., Coops, N.C., Wulder, M.A., Nielsen, S.E., McDermid, G.J., and Stenhouse, G. (2011). Design and installation of a camera network across an elevation gradient for habitat assessment. *Instrum. Sci. Technol.*, 39, 231–247

Baumann, M., Özdoğan, M., Richardson, A.D., and Radeloff, V.C. (2017). Phenology from Landsat when data is scarce: Using MODIS and Dynamic Time-Warping to combine multi-year Landsat imagery to derive annual phenology curves. *Int. J. Appl. Earth Obs. Geoinformation*, 54, 72–83

Beaubien, E.G., and Freeland, H.J. (2000). Spring phenology trends in Alberta, Canada: links to ocean temperature. *Int J of Biom*., 44, 53–59

Beaumont, L., Hartenthaler, T., Keatley, M., and Chambers, L. (2015). Shifting time: recent changes to the phenology of Australian species. *Clim. Res.*, 63, 203–214

Beck, P.S.A., Atzberger, C., Hogda, K.A., Johansen, B., and Skidmore, A.K. (2006). Improved monitoring of vegetation dynamics at very high latitudes: A new method using MODIS NDVI. *Remote Sensing of Environment*, 100, 321–334

Beer, C., Reichstein, M., Tomelleri, E., Ciais, P., Jung, M., Carvalhais, N., Rödenbeck, C., Arain, M., Baldocchi, D., and Bonan, G. (2010). Terrestrial gross carbon dioxide uptake: Global distribution and covariation with climate. *Sci.*, 329, 834–838

Beguería, S., Vicente-Serrano, S.M., Reig, F., and Latorre, B. (2013). Standardized precipitation evapotranspiration index (SPEI) revisited: parameter fitting, evapotranspiration models, tools, datasets and drought monitoring. *Int. J. Climatol*., 34, 3001–3023

Berg, A., Findell, K., Lintner, B. (2016). Land–atmosphere feedbacks amplify aridity increase over land under global warming. *Nature Clim Change*., 6, 869–874

Berra, E., and Gaulton, R. (2021). Remote sensing of temperate and boreal forest phenology: A review of progress, challenges and opportunities in the intercomparison of in-situ and satellite phenological metrics. *Forest Ecology and Management*, 480, 118663

Bonan, G. B. (2008). *Ecological Climatology*: Concepts and Applications (Cambridge Univ. Press, Cambridge, 2nd ed.)

Borchert, R., and Rivera, G. (2001). Photoperiodic control of seasonal development and dormancy in tropical stem–succulent trees. *Tree Physiol*, 21, 213–221

Bórnez, K., Descals, A., Verger, A., and Peñuelas, J. (2020a). Land surface phenology from VEGETATION and PROBA-V data. Assessment over deciduous forests. *Int. J. Appl. Earth Obs. Geoinf*., 84, 101974

Bórnez, K., Richardson, A.D., Verger, A., Descals, A., and Peñuelas, J. (2020b). Evaluation of VEGETATION and PROBA-V Phenology Using PhenoCam and Eddy Covariance Data. *Remote Sens*., 12, 3077

Bradley, A.V., Gerard, F.F., Barbier, N., Weedon, G.P., Anderson, L.O., Huntingford, C., Aragao, L.E., Zelazowski, P., and Arai, E. (2011). Relationships between phenology, radiation and precipitation in the Amazon region. *Global Change Biol*., 17, 2245–2260

Bradley, B.A., Jacob, R.W., Hermance, J.F., and Mustard, J.F. (2007). A curve fitting procedure to derive inter-annual phenologies from time series of noisy satellite NDVI data. *Remote Sens Environ.*, 106, 137–145

Brown, J., Wardlow, B., Tadesse, T., Hayes, M., and Reed, B. (2008). The vegetation drought response index (VegDRI): a new integrated approach for monitoring drought stress in vegetation. *GIScience Remote Sens*., 45, 16–46

Brown, T., Hultine, K.R., Steltzer, H., Denny, E., Denslow, M., Granados, J., Henderson, S., Moore, D.J.P., Nagai, S., and San Clements, M. (2016). Using phenocams to monitor our changing Earth: Toward a global phenocam network. *Front. Ecol. Environ*., 14, 84–93

Brus, D., Hengeveld, G., Walvoort, D., Goedhart, P., Heidema, A., Nabuurs, G., and Gunia, K. (2012). Statistical mapping of tree species over Europe. *Eur. J. Forest Res.*, 131, 145–157

Buermann, W., Forkel, M., O'Sullivan, M., Sitch, S., Friedlingstein, P., Haverd, V., Jain, AK., Kato, E., Kautz, M., Lienert, S., Lombardozzi, D., Nabel, JEMS., Tian, H., Wiltshire, AJ., Zhu, D., Smith, WK., and Richardson, AD. (2018). Widespread seasonal compensation effects of spring warming on northern plant productivity. *Nature*, 562(7725), 110-114

Buermann, W., Parida, B., Jung, M., Burn, D., and Reichstein, M. (2013). Earlier springs decrease peak summer productivity in North American boreal forests. *Environmental Research Letters*, 8, 024027

Butt, N., Seabrook, L., Maron, M., Law, B.S., Dawson, T.P., Syktus, J., and McAlpine, C.A. (2015). Cascading effects of climate extremes on vertebrate fauna through changes to low-latitude tree flowering and fruiting phenology. *Global Change Biol.*, 21(9), 3267–3277

C3S Global Land Cover Map. Available online: http://maps.elie.ucl.ac.be/CCI/viewer/download.php (accessed on 18 July 2021)

Cai, Z., Jönsson, P., Jin, H., and Eklundh, L. (2017). Performance of Smoothing Methods for Reconstructing NDVI Time-Series and Estimating Vegetation Phenology from MODIS Data. *Remote Sensing*, 9, 1271

Ceccherini, G., Gobron, N., and Migliavacca, M. (2014). On the Response of European Vegetation Phenology to Hydroclimatic Anomalies. *Remote Sens*., 6, 3143–3169

CGLS LAI V2 Data. Available online: https://land.copernicus.eu/global/themes/vegetation (accessed on 8 July 2021)

Chen, H., and Sun, J. (2015). Changes in drought characteristics over China using the standardized precipitation evapotranspiration index. *J Clim.*, 28, 5430–5447

Chen, J., Jönsson, P., Tamura, M., Gu, Z., Matsushita, B., and Eklundh, L. (2004). A simple method for reconstructing a high-quality NDVI time-series data set based on the Savitzky–Golay filter. *Remote Sens. Environ*., 91, 332–344

Chen, S., Zhang, L.G., Tang, R., Yang, K., and Huang, Y. (2017). Analysis on temporal and spatial variation of drought in Henan Province based on SPEI and TVDI. *Trans Chin Soc Agric Eng*., 33, 126–132

Chen, Z., Tang, X., Gu, Q., Wang, T., Wei, J., Song, L., and Ma, M. (2018). Climatic anomaly and its impact on vegetation phenology, carbon sequestration and water-use efficiency at a humid temperate forest. *Journal of Hydrology*., 565, 150-159

Cherlet, M., Hutchinson, C., Reynolds, J., Hill, J., Sommer, S., and von Maltitz, G. (Eds.). (2018). World Atlas of Desertification, *Publication Office of the European Union*, Luxembourg

Chmielewski, F.M., and Rötzer, T. (2001). Response of tree phenology to climate change across *Europe. Agric. For. Meteorol*., 108, 101–112

Chmielewski, F.M., and Rotzer, T. (2002). Annual and spatial variability of the beginning of growing season in Europe in relation to air temperature changes. *Climate Research*, 19, 257–264

Chmura, H.E. (2019). The mechanisms of phenology: the patterns and processes of phenological shifts. *Ecol. Monogr.*, 89, e01337

Chuine, I. (2010). Why does phenology drive species distribution? *Philos Trans R Soc B.*, 365, 3149–3160

Chuine, I., and Régnière, J. (2017). Process-based models of phenology for plants and animals. Annual Review of Ecology, *Evolution, and Systematics*, 48, 159–182

Churkina, G., Schimel, D., Braswell, B., and Xiao, X. (2005). Spatial analysis of growing season length control over net ecosystem exchange. *Glob. Change Biol.*, *11*, 1777–1787

Ciais, P., Reichstein, M., Viovy, N., Granier, A., Ogée, J., Allard, V., Aubinet, M., Buchmann, N., Bernhofer, C., and Carrara, A. (2005). Europe-wide reduction in primary productivity caused by the heat and drought in 2003. *Nature*, 437, 529–533

Cleland, E.E., Chuine, I., Menzel, A., Mooney, H.A., and Schwartz, M.D. (2017). Shifting plant phenology in response to global change. *Trends Ecol. Evol*., 22, 357–365

Cong, N., Shen, M.G., and Piao, S.L. (2017). Spatial variations in responses of vegetation autumn phenology to climate change on the Tibetan Plateau. *J. Plant Ecol*., 10, 744–752

D'Odorico, P., Besik, A., Wong, C.Y.S., Isabel, N., and Ensminger, I. (2020). High-throughput drone-based remote sensing reliably tracks phenology in thousands of conifer seedlings. *New Phytol*., 226, 1667–1681

Daham, A., Han, D., Jolly, WM., Rico-Ramirez, M., and Marsh, A. (2019). Predicting vegetation phenology in response to climate change using bioclimatic indices in Iraq. *J Water Clim Change*, 10 (4): 835–851

de Beurs, K., and Henebry, G. (2005). Land surface phenology and temperature variation in the International Geosphere–Biosphere Program high-latitude transects. *Global Change Biol*., 11, 779–790

de Beurs, K., and Henebry, G. (2010). Spatio-temporal statistical methods for modelling land surface phenology. In Hudson, & Keatley (Eds.), Phenological research: Methods for environmental and climate change analysis. Springer, Dordrecht

de Beurs, K.M., and Henebry, G.M. (2004). Land surface phenology, climatic variation, and institutional change: analyzing agricultural land cover change in Kazakhstan. *Remote Sens Environ.*, 89, 497–509

de Moura, Y.M., Galvao, L.S, Hilker, T., Wu, J., Saleska, S., do Amaral, C.H., Nelson, B.W., Lopes, A.P., Wiedeman, K.K., Prohaska, N., de Oliveira, R.C., Machado, C.B., and Aragao, L.E.O.C. (2017). Spectral analysis of amazon canopy phenology during the dry season using a tower hyperspectral camera and modis observations. ISPRS J. Photogramm. *Remote Sens*., 131, 52–64

Delbart, N., Beaubien, E., Kergoat, L., and Le Toan, T. (2015). Comparing land surface phenology with leafing and flowering observations from the PlantWatch citizen network. *Remote Sens. Environ*., 160, 273–280

Delbart, N., Kergoat, L., Le Toan, T., Lhermitte, J., and Picard, G. (2005). Determination of phe- nological dates in boreal regions using normalized difference water index. *Remote Sens. Environ*., 97, 26–38

Delbart, N., Picard, G., Le Toans, T., Kergoat, L., Quegan, S., Woodward, I., Dye, D., and Fedotova, V. (2008). Spring phenology in boreal Eurasia over a nearly century time scale, *Global Change Biol*., 14(3), 603–614

Denny, E., Gerst, K.L., Miller-Rushing, A.J., Tierney, G.L., Crimmins, T.M., Enquist, C.A.F., Guertin, P., Rosemartin, A.H., Schwartz, M.D., and Thomas, K.A., (2014). Standardized phenology monitoring methods to track plant and animal activity for science and resource management applications. *Int. J. Biometeorol.*, 58, 591–601

Descals, A., Wich, S., Wich., Meijaard, E., Gaveau, D., Peedell, S., and Szantoi Z. (2020). High-resolution global map of small holder and industrial closed-canopy oil palm plantations. *Earth Syst. Sci.* Data, 13, 1211–1231

Diffenbaugh, N. (2005). Sensitivity of extreme climate events to CO2 induced biophysical atmosphere-vegetation feedbacks in the western United States. *Geophys. Res. Lett*., 32, 1–4

Donnelly. A., and Yu, R. (2017). The rise of phenology with climate change: an evaluation IJB publications. *Int J Biometerol*, 61, 29–50

Du, J., He, Z., Piatek, K., Chen, L.F., Lin, P., and Zhu, Xi. (2019). Interacting effects of temperature and precipitation on climatic sensitivity of spring vegetation green-up in arid mountains of China. *Agric. For. Meteorol*., 269, 71–77

Duarte, L., Teodoro, A.C., Monteiro, A.T., Cunha, M., and Gonçalves, H. (2018). QPhenoMetrics: an open-source software application to assess vegetation phenology metrics. *Comput. Electron. Agric*., 148, 82–94

Duchemin, B., Goubier, J., and Courrier, G. (1999). Monitoring phenological key stages and cycle duration of temperate deciduous forest ecosystems with NOAA/AVHRR data. *Remote Sens. Environ*., 67, 68–82

Eerens, H., and Haesen, D. (2015). User's manual of Software for the Processing and Interpretation of Remotely Sensed Image Time Series. Version 1.4.0. Available at http://spirits.jrc.ec.europa.eu/files/SpiritsManual_140.pdf

Eerens, H., Haesen, D., Rembold, F., Urbano, F., Tote, C., and Bydekerke, L. (2014). Image time series processing for agriculture monitoring. *Environ. Model. Soft*., 53, 154–162

Eilers, P. H. C. (2003). A perfect smoother. *Analytical Chemistry*., 75(14), 3631–3636

Ellwood, E., Temple, S., Primack, R., Bradley, N., and Davis, C. (2013). Record-Breaking Early Flowering in the Eastern United States. *PLoS ONE.*, 8(1), e53788

ERA5 Climate Dataset. Available online: https://cds.climate.copernicus.eu/ (accessed on 2 May 2021)

ESA. Land Cover CCI Product C3S. Available online: http://maps.elie.ucl.ac.be/CCI/viewer/download.php (accessed on 2 May 2021)

Estiarte, M., and Peñuelas, J. (2015). Alteration of the phenology of leaf senescence and fall in winter deciduous species by climate change: effects on nutrient proficiency. *Glob Chang Biol*., 21(3), 1005–1017

Estrella, N., and Menzel, A. (2006). Responses of leaf colouring in four deciduous tree species to climate and weather in Germany. *Climate Research*., 32, 253–267

Fischer, A. (1994). A model for the seasonal variations of vegetation indices in coarse resolution data and its inversion to extract crop parameters. *Remote Sens. Environ*., 48, 220–230

Fischer, E.M., and Schär, C. (2010). Consistent geographical patterns of changes in high-impact European heatwaves. *Nat. Geosci*., 3(6), 398–403

Fischer, E.M., Seneviratne, S.I., Vidale, P., Lüthi, D., and Schär, C. (2007). Soil moisture–atmosphere interactions during the 2003 European summer heat wave. *J. Clim*., 20, 5081–5099

Fisher, J.I., and Mustard, J.F. (2007). Cross-scalar satellite phenology from ground, Landsat, and MODIS data. *Remote Sens. Environ*., 109, 261–273

Fisher, J.I., Mustard, J.F., and Vadeboncoeur, M.A. (2006). Green leaf phenology at Landsat resolution: Scaling from the field to the satellite. *Remote Sens. Environ*., 100, 265–279

Fitchett, J.M., Grab, S.W., and Thompson, D.I. (2015). Plant phenology and climate change: Progress in methodological approaches and application. *Progress in Physical Geography*, 39, 460–482

Forrest, J., and Miller-Rushing, A.J. (2010). Toward a synthetic understanding of the role of phenology in ecology and evolution. *Philos. Trans. R. Soc*., 365, 3101–3112

Forzieri, G., Feyen, L., Cescatti, A., and Vivoni, E.R. (2014). Spatial and temporal variations in ecosystem response to monsoon precipitation variability in southwestern North America. *J. Geophys. Res*., 119, 1999–2017

Funk, C., Pedreros, D., Nicholson, S., Hoell, A., Korecha, D., Galu, G., Artan, G., Segele, Z., Tadege, A., Atheru, Z., Teshome, F., Hailermariam, K., Harrison, L., and Pomposi, C. (2019). Examining the potential contributions of extreme "Western V" sea surface temperatures to the 2017 March–June East African Drought. *Bull Am Meteorol Soc.*, 100, 55–60

Ganguly, S., Friedl, M.A., Tan, B., Zhang, X., and Verma, M. (2010). Land surface phenology from MODIS: Characterization of the Collection 5 global land cover dynamics product. *Remote. Sens. Environ.*, 114, 1805–1816

García de Cortázar, I., Duchêne, E., Destrac-Irvine, A., Barbeau, G., de Rességuier, L., Lacombe, T., Parker, A.K., Saurin, N., and Van Leeuwen, C. (2017). Grapevine phenology in France: From past observations to future evolutions in the context of climate change. *OENO One.*, 51, 115–126

Garrity, S., Bohrer, G., Maurer, K., Mueller, K., Vogel, C., and Curtis, P. (2011). A comparison of multiple phenology data sources for estimating seasonal transitions in deciduous forest carbon exchange. *Agric. Forest Meteorol*., 151, 1741–1752

Gobron, N., Pinty, B., Mélin, F., Taberner, M., Verstraete, M., Belward, A., Lavergne, T., and Widlowski, J.L. (2005). The state of vegetation in Europe following the 2003 drought. *Int. J. Remote Sens*., 26, 2013–2020

Gonsamo, A., Chen, J., and D'Odorico, P. (2013). Deriving land surface phenology indicators from CO2 eddy covariance measurements. *Ecological Indicators*, 29, 203–207

Gonsamo, A., Chen, J.M., Price, D.T., Kurz, W.A., and Wu, C. (2012). Land surface phenology from optical satellite measurement and CO2 eddy covariance technique. *J. Geophys. Res.-Biogeosci*., 117, (G3):1-18

Gorelick, N., Matt, H., Mike, S., David, T., and Rebecca, M. (2017). Google Earth Engine: Planetary-Scale Geospatial Analysis for Everyone. *Remote Sens Environ.*, 202, 18–27

Guzmán., J.A., Sanchez-Azofeifa, G.A.; and Espírito-Santo, M.M. (2019). MODIS and PROBA-V NDVI Products Differ when Compared with Observations from Phenological Towers at Four Tropical Dry Forests in the Americas. *Remote Sens*., 11, 2316

Hanes, J.M., and Schwartz, M.D. (2011). Modeling land surface phenology in a mixed temperate forest using MODIS measurements of leaf area index and land surface temperature. *Theor. Appl. Climatol*., 105, 37–50

He, Z., Du, J., Chen, L., Zhu, X., Lin, P., Zhao, M., and Fang, S. (2018). Impacts of recent climate extremes on spring phenology in arid-mountain ecosystems in China. *Agric. For. Meteorol*., 260, 31–40

Held, I.M., and Soden, B. (2006). Robust responses of the hydrological cycle to global warming, *J. Clim*., 19(21), 5686–5699

Henebry, G.M., and de Beurs, K.M. (2013). Remote sensing of land surface phenology: a prospectus. In: Schwartz, M.D. (Ed.), Phenology: An Integrative Environmental Science. Springer, pp. 385–411

Heumann, B.W., Seaquist, J.W., Eklundh, L., and Jönsson, P. (2007). AVHRR derived phenological change in the Sahel and Soudan, Africa, 1982–2005. *Remote Sens. Environ*., 108, 385–392

Hmimina, G., Dufrêne, E., Pontailler, J., Delpierre, N., Aubinet, M., Caquet, B., De Grandcourt, A., Burban, B., Flechard, C., Granier, A., Gross, P., Heinesch, B., Bernard, L., Moureaux, C., Ourcival, J.M., Rambal, S., and Soudani, K. (2013). Evaluation of the potential of MODIS satellite data to predict vegetation phenology in different biomes: An investigation using ground-based NDVI measurements. *Remote Sens Environ.*, 132, 145–158

Hollinger, D.Y., and Richardson, A.D. (2005). Uncertainty in eddy covariance measurements and its application to physiological models. *Tree Physiol.*, 25, 873–885

Hou, W., Gao, J., Wu, S., and Dai, E. (2015). Interannual Variations in Growing-Season NDVI and Its Correlation with Climate Variables in the Southwestern Karst Region of China. *Remote Sens.*, 7(9), 11105–11124

Hufkens, K., Basler, D., Milliman, T., Melaas, E.K., and Richardson, A.D. (2018). An integrated phenology modelling framework in r. *Methods Ecol. Evol.*, 9, 1276–1285

Hufkens, K., Friedl, M., Sonnentag, O., Braswell, B.H., Milliman, T., and Richardson, A.D. (2012). Linking near-surface and satellite remote sensing measurements of deciduous broadleaf leaf forest phenology. *Remote Sens. Environ.*, 117, 307–321

Hufkens, K., Friedl, M.A., Keenan, T.F., Sonnentag, O., Bailey, A., O'Keefe, J., and Richardson, A.D. (2012). Ecological impacts of a widespread frost event following early spring leaf-out. *Glob. Chang. Boil.*, 18, 2365–2377

Ibáñez, I., Primack, R.B., Miller-Rushing, A.J., Ellwood, E., Higuchi, H., Lee, S.D., Kobori, H., and Silander, J.A. (2010). Forecasting phenology under global warming. *Philos Trans R Soc.*, 365, 3247–3260

Inouye, D.W. (2008). Effects of climate change on phenology, frost damage, and floral abundance of montane wildflowers. *Ecology*, 89, 353–362

IPCC. *Climate Change 2007. Contribution of Working Group 1 to the fourth assessment report of the Intergovernmental Panel on Climate Change*; Solomon, S., Qin, M., Manning, Z., Chen, M., Marquis, K.B., Averyt, M., and Miller, H., Eds.; Cambridge University Press: Cambridge, United Kingdom and New York, NY, USA, 2007; p 976

IPCC. *Climate Change 2013: The Physical Science Basis. Contribution of Working Group I to the Fifth Assessment Report of the Intergovernmental Panel on Climate Change*; Stocker, T.F., Qin, D., Plattner, G.-K., Tignor, M., Allen, S.K., Boschung,

J., Nauels, A., Xia, Y., Bex, V., and Midgley, P.M., Eds.; Cambridge University Press: Cambridge, UK, 2013; p. 1535

IPCC. *Climate Change, 2014. Impacts, Adaptation, and Vulnerability. Part a: Global and Sectoral Aspects. Contribution of Working Group II to the Fifth Assessment Report of the Intergovernmental Panel on Climate Change*. Cambridge University Press, Cambridge, United Kingdom and New York,NY, USA, 2014; p.1132

IPCC. *Climate Change 2012. Managing the Risks of Extreme Events and Disasters to Advance Climate Change Adaptation. A Special Report of Working Groups I and II of the Intergovernmental Panel on Climate Change*. Field, C.B., Barros, V., Stocker, T.F., Qin, D., Dokken, D.J., Ebi, K.L., Mastrandrea, M.D., Mach, K.J., Plattner, G., Allen, S.K., Tignor, M., and Midgley, P., Eds.; Cambridge University Press, Cambridge, UK, and New York, NY, USA, 2012; p. 582

Ivits, E., Cherlet, M., Mehl, W., and Sommer, S. (2009). Estimating the ecological status and change of riparian zones in Andalusia assessed by multi-temporal AVHHR datasets. *Ecol. Indic*., 9, 422–431

Ivits, E., Horion, S., Fensholt, R., and Cherlet, M. (2014). Drought footprint on European ecosystems between 1999 and 2010 assessed by remotely sensed vegetation phenology and productivity, *Global Change Biol*., 20(2), 581–593

Jacobs, N., Burgin, W., Fridrich, N., Abrams, A., Miskell, K., Braswell, B., Richardson, A.D., and Pless, R. (2009). The global network of outdoor webcams: Properties and applications In Proceedings of the 17th ACM International Conference on Advances in Geographic Information Systems, Seattle, WA, USA, 3–6 November; pp. 111–120

Javed, T., Li, Y., Feng, K. (2021). Monitoring responses of vegetation phenology and productivity to extreme climatic conditions using remote sensing across different sub-regions of China. *Environ Sci Pollut Res*., 28, 3644–3659

Jentsch, A., Kreyling, J., Boettcher, J., and Beierkuhnlein, C. (2009). Beyond gradual warming: Extreme weather events alter flower phenology of European grassland and heath species, *Global Change Biol*., 15(4), 837–849

Jeong, S. J., Ho, C.H., Gim, H. J., and Brown, M. E. (2011). Phenology shifts at start vs. end of growing season in temperate vegetation over the Northern Hemisphere for the period 1982–2008. *Global Change Biology*, 17, 2385–2399

Jia, K., Liang, S., Wei, X., Yao, Y., Su, Y., Jiang, B., and Wang, X. (2014). Land cover classification of Landsat data with phenological features extracted from time series MODIS NDVI data. *Remote Sens*., 6, 11518–11532

Joiner, J., Yoshida, Y., Zhang, Y., Duveiller, G., Jung, M., Lyapustin, A., Wang, Y., and Tucker, C.J. (2018). Estimation of terrestrial global gross primary production (GPP) with satellite data-driven models and eddy covariance flux data. *Remote. Sens.*, 10, 1346

Jones, H. G., and Vaughan, R. A. (2010). Remote sensing of vegetation: Principles, techniques, and applications. Oxford: Oxford University Press.

Jönsson, P., and Eklundh, L. (2002). Seasonality extraction by function fitting to time-series of satellite sensor data. *IEEE Transactions on Geoscience and Remote Sensing*., 40, 1824–1832

Jonsson, P., and Eklundh, L. (2004). TIMESAT—a program for analyzing time-series of satellite sensor data. *Comput. Geosci*., 30, 833–845

Jonsson, P., Cai, Z.Z., Melaas, E., Friedl, M.A., and Eklundh, L. (2018). A Method for Robust Estimation of Vegetation Seasonality from Landsat and Sentinel-2 Time Series Data. *Remote Sens*, 10(4), 635

Julien, Y., and Sobrino, J. (2009). Global land surface phenology trends from GIMMS database. *Int J Remote Sens*., 30, 13, 3495–3513

Kandasamy, S., and Fernandes, R. (2015). An approach for evaluating the impact of gaps and measurement errors on satellite land surface phenology algorithms: Application to 20year NOAA AVHRR data over Canada. *Remote Sensing of Environment*., 164, 114–129

Kandasamy, S., Baret, F., Verger, A., Neveux, P., and Weiss, M. (2013). A comparison of methods for smoothing and gap filling time series of remote sensing observations-Application to MODIS LAI products. *Biogeosciences.*, 10, 4055–4071

Kang, S., Running, S.W., Lim, J.H., Zhao, M., Park, C.R., and Loehman, R. (2003). A regional phenology model for detecting onset of greenness in temperate mixed forests, Korea: an application of MODIS leaf area index. *Remote Sens. Environ*., 86, 232–242

Kang, W., Wang, T., and Liu, S. (2018). The Response of Vegetation Phenology and Productivity to Drought in Semi-Arid Regions of Northern China. *Remote Sens*., 10, 727

Karl, T.R., Gleason, B., Menne, M., Mcmahon, J., Heim, J., Brewer, M., Kunkel, K., Arndt, D., Privette, J., Bates, J., and Groisman, P. (2012). Easterling, D. U.S. temperature and drought: Recent anomalies and trends. EoS *Transactions*., 93, 473–474

Keenan, T.F., Darby, B., Felts, E., Sonnentag, O., Friedl, M.A., Hufkens, K., O'Keef, J., Klosterman, S., Munger, J.W., Toome, M., and Richardson, A.D. (2014). Tracking forest phenology and seasonal physiology using digital repeat photography: a critical assessment. *Ecol Appl*., 24(6), 1478-1489

Keenan, T.F.; Gray, J., Friedl, M.A., Toomey, M., Bohrer, G., Hollinger, D.Y., Munger, J.W., O'Keefe, J, Schmid, H.P., Wing,I.S., Yang, B., and Richardson, A.D. (2014). Net carbon uptake has increased through warming-induced changes in temperate forest phenology. *Nature Climate Change*., 4(7), 598-604

Klosterman, S.T., Hufkens, K., Gray, J.M., Melaas, E., Sonnentag, O., LaVine, I., Mitchell, L., Norman, R., Friedl, M.A., and Richardson, A.D. (2014). Evaluating remote sensing of deciduous forest phenology at multiple spatial scales using PhenoCam imagery. *Biogeosciences*, 11, 4305–4320

Laskin, D.N., and McDermid, G.J. (2016). Evaluating the level of agreement between human and time-lapse camera observations of understory plant phenology at multiple scales. *Ecol. Informatics*, 33, 1–9

Li, Y., Zhang, Y., Gu, F., and Liu, S. (2019). Discrepancies in vegetation phenology trends and shift patterns in different climatic zones in middle and eastern Eurasia between 1982 and 2015. *Ecol Evol*., 9, 8664–8675

Lian, X., Piao, S., Li, L., Li, Y., Huntingford, C., Ciais, P., Cescatti, A., Janssens, I.A., Penuelas, J., Buermann, W., Chen, A., Li, X., Myneni, R., Wang, X., Wang, Y., Yang, Y., Zeng, Z., Zhang, Y., and Mcvicar, T.R. (2020). Summer soil drying exacerbated by earlier spring greening of northern vegetation. *Sci*. *Adv*., 6(1), eaax0255

Liang, E.Y., Liu, B., Zhu, L.P., and Yin, Z.Y. (2011). A short note on linkage of climatic records between a river valley and the upper timberline in the Sygera Mountains, southeastern Tibetan Plateau. *Global Planet Change*., 77, 97–102

Liang, L., Schwartz, M.D., and Fei, S. (2011). Validating satellite phenology through intensive ground observation and landscape scaling in a mixed seasonal forest. *Remote. Sens. Environ.*, 115, 143–157

Lieth, H., (edit.). (1974). Phenology and Seasonality Modeling, Springer Verlag, New York, 444pp

Lin, P., He, Z., Du, J., Chen, L., Zhu, X., and Li, J. (2017). Recent changes in daily climate extremes in an arid mountain region, a case study in northwestern China's Qilian Mountains. *Sci*. *Rep*., 7, 2245

Liu, L., Zhang, X., Yu, Y., and Guo, W. (2017). Real-time and short-term predictions of spring phenology in North America from VIIRS data. *Remote Sens. Environ*., 194, 89–99

Liu, Q., Fu, Y.S.H., Zhu, Z.C., Liu, Y.W., Liu, Z., Huang, M.T., Janssens, I.A., and Piao, S.L. (2016). Delayed autumn phenology in the Northern Hemisphere is related to change in both climate and spring phenology. *Global Change Biol*., 22, 3702–3711

Lloyd, D. (1990). A phenological classification of terrestrial vegetation cover using shortwave vegetation index imagery. *Remote Sens*., 11, 2269–2279

Lorenz, R., Davin, E., Lawrence, D., Stöckli, R., and Seneviratne, S. (2013). How important is vegetation phenology for European climate and heatwaves?. *J. Clim.*, 26, 10077–10100

Lu, P.L., Yu, Q., Liu, J.D., and He, Q.T. (2016). Effects of changes in spring temperature on flowering dates of woody plants across China. *Botanical Studies*., 47, 153–161

Luquez, V.M., Hall, D., Albrectsen, B.R., Karlsson, J., Ingvarsson, P., and Jansson, S. (2007). Natural phenological variation in aspen (*Populus tremula*): The SwAsp collection. *Tree Genet. Genomes*, 4, 279–292

Meroni, M., Marinho, E., Sghaier, N., Verstrate, M., and Leo, O. (2013). Remote sensing based yield estimation in a stochastic framework — case study of durum wheat in Tunisia. Remote Sens., 5, 539–557

Miao, L., Müller, D., Cui, X., and Ma, M. (2017). Changes in vegetation phenology on the Mongolian Plateau and their climatic determinants. *Plos One*., 12, e0190313

Miao, R., N. Lu, L. Yao, Y. Zhu, J. Wang, and J. Sun. (2013). Multi-year comparison of carbon dioxide from satellite data with ground-based FTS measurements (2003–2011), *Remote Sens*., 5(7), 3431–3456

Migliavacca, M., Galvagno, M., Cremonese, E., Rossini, M., Meroni, M., Sonnentag, O., Cogliati, S., Manca, G., Diotri, F., and Busetto, L. (2011). Using digital repeat photography and eddy covariance data to model grassland phenology and photosynthetic CO_2 uptake. *Agric. For. Meteorol., 151*, 1325–1337Monahan, W.B., Rosemartin, A., Gerst, K.L., Fisichelli, N.A., Ault, T., Schwartz, M.D., Gross, J.E., and Weltzin, J.F. (2013). Climate change is advancing spring onset across the US national park system. *Ecosphere*, 7, e01465

Moore, L.M., Lauenroth, WK., Bell, DM., and Schlaepfer, DR. (2015). Soil water and temperature explain canopy phenology and onset of spring in a semiarid steppe. *Great Plains Research*., 25, 121–138Morgenstern, K., Black, T.A., Humphreys, E., Griffis, T.J., Drewitt, G.B., Cai, T., Nesic, Z., Spittlehouse, D.L., and Livingston, N.J. (2004). Sensitivity and uncertainty of the carbon balance of a Pacific Northwest Douglas-fir forest during an El Niño/La Niña cycle. *Agric. For. Meteorol.*, 123, 201–219

Morin, X., Lechowicz, M.J., Augspurger, C., O'Keefe, J., Viner, D., and Chuine, I. (2009). Leaf phenology in 22 North American tree species during the 21st century. *Glob. Change Biol*., 15, 961–975

Morisette, J.T., Richardson, A.D., Knapp, A.K., Fisher, J.I., Graham, E.A., Abatzoglou, J., Wilson, B.E., Breshears, D.D., Henebry, G.M., and Hanes, J.M. (2009). Tracking the rhythm of the seasons in the face of global change: Phenological research in the 21st century. *Front. Ecol. Environ*., 7, 253–260

Mu, Q., Xiao, J., John, R., and Chen, J. (2011). Upscaling key ecosystem functions across the conterminous United States by a water-centric ecosystem model. J Geophys Res *Biogeosci*, 116, G00J05

Myneni, R. B., and Williams, D. L. (1994). On the relationship between FAPAR and NDVI. *Remote Sens. Environ*., 49(3), 200–211

Myneni, R. B., Hoffman, S., Knyazikhin, Y., Privette, J. L., Glassy, J., Tian, Y., Wang, Y., Song, X., Zhang, Y., Smith, G. R., Lotsch, A., Friedl, M., Morisette, J. T., Votava, P., Nemani, R. R., and Running, S. W. (2002). Global products of vegetation leaf area and absorbed PAR from year one of MODIS data. *Remote Sens. Environ*., 83, 214–231

Myneni, R.B., Keeling, C.D., Tucker, C.J., Asrar, G., and Nemani, R.R. (1997). Increased plant growth in the northern high latitudes from 1981–1991. *Nature*, 386, 698–702

Nijland, W., Bolton, D., Coops, N., and Stenhouse, G. (2016). Imaging phenology; scaling from camera plots to landscapes. *Remote Sens. Environ.*, 177, 13–20

Noormets, A., Chen, J., Gu, L., and Desai, A.R. (2009). The phenology of gross ecosystem productivity and ecosystem respiration in temperate hard-wood and conifer chronosequences. In Phenology of Ecosystem Processes: Applications in Global Change Research; Noormets A. (eds) Phenology of Ecosystem Processes. Springer, New York, NY. pp. 58–85

Palmer, W.C. (1965). Meteorological drought. U.S. Research Paper No. 45. US Weather Bureau, Washington, DC, p. 58

Parmesan, C. (2007). Influences of species, latitudes and methodologies on estimates of phenological response to global warming. *Global Change Biology*, 13, 1860–1872

Peng, D., Wu, C., Li, C., Zhang, X., Liu, Z, Ye, H., Luo, S., Liu, X., Hu, Y., and Fang, B. (2017). Spring green-up phenology products derived from MODIS NDVI and EVI: Intercomparison, interpretation and validation using National Phenology Network and AmeriFlux observations. *Ecol. Indic*., 77,. 323–336

Peñuelas J., and Filella I. (2001). Phenology: Responses to a warming world. *Sci*., 294, 793–795

Peñuelas J., Filella I., and Comas P. (2002). Changed plant and animal life cycles from 1952-2000 in the Mediterranean region. *Global Change Biology*, 8, 531–544

Peñuelas, J., Rutishauser, T., and Filella, I. (2009). Phenology feedbacks on climate change. *Science*., 324 (5929), 887-888

Pettitt, A.N. (1979). A non-parametric approach to the change-point problem. *Appl. Stat.*, 351, 126–135

PhenoCam Dataset v1.0 used in this study is publicly available through the ORNL DAAC (https://daac.ornl.gov/VEGETATION/guides/PhenoCam_V1.html) (accessed on 12 July 2021)

Piao S.L., Friedlingstein, P., Ciais, P., Viovy, N., and Demarty, J. (2007). Growing season extension and its effects on terrestrial carbon flux over the last two decades. *Global Biogeochemical Cycles*., 21, GB3018Piao, S., Fang, J., Zhou, L.M., Ciais, P., and Zhu, B. (2006). Variations in satellite-derived phenology in China's temperate vegetation. *Global Change Biol*., 12, 672–685

Piao, S., Friedlingstein, P., Ciais, P., Zhou, L., and Chen, A. (2006). Effect of climate and CO_2 changes on the greening of the Northern Hemisphere over the past two decades. *Geophys. Res. Lett.*, 33, 23402

Piao, S., Liu, Q., Chen, A., Janssens, I.A., Fu, Y., and Dai, J. (2019). Plant phenology and global climate change: current progresses and challenges. *Glob. Change Biol*., 25, 1922–1940

Piao, S., Tan, J., Chen, A., Fu, Y.H., Ciais, P., and Liu, Q. (2015). Leaf onset in the northern hemisphere triggered by daytime temperature. *Nat. Commun*., 6, 6911

Piao, S., Wang, X., Ciais, P., Zhu, B.,Wang, T., and Liu, J. (2011). Changes in satellite-derived vegetation growth trend in temperate and Boreal Eurasia from 1982 to 2006. *Glob. Chang. Biol*., 17, 3228–3239

Ponce-Campos, G., Moran, M., Huete, A., Zhang, Y., Bresloff, C., Huxman, T., and Starks, P. (2013). Ecosystem resilience despite large-scale altered hydroclimatic conditions, *Nature*., 494 (7437), 349–52

Primack, D., Imbres, C., Primack, R.B., Miller-Rushing, A.J., and Del Tredici, P. (2004). Herbarium specimens demonstrate earlier flowering times in response to warming in Boston. *Am. J. Bot*., 91, 1260–1264

Ramos, A., Pereira, M.J., Soares, A., Rosário, L.D., Matos, P., and Nunes, A. (2015). Seasonal patterns of Mediterranean evergreen woodlands (Montado) are explained by long term precipitation. *Agric. For. Meteorol*., 202, 44–50

Reed, B.C., Brown, J.F., VanderZee, D., Loveland, T.R., Merchant, J.W., and Ohlen, D. O. (1994). Measuring phenological variability from satellite imagery. *Journal of Vegetation Science*, 5, 703–714

Reed, B.C., White, M., and Brown, J.F. (2003). Remote sensing phenology. In Phenology: An integrative Environmental Science; Tasks for Vegetation Science, vol 39. Springer, Dordrecht

Reichstein, M. (2013). Climate extremes and the carbon cycle, *Nature*, 500(7462), 287–295

Reichstein, M., Ciais, P., Papale., D. (2007). Reduction of ecosystem productivity and respiration during the European summer 2003 climate anomaly: A joint flux tower, remote sensing and modelling analysis, *Global Change Biol*., 13(3), 634–651

Reichstein, M., Falge, E., Baldocchi, D., Papale, D., Aubinet, M., Berbigier, P., Bernhofer, C., Buchmann, N., Gilmanov, T., and Granier, A. (2005). On the separation of net ecosystem exchange into assimilation and ecosystem respiration: Review and improved algorithm. *Glob. Chang. Biol.*, 11, 1424–1439

Rembold F., Meroni M., Urbano F., Royer A., Atzberger C., Lemoine G., Eerens H., Haesen D., Aidco D.G., and Klisch A. (2015). Remote sensing time series analysis for crop monitoring with the SPIRITS software: new functionalities and use examples. *Front. Environ. Sci*., 3, 129–134

Richardson, A.D., Black, T.A., Ciais, P., Delbart, N., Friedl, M.A., Gobron, N., Hollinger, D.Y., Kutsch, W.L., Longdoz, B., and Luyssaert, S. (2010). Influence of spring and autumn phenological transitions on forest ecosystem productivity. *Philos. Trans. R. Soc. B: Boil. Sci.*, 365, 3227–3246

Richardson, A.D., Braswell, B., Hollinger, D.Y., Jenkins, J.P., and Ollinger, S.V. (2009). Near-surface remote sensing of spatial and temporal variation in canopy phenology. *Ecol. Appl.*, 19, 1417–1428

Richardson, A.D., Hufkens, K., Li, X., and Ault, T.R. (2019). Testing Hopkins' Bioclimatic Law with PhenoCam data. *Appl. Plant Sci.*, 7, e01228

Richardson, A.D., Hufkens, K., Milliman, T., and Frolking, S. (2018). Intercomparison of phenological transition dates derived from the PhenoCam Dataset V1.0 and MODIS satellite remote sensing. *Sci. Rep.*, 8, 5679

Richardson, A.D., Hufkens, K., Milliman, T., Aubrecht, D.M., Chen, M., Gray, J.M., Johnston, M.R., Keenan, T.F., Klosterman, S.T., and Kosmala, M. (2018). Tracking vegetation phenology across diverse North American biomes using PhenoCam imagery. *Sci. Data*, 5, 180028

Richardson, A.D., Jenkins, J.P., Braswell, B., Hollinger, D.Y., Ollinger, S.V., and Smith, M.L. (2007). Use of digital webcam images to track spring green-up in a deciduous broadleaf forest. *Oecologia*, 152, 323–334

Richardson, A.D., Keenan, T.F., Migliavacca, M., Ryu, Y., Sonnentag, O., and Toomey, M. (2013). Climate change, phenology, and phenological control of vegetation feedbacks to the climate system. *Agricultural and Forest Meteorology*, 169, 156–173

Richardson, A.D., Milliman, T., Hufkens, K., Aubrecht, D.M.L., Chen, M., Gray, J.M., Johnston, M.R., Keenan, T., Klosterman, S.T., and Kosmala, M. (2017). PhenoCam Dataset v1.0: Vegetation Phenology from Digital Camera Imagery, 2000–2015; ORNL Distributed Active Archive Center: Washington, DC, USA

Richardson, AD., Bailey, AS., Denney, EG., Martin, CW., Keenan, T.F., and O'Keefe, J. (2006). Phenology of a northern hardwood forest canopy. *Glob Chang Biol.*, 12(7), 1174–1188

Rodrigues, A., Marcal, A.R.S., and Cunha, M. (2013). Monitoring vegetation dynamics inferred by satellite data using the PhenoSat tool. *IEEE Trans. Geosci. Remote Sens*., 51, 2096–2104

Rodriguez-Galiano, V.F., Dash, J., and Atkinson, P.M. (2015). Characterising the land surface phenology of Europe using decadal MERIS data. *Remote. Sens.*, 7, 9390–9409

Rouse, J.W., R.H. Haas, J.A. Schell, and D.W. Deering. (1974). Monitoring vegetation systems in the Great Plains with ERTS, In: S.C. Freden, E.P. Mercanti, and M. Becker (eds) *Third Earth Resources Technology Satellite–1 Syposium. Volume I: Technical Presentations.*, NASA SP-351, NASA, Washington, D.C., pp. 309-317

Ryu, Y., Lee, G., Jeon, S., Song, Y., and Kimm, H. (2014). Monitoring multi-layer canopy spring phenology of temperate deciduous and evergreen forests using low-cost spectral sensors. *Remote Sens. Environ.*, 149, 227–238

Savitzky, A., and Golay, M.J.E. (1964). Smoothing and differentiation of data by simplified least squares procedures. *Anal. Chem.*, 36, 1627–1639

Saxena, K.G., and Rao, K.S. (2020). Climate Change and Vegetation Phenology. In: Tandon R., Shivanna K., Koul M. (eds) *Reproductive Ecology of Flowering Plants*: Patterns and Processes. Springer, Singapore, pp. 25–39

Schnelle, F. (1955). Pflanzen-Phänologie. Akademische VerlagsgeselIschaft, Leipzig.

Schwartz, M. D., and Hanes, J. M. (2010). Continental-scale phenology: warming and chill. *Int. J. Climatol*., 30, 1595–1598

Schwartz, M., Betancourt, J., and Weltzin, J. (2012). From Caprio's lilacs to the USA National Phenology Network Front. *Ecol. Environ*., 10, 324-327

Schwartz, M.D., Ahas, R., and Aasa, A. (2006). Onset of spring starting earlier across the Northern Hemisphere. *Global Change Biol*., 12, 343–351

Schwartz, M.D., and Hanes, J.M. (2009). Intercomparing multiple measures of the onset of spring in eastern North America. *Int. J. Clim*., 30, 1614–1626

Schwartz, M.D., Ault, T.R., and Betancourt, J.L. (2013). Spring onset variations and trends in the continental United States: past and regional assessment using temperature-based indices. *Int. J. Climatol*., 33, 2917–2922

Schwartz, M.D., Reed, B.C., and White, M.A. (2002). Assessing satellite-derived start-of-season measures in the conterminous USA. *Int. J. Climatol*., 22, 1793–1805

Sen, P.K. (1968). Estimates of the regression coefficient based on kendall's tau. *J. Am. Stat. Assoc*., 63, 1379–1389

Seneviratne, S. I., Luthi, D., Litschi, M., and Schar, C. (2006). Land atmosphere coupling and climate change in Europe, *Nature*., 443, 205–209

Sheffield, J., and Wood, E. (2008). Projected changes in drought occurrence under future global warming from multi-model, multi-scenario, IPCC AR4 simulations, *Clim. Dyn*., 31(1), 79–105

Shen, M., Piao, S., Dorji, T., Liu, Q., Cong, N., Chen, X., An, S., Wang, S., Wang, T., and Zhang, G. (2015). Plant phenological responses to climate change on the Tibetan plateau: research status and challenges. *Natl Sci Rev.*, 2, 454–467

Shen, M., Tang, Y., Chen, J., Yang, X., Wang, C., Cui, X., Yang, Y., Han, K., Li, L., Du, J., Zhang, G., and Cong, N.(2014). Earlier-Season Vegetation Has Greater

Temperature Sensitivity of Spring Phenology in Northern Hemisphere. *PLoS ONE*, 9(2), e88178

Shen, M.G., Piao, S.L., Cong, N., Zhang, G.X., and Jassens, I.A. (2015). Precipitation impacts on vegetation spring phenology on the Tibetan Plateau. Glob. *Change Biol. Bioenergy*., 21, 3647–3656

Siegmund, J.F., Wiedermann, M., Donges, J.F., and Donner, R.V. (2016). Impact of temperature and precipitation extremes on the flowering dates of four German wildlife shrub species. *Biogeosciences*., 13(19), 5541

Snyder, K.A., Huntington, J.L., Wehan, B.L., Morton, C.G., and Stringham, T. (2019). Comparison of Landsat and Land-based phenology camera Normalized Difference Vegetation Index (NDVI) for dominant plant communities in the Great Basin. *Sensors*, 19, 1139

Sonnentag, O., Hufkens, K., Teshera-Sterne, C., Young, A.M., Friedl, M., Braswell, B.H., Milliman, T., O'Keefe, J., and Richardson, AD. (2012). Digital repeat photography for phenological research in forest ecosystems. *Agric. For. Meteorol*., 152, 159–177

Sparks, TH., and Carey, PD. (1995). The response of species to climate over two centuries: an analysis of the Marsham phenological record, 1736–1947. *Journal of Ecology*, 83, 321–329

SPEI database. Available online: https://spei.csic.es/database.html (accessed on 2 May 2021)

Stéfanon, M., Drobinski, P., NOBLET, N., and D'Andrea, F. (2012). Effects of interactive vegetation phenology on the 2003 summer heat waves. *Journal of Geophysical Res*., 117, D24103

Swets, D. L., Reed, B. C., Rowland, J. R., and Marko, S. E. (1999). A weighted least-squares approach to temporal smoothing of NDVI. In Proceedings of the ASPRS Annual Conference, Portland, OR, USA, 17-21 May 1999; pp. 526–536

Sykes, M.T. (2009). Climate Change Impacts: Vegetation. In: *Encyclopedia of Life Sciences* (ELS). John Wiley & Sons, Ltd: Chichester

Tan, B., Morisette, J.T., Wolfe, R.E., Gao, F., Ederer, G.A., Nightingale, J., and Pedelty, J.A. (2011). An enhanced TIMESAT algorithm for estimating vegetation phenology metrics from MODIS data. *IEEE J. Sel. Top. Appl. Earth Observ. Remote Sens*., 4, 361–371

Tang, X.G., Li, H.P., Ma, M.G., Yao, L., Peichl, M., Arain, A., Xu, X.B., and Goulden, M. (2017). How do disturbances and climate effects on carbon and water fluxes differ between multi-aged and even-aged coniferous forests? *Sci. Total Environ*., 599, 1583–1597

Tateishi, R., and Ebata, M. (2004). Analysis of phenological change patterns using 1982–2000 Advanced Very High-Resolution Radiometer (AVHRR) data. *International Journal of Remote Sensing*, 25, 2287–2300

Templ, B., Koch, E., Bolmgren, K., Ungersböck, M., Paul, A., and Scheifinger, H. (2018). Pan European Phenological database (PEP725): a single point of access for European data. *Int. J. Biometeoroly*, 62, 1109–1113

Thackeray, S., Henrys, P. and Hemming, D. (2016). Phenological sensitivity to climate across taxa and trophic levels. *Nature*., 535, 241–245

Theil, H. (1992). A rank-invariant method of linear and polynomial regression analysis. In Henri Theil's Contributions to Economics and Econometrics; *Springer*: Berlin, Germany; pp. 345–381

Thompson, R., and Clark, R. M. (2008). Is spring starting earlier? *The Holocene*, 18(1), 95–104

Tierney, G., Mitchell, B., Miller-Rushing, A., Katz, J., Denny, E., Brauer, C., Donovan, T., Richardson, A., Toomey, M., Kozlowski, A. (2013). Phenology Monitoring Protocol: Northeast Temperate Network; Technical Report No. NPS/NETN//NRR-2013/681; National Park Service: Fort Collins, CO, USA; pp. 254.

Toté, C., Swinnen, E., Sterckx, S., Clarijs, D., Quang, C., and Maes, R. (2017). Evaluation of the SPOT/VEGETATION collection 3 reprocessed dataset: surface reflectances and NDVI. *Remote Sens. Environ*., 201, 219–233

Trumbore, S., Brando, P., and Hartmann, H. (2015). Forest health and global change. *Sci*., 349, 814–818

Tucker, C. J. (1979). Red and photographic infrared linear combination for monitoring vegetation. *Remote Sensing of Environment*, 8(2), 127-150

Verger, A., Baret , F., and Weiss, M. (2014). Near real time vegetation monitoring at global scale. *IEEE Journal of Selected Topics in Applied Earth Observations and Remote Sensing*, 7, 3473–3481

Verger, A., Baret, F., and Weiss, M. (2008). Performances of neural networks for deriving LAI estimates from existing CYCLOPES and MODIS products. *Remote. Sens. Environ.*, 112, 2789–2803

Verger, A., Baret, F., and Weiss, M. (2017). Algorithm Theoretical Basis Document: LAI, FAPAR, FCOVER Collection 1km, Version 2, Issue I1.40. Available at: https://land.copernicus.eu/global/sites/cgls.vito.be/files/products/GIOGL1_ATBD_FAPAR1kmV2_I1.40.pdf.

Verger, A., Baret, F., and Weiss, M. (2019). Algorithm Theoretical Basis Document: LAI, FAPAR, FCOVER Collection 1km, Version 2, Issue I1.41.. Available online: https://land.copernicus.eu/global/sites/cgls.vito.be/files/products/CGLOPS1_ATBD_LAI1km-V2_I1.41.pdf (accessed on 10 July 2021)

Verger, A., Baret, F., Weiss, M., Kandasamy, S., and Vermote, E. (2013). The CACAO method for smoothing, gap filling and characterizing seasonal anomalies in satellite time series. *IEEE transactions on Geoscience and Remote Sensing*., 51, 1963–1972

Verger, A., Bater, M., Weiss, M., Filella, and Peñuelas, J. (2015). GEOCLIM A global climatology of LAI, FAPAR, and FCOVER from VEGETATION observations for 1999-2010. *Remote Sens. Environ*., 166, 126–137

Verger, A., Filella, I., Baret, F., and Penuelas, J. (2016). Vegetation baseline phenology from kilometric global LAI satellite products. *Remote Sens. Environ*., 178, 1–14

Vicente-Serrano, S. M., Beguería, S., and López-Moreno, J. (2010). A multiscalar drought index sensitive to global warming: The Standardized Precipitation Evapotranspiration Index, *J. Clim*., 23(7), 1696–1718

Vicente-Serrano, S. M., Gouveia, C., Camarero, J., Beguería, S., Trigo, R., López-Moreno, J., Azorín-Molina, C., Pasho, E., Lorenzo-Lacruz, J., Revuelto, J., Morán-Tejeda, E., and Sánchez-Lorenzo, A. (2013). Response of vegetation to drought time-scales across global land biomes, *Proc. Natl. Acad. Sci*., 110(1), 52–57

Viovy, N., Arino, O., and Belward, A. S. (1992). The best index slope extraction (BISE): A method for reducing noise in NDVI time-series. *Int J of Remote Sens*., 13, 1585–1590

Visser, ME., Caro. SP., Van Oers, K., Schaper, SV., and Helm, B. (2010). Phenology, seasonal timing and circannual rhythms: towards a unified framework. *Philos Trans R Soc B.*, 365, 3113–3127

Vitasse, Y., Delzon, S., Dufrêne, E., Pontailler, J.Y., Louvet, J.M., Kremer, A., and Michalet, R. (2009). Leaf phenology sensitivity to temperature in European trees: do within-species populations exhibit similar responses? *Agric. For. Meteorol*., 149, 735–744

Vliet, A.J.H.V., de Groot, R.S., Bellens, Y., Braun, P., Bruegger, R., Bruns, E., Clevers, J., Estreguil, C., Flechsig, M., and Jeanneret, F.O. (2003). The European Phenology Network

Vrieling, A., Meroni, M., Darvishzadeh, R., Skidmore, A., Wang, T., Zurita-Milla, R., Oosterbeek, K., O'Connor, B., and Paganini, M. (2018). Vegetation phenology from Sentinel-2 and field cameras for a Dutch barrier island. *Remote Sensing of Environment,*, 215, 517–529

Vuichard, N., and Papale, D. (2015). Filling the gaps in meteorological continuous data measured at FLUXNET sites with ERA-Interim reanalysis. *Earth Syst. Sci. Data*, 7, 157–171

Walther, G.R. (2010). Community and ecosystem responses to recent climate change. *Philos. Trans. R. Soc. Lond. Ser. B.*, 365, 2019–2024

Walther, G.R., Post, E., Convey, P., Menzel, A., Parmesan, C., Beebee, T.J., Fromentin, J.M., Hoegh-Guldberg, O., and Bairlein, F. (2002). Ecological responses to recent climate change. *Nature*, 416(6879), 389–395

Wang, C., Li, J., Liu, Q., Zhong, B., Wu, S., and Xia, C. (2017). Analysis of differences in phenology extracted from the enhanced vegetation index and the leaf area index. *Sensors*, 17, 1982

Wang, H., Dai, J., and Ge, Q. (2014). Comparison of Satellite and Ground-Based Phenology in China's Temperate Monsoon Area. Advances in Meteorology 2014

Wang, H., Tetzlaff, D., Buttle, J., Carey, SK., Laudon, H., McNamara, JP., Spence, C., and Soulsby, C. (2019). Climate-phenology-hydrology interactions in northern high latitudes: assessing the value of remote sensing data in catchment ecohydrological studies. *Sci Total Environ.*, 656, 19–28

Wang, W., Anderson, B., Entekhabi, D., Huang, D., Su, Y., Kaufmann, R., and Myneni, R. (2007). Intraseasonal interactions between temperature and vegetation over the boreal forests. *Earth Interact*., 11, 1–30

Wang, X., Piao, S., Ciais, P., Li, J., Friedlingstein, P., Koven, C., and Chen, A. (2011). Spring temperature change and its implication in the change of vegetation growth in North America from 1982 to 2006. *Proceedings of the National Academy of Sciences*, 108, 1240–1245

Wang, X., Piao, S., Xu, X., Ciais, P., MacBean, N., Myneni, R.B., and Li, L. (2015). Has the advancing onset of spring vegetation green-up slowed down or changed abruptly over the last three decades? *Global Ecol. Biogeogr*., 24, 621–631

Wang, Z., Li, J., Lai, C., Huang, Z., Zhong, R., Zeng, Z., and Chen, X. (2017). Increasing drought has been observed by SPEI_pm in Southwest China during 1962–2012. *Theor Appl Climatol.*, 133, 23-28

White, K., Pontius, J., and Schaberg, P. (2014). Remote sensing of spring phenology in northeastern forests: A comparison of methods, field metrics and sources of uncertainty. *Remote Sensing of Environment*, 148, 97–107

White, M. A., de Beurs, K. M., Didan, K., Inouye, D. W., Richardson, A. D., Jensen, O. P., and Lauenroth, W. K. (2009). Intercomparison, interpretation, and assessment of spring phenology in North America estimated from remote sensing for 1982–2006. *Global Change Biology*, 15, 2335–2359

White, M. A., Thornton, P. E., and Running, S.W. (1997). A continental phenology model for monitoring vegetation responses to interannual climatic variability. *Global Biogeochemical Cycles,* 11, 217–234

White, M.A., Hoffman, F., and Hargrove, W.W. (2005). A global framework for monitoring phenological responses to climate change. *Geophys. Res. Lett.*, 32, L04705

Wingate, L., Ogée, J., Cremonese, E., Filippa, G., Mizunuma, T., Migliavacca, M., Moisy, C., Wilkinson, M., Moureaux, C., and Wohlfahrt, G. (2015). Interpreting canopy development and physiology using a European phenology camera network at flux sites. *Biogeosciences*, 12(20), 7979–8034

Wu, C., and Chen, J.M. (2013). Deriving a new phenological indicator of interannual net carbon exchange in contrasting boreal deciduous and evergreen forests. *Ecol. Indic.*, 24, 113–119

Wu, C., Gonsamo, A., Gough, C. M., Chen, J. M., and Xu, S. (2014). Modeling growing season phenology in North American forests using seasonal mean vegetation indices from MODIS. *Remote Sensing of Environment*, 147, 79–88

Wu, C., Peng, D., Soudani, K., Siebicke, L., Gough, C.M., Arain, M.A., Bohrer, G., LaFleur, P.M., Peichl, M., Gonsamo, A., Xu, S., Fang, B., and Ge, Q. (2017). Land

surface phenology derived from normalized difference vegetation index (NDVI) at global FLUXNET sites. *Agric. For. Meteorol.*, 233, 171–182

Xiao, X., Zhang, J., Yan, H., Wu, W., and Biradar, C. (2009). Land surface phenology. Convergence of satellite and Co2 eddy flux observations in *Phenology of Ecosystem Processes: Applications in Global Change Research* edited by Noormets, A, pp. 247–270, Springer, New York

Xiao, X., Zhang, Q., Hollinger, D., Aber, J., and Moore, B. (2005). Modeling gross primary production of an evergreen needleleaf forest using MODIS and climate data. *Ecol. Appl.*, 15, 954–969

Xie, Y., Sha, Z., and Yu, M. (2008). Remote sensing imagery in vegetation mapping: a review, *Journal of Plant Ecology*, 1, 9–23

Yan, D., Scott, R., Moore, D., Biederman, J., and Smith, W. (2019). Understanding the relationship between vegetation greenness and productivity across dryland ecosystems through the integration of PhenoCam, satellite, and eddy covariance data. *Remote Sens. Environ.*, 223, 50–62

Yu, F., Price, K.P., Ellis, J., and Shi, P. (2003). Response of seasonal vegetation development to climatic variations in eastern central Asia. *Remote Sens. Environ*., 87, 42–54

Yu, L., Liu, T., Bu, K., Yan, F., Yang, J., Chang, L., and Zhang, S. (2017). Monitoring the long-term vegetation phenology change in northeast China from 1982 to 2015. *Scientific Report*., 7, 14770

Zeng, H., Jia, G., and Epstein, H. (2011). Recent changes in phenology over the northern high latitudes detected from multi-satellite data. *Environ. Res. Lett.*, 6, 045508

Zeng, L., Wardlow, B., Xiang, D., Hu, S., and Li, D. (2020). A review of vegetation phenological metrics extraction using time-series, multispectral satellite data. *Remote Sensing of Environment*, 237, 111511

Zhang, X., Friedl, M. A., Schaaf, C. B., Strahler, A. H., Hodges, J. C. F., Gao, F., and Huete, A. (2003). Monitoring vegetation phenology using MODIS. *Remote Sens. Environ*., 84, 471-475

Zhang, X., Friedl, M.A., and Schaaf, C. (2006). Global vegetation phenology from Moderate Resolution Imaging Spectroradiometer (MODIS): Evaluation of global patterns and comparison with in situ measurements. *J. Geophys. Res. Space Phys*., 111, G04017

Zhang, X., Friedl. M,, Schaaf. CB., and Strahler, AH. (2004). Climate controls on vegetation phenological patterns in northern mid-and high latitudes inferred from MODIS data. *Glob Chang Biol.*, 10, 1133–1145

Zhang, X., Jayavelu, S., Liu, L., Friedl, M.A., Henebry, G.M., Liu, Y., Schaaf, C.B., Richardson, A.D., and Gray, J. (2018). Evaluation of land surface phenology from VIIRS data using time series of PhenoCam imagery. *Agr. Forest Meteorol*., 256, 137-149

Zhang, X., Tarpley, D., and Sullivan, J. (2007). Diverse responses of vegetation phenology to a warming climate, *Geophys. Res. Lett*., 34, L19405

Zhao, A., Zhang, A., Cao, S., Liu, X.F., Liu, J.H., and Cheng, D. (2018). Responses of vegetation productivity to multi-scale drought in Loess Plateau, China. *Catena*., 163, 165–171

Zhao, J., Zhang, H., Zhang, Z., Guo, X., Li, X., and Chen, C. (2015). Spatial and Temporal Changes in Vegetation Phenology at Middle and High Latitudes of the Northern Hemisphere over the Past Three Decades. *Remote Sens*., 7, 10973–10995

Zhao, M., Peng, C., Xiang, W., Deng, X., Tian, D., Zhou, X., Yu, G., He, H., and Zhao, Z. (2013). Plant phenological modeling and its application in global climate change research: overview and future challenges. *Environ Rev.*, 21, 1–14

Zheng, C., Tang, X, Gu, Q., Wang, T., Wei, J., Song, L., and Ma, M. (2018). Climatic anomaly and its impact on vegetation phenology, carbon sequestration and water-use efficiency at a humid temperate forest. *J. Hydrol*., 565, 150–159

Zheng, Z., Zhu, W., and Zhang, Y. (2020). Seasonally and spatially varied controls of climatic factors on net primary productivity in alpine grasslands on the Tibetan Plateau. *Glob. Ecol. Conserv*., 21, e00814

Zhou, J., Jia, L., and Menenti, M. (2015). Reconstruction of global MODIS NDVI time series: performance of harmonic ANalysis of time series (HANTS). *Remote Sens. Environ*., 163, 217–228

Zhou, J.H., Cai, W.T., Qin, Y., Lai, L.M., Guan, T.Y., Zhang, X.L., Jiang, L.H., Du, H., Yang, D.W., Cong, Z.T., and Zheng, Y.R. (2016). Alpine vegetation phenology dynamic over 16 years and its covariation with climate in a semi-arid region of China. *Sci. Total Environ*., 572, 119–128

Zhou, L., Tucker, C.J., Kaufmann, R.K., Slayback, D., Shabanov, N.V., and Myneni, R.B. (2001). Variations in northern vegetation activity inferred from satellite data of vegetation index during 1981–1999. *J of Geophy Research*., 106, 20069–20083